HUMANIZED ANTIBODY DEVELOPMENT USING PHAGE DISPLAY: APPLICATIONS TO SOLID TUMOR METASTASIS

A DISSERTATION
SUBMITTED TO THE FACULTY OF
UNIVERSITY OF MINNESOTA
BY

STEPHEN KALSCHEUER

IN PARTIAL FULFILLMENT OF THE REQUIREMENTS
FOR THE DEGREE OF
DOCTOR OF PHILOSOPHY

JAYANTH PANYAM
ADVISOR

JULY 2016

Abstract

The outlook for cancer patients who present with evidence of metastasis is best characterized as a precipitous decline in prognosis and overall survival. This dramatic reduction in survival suggests a need to focus on the development of therapeutic and diagnostic reagents that are tailored to cancer in its disseminated form. In pursuit of this goal, a phage display based phenotype screening platform was developed to generate humanized antibodies for use in both circulating tumor cell detection, and therapeutic intervention, using *in vivo* models of breast cancer metastasis.

A broader perspective on this work is that it highlights methods that focus on biologic drug development based on disease phenotype, as opposed to conventional target-based methods. In the context of metastasis, the present work focused on the relevant cancer cell phenotype, termed epithelial to mesenchymal transition, which is believed to be the driver phenotype of cancer dissemination. Phenotype screening approaches do not require prior knowledge of potential targets, and are thus amenable to cancer biomarker discovery, which in turn can lead to innovative, first-in-class approaches to cancer management. A broadly applicable method for deriving humanized antibodies from cell based phenotype screening was developed. Target deconvolution approaches to identify the binding partner of candidate antibodies were also explored. Finally, the fine tuning of antibody binding affinity via affinity maturation methods was also explored through physiologically based pharmacokinetic modelling, in an attempt to establish optimal targeting affinities for both solid tumors and metastases. The work concludes with *in vitro* and *in vivo* characterization of two candidate antibodies as therapeutic agents.

TABLE OF CONTENTS

SECTION 2: THERAPEUTIC ANTIBODY DEVELOPMENT

List of Tables

List of Figures

List of Abbreviations

[Ab]	antibody concentration
[Ag]	antigen concentration
ASCO	American society for clinical oncology
AUC	area under the curve
BC	breast cancer
BSA	bovine serum albumin
BSB	binding site barrier
CDH1	E-Cadherin
CDR	complementarity determining region
CFSE	carboxy fluorescein
CIP	calf intestinal phosphatase
C_{max}	maximum concentration achieved
CSPG	chondroitin sulfate proteoglycan
CTC	circulating tumor cell
DAPI	4',6-diamidino-2-phenylindole
DNA	deoxyribonucleic acid
DTC	disseminated tumor cell
ECM	extracellular matrix
EDTA	Ethylenediaminetetraacetic acid
EGF	epidermal growth factor
ELISA	enzyme linked immunosorbent assay
EMT	epithelial to mesenchymal transition
EpCAM	epithelial cell adhesion molecule
FACS	fluorescence activated cell sorting
Fc	fragment crystallizable region
FcRN	neonatal Fc Receptor
FDA	food and drug administration
FGF	fibroblast growth factor
GF	growth factor
GFP	green fluorescent protein
HER2	human epidermal growth factor receptor 2
HMLE	human mammary epithelial cells
HRP	horse radish peroxidase
HS	heparan sulfate
HSPE	heparanase
HSPG2	heparan sulfate proteoglycan 2/perlecan
i.v.	intravenous
IgG	Immunoglobulin G
IHC	immunohistochemistry
IMAC	immobilized metal ion affinity chromatography
IPTG	Isopropyl β-D-1-thiogalactopyranoside

K_D	equilibrium dissociation constant
MBC	metastatic breast cancer
MET	mesenchymal to epithelial transition
METS	metastasis
MFI	mean fluorescence intensity
MIC	metastasis initiating cell
mRNA	messenger RNA
NCCN	national comprehensive cancer network
PBMC	peripheral blood mononuclear cell
PBS	phosphate buffered saline
PCR	polymerase chain reaction
PDGF	platelet derived growth factor
PDX	patient derived xenograft
P_{eff}	effective permeability
PFS	progression free survival
PFU	plaque forming units
PI	propidium iodide
RE	restriction enzyme
RNA	ribonucleic acid
RT-PCR	Reverse transcription polymerase chain reaction
S/V	surface area to volume
SCC	squamous cell carcinoma
scFv	single chain variable domain
shRNA	short hairpin RNA
SWOG	southwest oncology group
TKI	tyrosine kinase inhibitor
TMB	3,3',5,5'-Tetramethylbenzidine
TMDD	target mediated drug disposition
USD	united states dollar
VEGF	vascular endothelial growth factor
V_H	heavy chain variable domain
VIM	Vimentin
V_L	light chain variable domain

CHAPTER 1

INTRODUCTION

1.1 metastatic breast cancer

Early detection and screening methods result in a favorable prognostic outlook in newly diagnosed breast cancer patients, however patients who present with evidence of metastasis have a five year survival rate of 23% from initial diagnosis[1]. The idea of metastasis as a late stage event in tumor progression has been challenged in recent years, with emerging evidence to suggest its appearance relatively early in tumorigenesis. Conventional diagnosis of metastatic cancer via detection of spread to regional lymphatics confers a poor prognosis in breast cancer patients, yet 20-40% of lymph node negative patients are believed to harbor occult metastases in bone marrow and other sites, at the time of diagnosis.[2,3] The presence of occult metastases at the time of diagnosis suggests a need for refinement of diagnostic methods, ideally through technologies capable of monitoring cancer cell dissemination in real-time. Such technologies would better inform clinicians of disease progression, therapy response, and relapse potential.

Current strategies for therapy management of metastatic breast cancer (MBC) patients is determined on an individual basis, taking into consideration several diagnostic criteria that include hormone receptor expression, HER2 expression, extent and location of detectable metastatic lesions, and duration of the relapse free interval following primary diagnosis and treatment. Therapy options include anthracycline and taxane monotherapy and/or aromatase inhibitors in hormone receptor positive patients, and the HER2 targeted

monoclonal antibody trastuzumab in combination with anthracyclines/taxanes in HER2 positive MBC patients.[4] Treatment goals are often focused on palliative care, however, suggesting a further need to elucidate the molecular mechanisms of cancer spread. With this knowledge, identification of stage specific events and biomarkers that will aid in diagnosis, and serve as points for therapeutic intervention will be critical in the future to improve cancer outcomes.

1.2 Epithelial to mesenchymal transition in metastasis

The formation of metastases in breast carcinoma proceeds through a series of steps, including invasion, intravasation into the circulation, survival, extravasation out of the circulation, and seeding of distant micrometastatic lesions.[5] The key cellular/molecular events that give rise to eventual dissemination begin as a histologically detectable transition from *in situ* to invasive carcinoma,[6] a process mediated by an abundance of inflammatory, endothelial and resident fibroblast cells within the reactive tumor stroma. Elevated levels of cytokines, growth factors and matrix proteases produced by these cells ultimately lead to dissolution of the basement membrane that separates *in situ* carcinoma, most frequently within mammary ductal epithelium, from the surrounding reactive tumor stroma. Upon dissolution of basement membrane, tumor cell – stromal interactions produce profound morphological changes within tumor cells, owing to the presence of secreted factors in tumor stroma. These cellular changes manifest as a loss of the polarized, cell-cell adhesion characteristics of epithelium. Cancer cells can, subsequently, acquire a motile, invasive, protease- and extracellular matrix component-secreting fibroblast like phenotype.[7]

The use of biomarker expression profiling to classify breast tumor subtypes has been

used to identify those subtypes displaying increased propensity for metastatic spread. Notably, the basal-like and HER2 positive subtypes display increased propensity to spread.[8,9] Immunohistochemical (IHC) characterization of basal-like primary breast tumors demonstrates high levels of EMT biomarker expression,[10] while gene expression profiling of cell lines from basal-like tumors define the EMT gene expression profile, relative to the non-invasive luminal phenotype.[11,12]

1.3 Role of EMT in generating circulating tumor cells

Advances in microfluidics and rare cell capture have resulted in development of a multitude of diagnostic medical devices aimed at detecting the presence of circulating tumor cells (CTCs) in peripheral blood of cancer patients. Evidence from a large, multi-center retrospective study of ca. 4,700 patients revealed that the presence of either disseminated tumor cells in bone marrow (DTC)s,[13] or CTCs[14] at time of diagnosis confers a poor prognosis. A landmark development in CTC diagnostics was the demonstration that monitoring of patient response to chemotherapy regimens at initial follow-up can predict disease progression.[15] The search for EMT marker gene expression has been extended to the CTC diagnostics field, with a number of recent studies demonstrating EMT marker gene expression in CTCs from BC patients. A frequent observation has been the enrichment of EMT associated genes within CTCs captured following conventional therapy regimens,[16–18] suggesting that EMT promotes an acquired resistance phenotype. Taken together, the aforementioned results point to the role of EMT in the generation of CTCs, and eventual metastases by generating invasive cells that can enter the circulation and have acquired therapeutic resistance, to enable viability prior to seeding a metastatic

lesion. Therapeutic targeting of EMT cells to prevent metastases represents a significant challenge however, owing to a number of factors that include; the complexity of EMT cell signaling, diversity of tumor microenvironmental factors in initiating EMT, and plasticity/transience of the acquired phenotype.[19]

1.4 Inter-relatedness of EMT and cancer stem cells

As mentioned above, EMT plays an important role in the early events of the metastatic cascade, yet evidence exists to suggest that, while EMT does govern the process of invasion and entry into the systemic circulation, it does not govern the process of seeding metastases.[20] As a consequence of this finding, inter-relatedness of EMT and the cancer stem cell (CSC) hypotheses has been postulated. Characteristics commonly ascribed to CSCs closely parallel those ascribed to EMT cells, with important additional properties harbored within CSCs that could help to explain the later stages of the metastatic cascade. The CSC hypothesis states that a minority of cancer cells exhibit properties of self-renewal, intrinsic therapy resistance, and proliferation/survival under various conditions of stress. CSCs are operationally defined by tumor seeding in immunocompromised hosts, dye effux as a surrogate to chemotherapy resistance, and growth in suspension culture. Application of the CSC hypothesis to the end stages of metastasis can also help to explain the observed cellular heterogeneity of metastatic tumors, which would suggest the presence of a metastatic founder cell capable of asymmetric cell division to produce a diversity of cell types.[21]

Normal tissue stem cells are long lived cells, possessing an indefinite replicative life cycle. The cancer correlates of normal tissue stem cells have been postulated to be putative

cells of origin in cancer.[22] The initial identification of breast cancer stem cells through immunophenotyping demonstrated a minority of cells exist in the primary tumor with the potential for self-renewal and tumorigenicity, as fewer than 200 of these CSCs were required to seed tumors in immunocompromised hosts, a phenomena that required $\geq 10^4$ non-stem cancer cells.[23] Subsequent studies, relying on immunophenotyping for CSC identification, conclusively demonstrated an inter-relatedness of EMT and CSC by showing that induced passage through an EMT in BC cell lines is accompanied by acquisition of CSC properties.[24] This landmark finding established an *in vitro* system that provided stable cell line models to interrogate critical aspects of both metastasis and therapy resistance.

The results pertaining to the inter-relatedness of EMT and CSC processes in metastasis pose an interesting question as to whether these properties can coexist in individual cancer cells. Kirchner has suggested the existence of two distinct cancer stem cell populations, one being static and the other being migratory. Migratory CSCs exist at the invasive front of primary tumors, near tumor – host interface. In a stepwise fashion, static CSCs are exposed to soluble factors in tumor stroma that can lead to EMT, thus generating migratory CSCs.[25] Attempts to identify true migratory CSCs, or "metastatic founder cells", has accelerated in the recent past, often through *ad hoc* assignment of cell surface biomarker expression to facilitate the sorting of CTC subsets believed to harbor such cells.[26,27]

From a drug development perspective, the rational design of therapies that target EMT biomarkers offers the opportunity to impede cancer dissemination by targeting those

cells at the invasive front or the primary tumor, as well as EMT cells harbored in micrometastatic lesions. The initial reports, outlined above, that demonstrate passage through EMT results in acquisition of stem cell like properties represents a valuable *in vitro* tool for drug development in CSC and metastasis research, due to the inter-relatedness of these two phenotypes. These same isogenic cell line pairs are employed in this thesis as a means of obtaining robust quantities of both EMT and non EMT cancer cells, with the goal of developing antibody based diagnostics and therapeutics that can selectively bind to potentially uncharacterized cell surface biomarkers of EMT.

1.5 Perspective on current MBC diagnostics and therapy

From the perspective of cancer immunodiagnostics, CTC and disseminated tumor cell (DTC) detection has emerged through the duration of this thesis as a relevant diagnostic biomarker of metastasis. DTC detection in bone marrow and draining lymphatics at the time of surgical tumor resection is standard practice, with CTC enumeration likely to be implemented in the near future. In the past five years, CTC detection platform development has made enormous strides to not only detect the presence of CTCs, but to investigate molecular and genomic aberrations, frequently at the single cell level. There are limitations to existing CTC detection platforms, which will be outlined extensively in this thesis, that make the development of antibodies capable of discriminating EMT a potentially valuable tool. The current state of the art microfluidics platform for CTC capture, the CTC ichip, is antigen independent, relying on biophysical parameters to separate CTCs from blood mononuclear cells. It is likely to be implemented in the stead of immunomagnetic capture platforms such as the Veridex Cellsearch platform

due to its ability to separate CTCs in an antigen independent fashion. From the perspective of antibody based therapy of MBC, the primary focus has been to employ the HER2 targeted antibody trastuzumab either alone, or in combination with chemotherapy regimens, to prolong progression free survival (PFS).[4,28] More recently, HER2 targeted antibody combinations have been employed in combination with conventional chemotherapy to further lengthen the PFS interval.[29] Antibody drug conjugate forms of Trastuzumab have also demonstrated improvements in PFS.[30] Approximately 20% of advanced/MBC patients are positive for HER2 expression however[31], suggesting an urgent need to increase the available repertoire of targeted therapies in MBC, ideally through development of antibodies and other targeted reagents with alternative mechanisms of action. Novel antibody development platforms presents the opportunity to both improve patient outcomes beyond what has been observed for HER2 targeted reagents, as well as increase the potential patient pool that could realize a benefit from target therapies in MBC.

1.6 Overview of Thesis

An overview to the structure of this thesis is given below. Two distinct sections exploring the development of diagnostic and therapeutic antibodies, respectively, provide the bulk of the material. The introduction sections that begin each chapter will highlight emerging trends pertaining to the contents of each chapter. The field of cancer immunotherapy is a rapidly evolving and exciting one. As a result, many landmark findings and advancements, particularly with regards to the evolution of CTC diagnostic platforms, were being published in high impact journals concurrent to the development of this thesis. An attempt has been made to highlight those emerging trends, so as to place the body of

work contained within this thesis in the context of a rapidly evolving field.

The work contained in this thesis is best characterized as being focused on method development and refinement, for the purpose of humanized antibody development. Absent established protocols in the laboratory, a substantial time investment was made to develop protocols for using phage display libraries to derive antibody variable domains to cancer relevant targets. The trajectory to human IgG development from phage display scFv was not a linear one, however. The initial focus was to develop bivalent scFvs (diabodies), outlined in the second chapter of the first section, for use in both CTC and imaging based diagnostics. This approach yielded positive results, including some positive preliminary work developing near infrared dye conjugated diabodies as a means to detect occult metastases via *in vivo* imaging. Issues related to diabody production, including yield and purity, led to this approach being replaced by engineering scFv variable domains onto an IgG backbone. Dividends were realized immediately in terms of yield, purity, and biological activity. Mono and bivalent scFv are ideally suited for imaging based diagnostics owing to rapid systemic clearance, creating favorable image contrast. The prolonged circulation half-life of IgG relative to scFv and diabody led to the imaging based approaches being replaced with therapeutic applications.

SECTION 1: DIAGNOSTIC ANTIBODY DEVELOPMENT

CHAPTER 2

PHAGE DISPLAY BASED CELL PHENOTYPE SCREENING FOR NOVEL CANCER BIOMARKER DISCOVERY

Summary

Circulating tumor cells (CTCs) have potential value in predicting drug sensitivity and informing therapy management for patients diagnosed with metastatic cancers. The currently approved method of CTC detection does not capture mesenchymal CTCs, a subset considered important for tumor dissemination. Using a phage display-based biopanning procedure, we developed antibodies that discriminate mesenchymal CTCs from epithelial CTCs in multiple in vivo models of metastatic carcinoma. Our studies further identified HSPG2/Perlecan as the cognate cell surface antigen bound by the antibodies. When used in conjunction with EpCAM based reagents, the antibodies developed here could potentially achieve a more comprehensive phenotype read-out of CTCs than EpCAM-based reagents alone. The results also provide evidence for a role that proteoglycans play in cancer dissemination.

Introduction

The outlook for patients who present with evidence of metastasis derived from carcinoma is best characterized as a precipitous decline in prognosis and overall survival.[1] The dramatic reduction in survival rates upon finding evidence of dissemination suggests an urgent need to focus on the development of therapeutic and diagnostic reagents that are tailored to cancer in its disseminated form. The recent development of point-of-care fluidics platforms have enabled oncologists to obtain evidence of dissemination in real-time via detection of circulating tumor cells (CTCs) in blood of patients, a so called liquid biopsy. While numerous CTC analysis technologies exist at various stages of development[32], the Veridex Cellsearch platform is the only method currently approved by the FDA for this purpose. Concerns have been raised regarding the method of CTC detection using CellSearch, which is reliant upon epithelial cell adhesion molecule (EpCAM) dependent immunomagnetic capture. Attempts to circumvent this limitation have focused on the further refinement of the fluidics function of CellSearch, such efforts being pioneered principally by Toner and colleagues. These next generation CTC fluidics platforms have demonstrated the ability to capture both solitary CTCs[33], as well as CTC clusters,[34] from patient blood. These platforms are reliant on biophysical separation parameters, and are thus 'label-free' approaches to CTC capture. Extending the utility of this technology beyond an enumeration of the presence/absence of CTCs, and towards the use of CTC counts to inform patient management is however the overarching goal, and a prerequisite for its recommendation as a tumor marker by clinical governing bodies like the ASCO[35]. With the demonstration that CTCs can be cultured *ex vivo* for use in modest-

throughput screening procedures to predict patient drug susceptibility, Toner and colleagues have taken a giant step towards the realization of this goal[36].

Concurrent to advances in biophysical CTC capture technology is work that is directed towards better understanding the phenotypic heterogeneity of isolated CTCs. Transgenic lineage tracing models have established a rate limitation to cancer dissemination occurring as a result of epithelial to mesenchymal transition[37]. Canonical EMT biomarkers have now been detected in CTCs derived from a diversity of primary tumor types[38–40], lending support to the critical role EMT plays in orchestrating cancer dissemination. Given the phenotypic heterogeneity of CTCs, represented by the existence of CTCs that have shed epithelial characteristics, one important question is whether these phenotypically distinct CTC populations are equivalent in their ability to seed metastases. It was recently demonstrated that minority CTCs from breast cancer patients, bearing a unique cell surface antigen profile that excludes EpCAM, are competent to seed brain metastasis in nude mice[41]. Within the EpCAM+ CTC population captured by CellSearch from breast cancer patients, greater than 1000 CTCs are required to initiate metastasis in mouse models, with the expression of a suite of tumor antigens known to facilitate osteolytic bone metastasis, including cancer stem cell marker CD44, being present in CTC derived bone lesions[42]. These seminal reports suggest the existence of metastasis initiating cells (MICs) within the bulk CTC population that likely require specialized gene expression profiles to facilitate colonization[43]. It is therefore apparent that, in addition to improvements in fluidics capacity of CTC devices, improvements in immunocapture and

post-capture analysis are needed to provide a more comprehensive phenotypic characterization of CTCs.

The *ad hoc* assignment of MIC surface marker expression to identify metastatically virulent CTC populations proved highly successful in the examples mentioned above. Yet this approach, being relient on literature precedent for MIC biomarker assignment, precludes the ability to identify novel, or previously uncharacterized cell surface markers of MICs. Given the functional inter-relateness of EMT and cancer stem cells, it is likely that MICs reside within the EMT transitioned population of CTCs, or within more specialized subsets of EpCAM+ CTCs [43], and it is this population of CTCs that needs to be efficiently captured and subsequently characterized by CTC fluidics platforms. Development of an immunoreagent that is selective to this CTC population could be coupled to existing EpCAM based immunocapture reagents to enable the full phenotypic suite of CTCs to be characterized.

One technique well suited for cell surface antigen identification within minority cell populations is phenotype based screening. When whole cells are used as an antigen source, combinatorial library screens can be designed to identify binders to a relevant cellular phenotype. Screening approaches that employ combinatorial antibody libraries can be designed to identify functional candidate antibodies that bind to a relevant phenotype, capturing the target antigen as it would exist in its native confirmation, providing a direct route to antibody drug or diagnostic reagents that would likely be readily translated into diagnostic/therapeutic relevance[44]. Given that prior knowledge of a potential target is not needed, this approach is also highly amenable to novel biomarker discovery via target

deconvolution. Indeed, recent evidence of new molecular entities and biologic drug approvals by the FDA suggests that truly innovative, first in class medicines are more frequently being derived from phenotype screening approaches as opposed to conventional target based screens[45].

We report the development of a whole cell competition based panning procedure that employs a single chain Fv (scFv) phage display library, to identify candidate scFv capable of selective binding to EMT transitioned, immortalized mammary epithelial cells. The candidate scFv, termed Tw1S4_6, is subsequently reformatted to human IgG, and demonstrates the ability to discriminate EMT like CTCs from EpCAM +, epithelial CTCs in multiple in vivo models of metastatic carcinoma. The approach results in rapid generation of humanized antibodies from cell based phenotype screening and is broadly applicable. A simplified target deconvolution approach was used to identify HSPG2/Perlecan as the cognate EMT cell surface antigen bound by Tw1S4_6. The results contained herein identify a suitable immunocapture reagent that could conceivably be coupled to EpCAM based reagents to give a more comprehensive phenotype read-out of CTCs than either EpCAM alone, or multi-parameter based cell sorting techniques. The results also provide evidence for a role that a historically well characterized class of tumor antigens, the proteoglycans, play in cancer dissemination.

Methods

Cell culture conditions

HMLE isogenic cell lines were cultured in MEGM media (Lonza). LM2 cells were cultured in MEM supplemented with 10%FBS and antibiotics. M12 cells were cultured in MEM, 10%FBS, and insulin (Life technologies, Carlsbad, CA).

Phage display bio-panning procedure

The Tomlinson phage display library has on the order 10^9 structurally distinct scFv displayed on the surface of bacteriophage, in monovalent format. Methods involved in propagation and purification of bacteriophage were performed according to the supplier protocol (Source Bioscience, Santa Fe Springs, CA). For competitive cell panning, two fluorescent cell viability dyes, Calcein AM-450 and CFSE, were used to discriminate human mammary epithelial cells (HMLE), from a sub-population of HMLE cells stably expressing Twist1, a transcription factor known to induce EMT. HMLE cells were labeled with 10μM CFSE at 10^6 cells/mL and mixed at 100:1 ratio with Calcein AM-450 labelled HMLE-Twist1 cells, dye labelling was performed according to manufacturer protocol (ebioscience, San Diego, CA). 10^9 PFU naive phage library was added to the cell suspension. Following incubation, the target HMLE-Twist1 cells are sorted from the mixed population using BD FACS Aria cell sorting equipment. Phage bound to the sorted HMLE Twist1 cells are eluted in pH 2 glycine buffer, and propagated in TG1 bacteria to generate sub-libraries. Sub-libraries, designated Tw1_S1 through Tw1_S4, represent polyclonal populations of recovered phage from target cells. After 4 competitive enrichment experiments performed in series, the original library diversity of 10^9 is thus sequentially

narrowed to a manageable population of candidate clones displaying selective binding to HMLE-Twist1 cells. After completion of 4 competition panning experiments, polyclonal sub-libraries were evaluated for relative binding affinity to HMLE and HMLE-Twist1 cells. The same two color discrimination scheme was employed. After labelling, $1*10^9$ PFU of phage from each sub-library were incubated with a 1:1 cell suspension HMLE:HMLE-Twist1 cells. Analysis of phage bound to cells was determined with an alexa-fluor647 conjugated antibody recognizing the C-Myc epitope tag present on phage particles. As depicted in figure 1B, a clear distinction in relative binding of polyclonal phage sub-libraries to HMLE-Twist1 cells is discernable by the second sub-library. This distinction is maintained in the third sub-library, and increased to approximately 8 fold selective binding in the fourth sub-library (figure 1C).

Phagemid clone analysis, both polyclonal and monoclonal populations, was assessed via indirect flow cytometry staining. Following incubation with phage and washing steps, a monoclonal antibody recognizing the Myc-epitope (9E10, Abcam), followed by goat-anti mouse dylight 650 Sigma Aldrich, St. Louis, MO) was used to assess relative binding.

Soluble scFv production

Tw1S4_6 scFv in phagemid vector was isolated from a single TG1 colony following the fourth round of competitive flow sorting. For soluble scFv production, one microgram of phagemid DNA was digested with Nco1 and Not1 (New England Biolabs, Ipswich, MA). The scFv sequence was purified following 1% agarose gel electrophoresis using the Quick gel extraction kit (Qiagen) according to manufacturer protocol. pET22b(+) was digested with Nco1 and Not1. Ligation of the phagemid derived scFv sequence to pET22b(+) was

performed using T4 DNA ligase (New England biolabs) according to manufacturer protocol. A molar ratio of 1:3 vector to insert was used for ligation. The ligation was transformed in to BL21 (DE3) chemically competent cells (New England biolabs). DNA sequencing was used to confirm successful sub-cloning. Soluble scFv production was induced by the addition of IPTG to a final concentration of 1mM to log-phase culture, and incubated for 3-4 hours at 30 degrees. Bacteria were pelleted at 4000rpm for 30 minutes. The pellet was resuspended in B-PER reagent (Thermo Fisher, San Jose, CA) to extract the periplasmic fraction containing soluble scFv. This fraction was passed over nickel-NTA agarose resin (5 prime), followed by wash and elution using an imidazole gradient (40mM imidazole for washing, 250mM for elution). Eluted fractions were concentrated and buffer exchanged to DPBS using Amicon ultra centrifugal concentrators, having a 10kD molecular weight cut off.

To assess relative binding to soluble phage, indirect flow cytometry staining was employed. scFvs are incubated with indicated cell lines in flow buffer (DPBS, 0.5%w/v BSA, 2mM EDTA) for 1 hour. Following washes, monoclonal antibody recognizing 6x His tag-Dylight 647 conjugate (AbCAM, Cambridge, UK) was used to assess binding.

scFv reformatting to human IgG1

Vectors encoding constant regions of the heavy chain human IgG1 (pFUSE2ss-CHIg-hG1) and light chain κ (pFUSE2ss-CLIg-hk) were purchased from Invivogen. PCR Primers were designed to amplify the corresponding variable region from Tw1S4_6 scFv, with appended restriction enzyme sites introduced into the primer, according to the manufacturers recommendations. Primers were as follows:

Vl_R_BsiWI: TAAACGTACGTTTGATTTCCACCTTGGT

Vl_F EcoR1: TAAGCAGAAGGCAACGGACATCCAGATGACC

Vh_R_nhe1: AAGCGCTAGTCGCTCGAGACGGTGACCAGGGT

Vh_F_EcoR1: TAAGCAGAATTTCGAGGTGCAGCTGTTGGAGTC

PCR of the corresponding variable domain was performed with Phusion HF DNA polymerase (NEB) and the following thermal cycling protocol:

For V_H: 98C for 30sec, followed by 35 cycles of [98C – 10sec, 67C – 15sec, 72C – 15sec].

For V_L: 98C for 30sec, followed by 35 cyles of [98C – 10sec, 65C – 15sec, 72C – 15sec]

PCR amplicons were resolved on a 1% agarose gel, excised and purified using QiaQuick gel extraction kit according to manufacturer protocol (Qiagen). RE digestion of V_L and pFUSE2ss-CLIg-hk was performed with EcoR1 and BsiWI. RE digestion of V_H and pFUSE2ss-CHIg-hG1 was performed with EcoR1 and Nhe1. Variable region fragments were again gel purified following RE digestion. RE digested pFUSE2ss vectors were treated with CIP phosphatase (NEB) according to manufacturer protocol, and purified from the enzyme reaction with GET Clean DNA plasmid columns (G Biosciences). A molar ratio of 1:3 vector to insert was used for ligation with T4 DNA ligase. The ligation reaction was transformed into Novablue strain (Merck Millipore). Proper variable domain insertion into pFUSE2ss vectors was confirmed by sequencing, using primer Antibody vector seq: TGCTTGCTCAACTCTACGTC.

Detection of Tw1S4_6 IgG binding to cell lines was determined by flow cytometry using a goat anti-human IgG dylight 647 antibody. Flow cytometric analysis was carried out on a BD LSR2 cytometer.

Cognate antigen Immunoprecipitation and MS/MS identification

300 micrograms of Tw1S4_6 scFv, produced in pET vector, bearing a C-terminal His tag, was immobilized on nickel agarose. Gravity flow chromatography cartridges were used to contain the sample. $1*10^7$ HMLE-Twist1 cells were lysed in 3mL RIPA buffer. Following centrifugation to clear the insoluble lysate debris, the total cell lysate was passed over scFv.- Agarose beads, which were subsequently washed four times using 20mM imidazole in DPBS, pH 7.5, followed by elution of scFv – antigen complex with 250mM imidazole in DPBS, pH 7.5. The eluant was concentrated using Amicon ultra-filtration dialysis units bearing a 10kD molecular weight cut-off. The concentrated sample was prepared for acrylamide gel electrophoresis in laemmli sample buffer, and boiled for 10 minutes to denature scFv – antigen complex. Sample was resolved on a 4-15% gradient acrylamide gel, and stained with coomassie blue to identify scFv and immunoprecipitated antigen. A band of >250kD molecular weight was excised from the acrylamide gel with a sterile scalpel and placed in a micro-centrifuge tube. An in gel tryptic digestion kit (Pierce) was used according to the manufacturer protocol to prepare the excised protein band for MS/MS analysis of trypsin digested product.

Database searching-- Charge state deconvolution and deisotoping were not performed. All MS/MS samples were analyzed using Sequest (Thermo Fisher Scientific, San Jose, CA, USA; version 27, rev. 12). Sequest was set up to search the rs_human_041912_cRAP database (unknown version, 33986 entries) assuming the digestion enzyme trypsin. Sequest was searched with a fragment ion mass tolerance of 0.80 Da and a parent ion tolerance of

1.00 Da. Iodoacetamide derivative of cysteine was specified in Sequest as a fixed modification. Oxidation of methionine was specified in Sequest as a variable modification.

Criteria for protein identification-- Scaffold (version Scaffold_4.2.1, Proteome Software Inc., Portland, OR) was used to validate MS/MS based peptide and protein identifications. Peptide identifications were accepted if they could be established at greater than 95.0% probability by the Peptide Prophet algorithm (Anal. Chem. 2002;74(20):5383-92). Protein identifications were accepted if they could be established at greater than 99.0% probability and contained at least 2 identified peptides. Protein probabilities were assigned by the Protein Prophet algorithm. Proteins that contained similar peptides and could not be differentiated based on MS/MS analysis alone were grouped to satisfy the principles of parsimony.

Coarse linear epitope mapping against HSPG2

Linear 20-mer peptides corresponding to human HSPG2, having a 16 residue overlap with adjacent sequence, were synthesized in an array format by Pepscan Presto using proprietary methods. Tw1S4_6 IgG, along with commercially available anti-human HSPG2 antibody (Sigma), were tested in a PEPSCAN-based ELISA.

HSPG2 Domain 1 expression

HSPG2 domain 1 construct was generously provided by Dr. Arthur DeCarlo. DNA sequence encoding the first 247 amino acids of human HSPG2 was cloned into pcDNA 3.3+ vector bearing a C terminal His tag, and purified according to previously reported methods.[46] HSPG2 domain 5 is supplied as a commercially available reagent (Santa Cruz Biotechnology).

Immunofluorescence microscopy

Cells were plated onto 8 well CC2 chamber slides (Lab Tek), and allowed to adhere prior to fixation with 3% formaldehyde for 10 minutes. Cells were subsequently permeabilized with 0.5%v/v Triton-X 100. Following a 1 hour blocking step in 5%w/v BSA in PBS, cells were stained with dye conjugate antibodies for 1 hour in blocking buffer. Antibodies used in fluorescence microscopy experiments were:

- PE anti human ECadherin, clone 67A4 (Biolegend)
- PE anti human EpCAM, clone 1B7 (Biolegend)
- Efluor 660 anti human Vimentin, clone V9 (ebioscience)
- Biotinylated anti human perlecan antibody, clone A7L6 (neomarkers) and streptavidin dylight 488 (Biolegend), or streptavidin APC depending on the other fluorophores in the antibody panel.

All antibodies were used at 1:250 dilution. Following staining, cells were mounted in prolong gold anti-fade mounting medium (Life technologies) and imaged within 24 hours. Image acquisition was performed on an Olympus Fluoview FV1000 BX2 upright confocal microscope. This instrument operates as a shared resource within the University Imaging Centers at the University of Minnesota.

ELISA

HSPG2 domains 1 and 5 were coated onto elisa plates for 2 hours at RT, using a concentration of 10µg/mL. Following three PBS washes, plates were blocked in block buffer (PBS, 2%BSA) for 2 hours at RT. Tw1S4_6 IgG diluted in block buffer at the indicated concentrations was plated in triplicate and incubated overnight at 4 degrees. The

following morning, plates were washed and incubated with 1:20,000 Protein-L HRP (Genscript) for 2 hours at RT. Three washes in PBS, followed by incubation with TMB substrate (Sigma) for 15 minutes was performed. The peroxide solution was quenched with stop solution (Sigma), and signal intensity was quantified on a UV/Vis 96 well plate reader using absorbance at 450nm. Log concentration - response plots were generated in GraphPad Prism software. Nonlinear regression analysis was employed to generate fitted curves to the data, and estimate the equilibrium dissociation constant, K_D

Circulating tumor cell isolation and detection

Animals were euthanized, and peripheral blood was harvested via cardiac puncture into EDTA tubes. Blood samples from tumor bearing mice were pooled (n=3), diluted 1:1 with PBS containing 1% v/v FBS, and layered onto histopaque ficoll gradient (Sigma). Samples were centrifuged at 400xg for 30 minutes with the brake off. The buffy coat containing mononuclear cells was isolated, and residual RBCs were lysed with BD Pharm lyse (BD bioscience). Cells were washed three times in PBS. Antibodies were diluted in flow buffer (PBS, 0.5% BSA, 2mM EDTA) to 100nM concentration, and cells were incubated on a rotating platform for 1hour at 4 degrees. Following three PBS washes, cells were sorted based on fluorescent profile on BD FACSAria 2 cell sorting equipment, housed in the University of Minnesota Masonic Cancer Center flow cytometry core facility.

Results

To accomplish our goal of identifying an antibody suitable for immunocapture of EMT CTCs, we first developed an in vitro competition based panning procedure, employing the Tomlinson scFv phage display library, and fluorescent viability dyes to enable sorting of

target cell populations. For the panning procedure, an isogenic matched mammary epithelial cell line pair was employed (HMLE–human mammary epithelial cells, and HMLE Twist1 - an EMT transitioned derivative cell line). HMLE are an hTERT immortalized primary breast epithelial cell line that is heterogenous in epithelial lineage and propagated in defined serum free media.[47] While not a transformed cell line, the inclusion of this cell line pair is based on the ability to establish the greatest contrast between the mammary epithelial and EMT transitioned phenotype. Ras transformed derivatives of HMLE display an elevated baseline EMT phenotype,[48] so given the goal of identifying antibodies with selective affinity to the EMT phenotype, the inclusion of HMLE-Ras cells would thus impair the ability to discriminate EMT from non-EMT cell populations. The overexpression of the EMT inducing transcription factor Twist1 in HMLE cells results in global changes in gene expression that mirror the claudin low/metaplastic breast tumor subtype[49], resulting in increased invasiveness[50], and cancer stem cell like behavior[51].

Initial characterization of HMLE and HMLE-Twist1 cells were performed to insure reproducibility and consistency with the literature. Confirmation of Epithelial marker E-Cadherin expression in HMLE cells and corresponding absence of Mesenchymal intermediate filament Vimentin is shown in figure 1a – left panel. EMT transitioned HMLE-Twist1 cells display an inverse Epithelial/Mesenchymal expression profile to that of HMLE (Figure 1a right panel). In addition, HMLE-Twist1 cells are less sensitive to conventional chemotherapy relative to HMLE (Figure 1b), a phenomena ascribed to the cancer stem cell-like behavior of EMT transitioned cells. Further confirmation of the stem

cell properties of HMLE-Twist1 is enrichment of the cancer stem cell surface CD44hi/CD24 low phenotype in HMLE-Twist1 cells relative to HMLE (figure 1c). This initial characterization data establishes the utility of this isogenic matched cell line pair for subsequent phenotype screening to identify EMT selective antibodies.

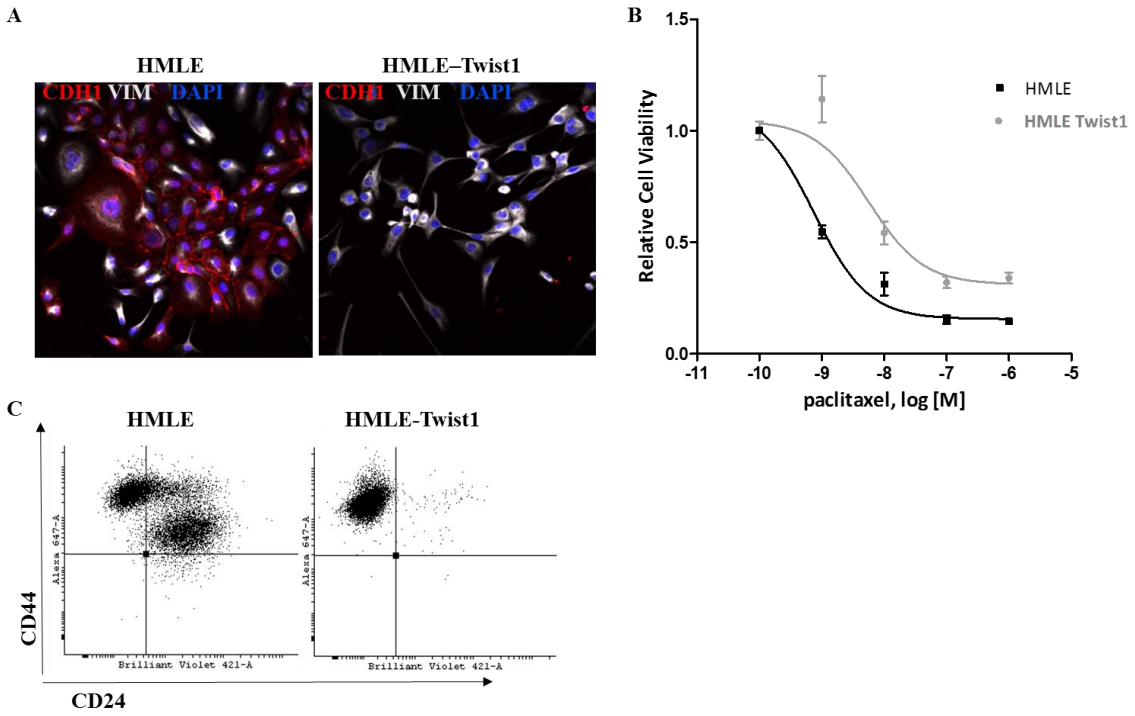

Figure 1 EMT Characteristics of isogenic EMT Cell lines. (A) Immunofluorescence staining of HMLE and HMLE-Twist1 cells for canonical epithelial and mesenchymal protein markers E-Cadherin (CDH1) and Vimentin (VIM), respectively. (B) Dose-response curve showing differential sensitivity of HMLE and HMLE-Twist1 cells to chemotherapeutic agent paclitaxel. (C) Cell surface cancer stem cell immunophenotyping demonstrates HMLE-Twist1 is predominately $CD44^{+}/CD24^{low}$ (right panel), relative to HMLE cells which have a mixed phenotype.

The Tomlinson phage scFv display library has on the order 10^{9} sequence unique scFv displayed on the surface of bacteriophage in monovalent format, with sequence diversity introduced into the complementarity determining regions via affinity maturation[52]. Two fluorescent viability dyes were used to discrimate mixed populations of HMLE and

HMLE-Twist1. Following incubation with phage library, HMLE-Twist1 cells are subsequently sorted from the mixed population, and bound phage eluted for sub-library generation. Critical to this approach is the initial fold dilution of Twist1 cells relative to HMLE. A mixing ratio of 100:1 HMLE:Twist1 provides a selective pressure for deriving antibody binders that are selective to Twist1 cells via creation of a cell surface antigen sink that is provided by excess HMLE cells. Thus, binders to genes whose products serve generalized functions or are expressed in equal abundance would be bound to HMLE and, following repeated iterations of the procedure, progressively eliminated from sorted sub-libraries. Phage bound to target cells are eluted and subsequently propagated in a permissive bacterial host to generate sub-libraries. Sub-libraries, designated Tw1_S1 through Tw1_S4, represent polyclonal populations of recovered phage from the target Twist1 cells. After 4 competitive cell sorting experiments, the original library diversity of 10^9 is sequentially narrowed to a manageable population of candidate clones displaying selective binding to Twist1 cells. Polyclonal sub-libraries were next evaluated for relative binding affinity to HMLE and Twist1 cells. The same two color, cell line discrimination scheme was employed (Figure 2A). After dye labelling, 10^9 PFU of phage from each sub-library were incubated with a 1:1 cell suspension HMLE:Twist1 cells. Analysis of phage bound to cells was determined with an antibody recognizing the Myc epitope tag present on scFv displaying phage. A clear distinction in relative binding of polyclonal phage sub-libraries to HMLE-Twist1 cells is discernable by the second sub-library (Figure 2B). This distinction is maintained in the third sub-library, and increased to approximately 8 fold selective binding in the fourth sub-library (Figure 2C). A monoclonal candidate scFv was

isolated from the fourth sorted sub-library which demonstrated selective binding to Twist1 relative to HMLE cells (Fig 2D), which is hereafter designated Tw1S4_6.

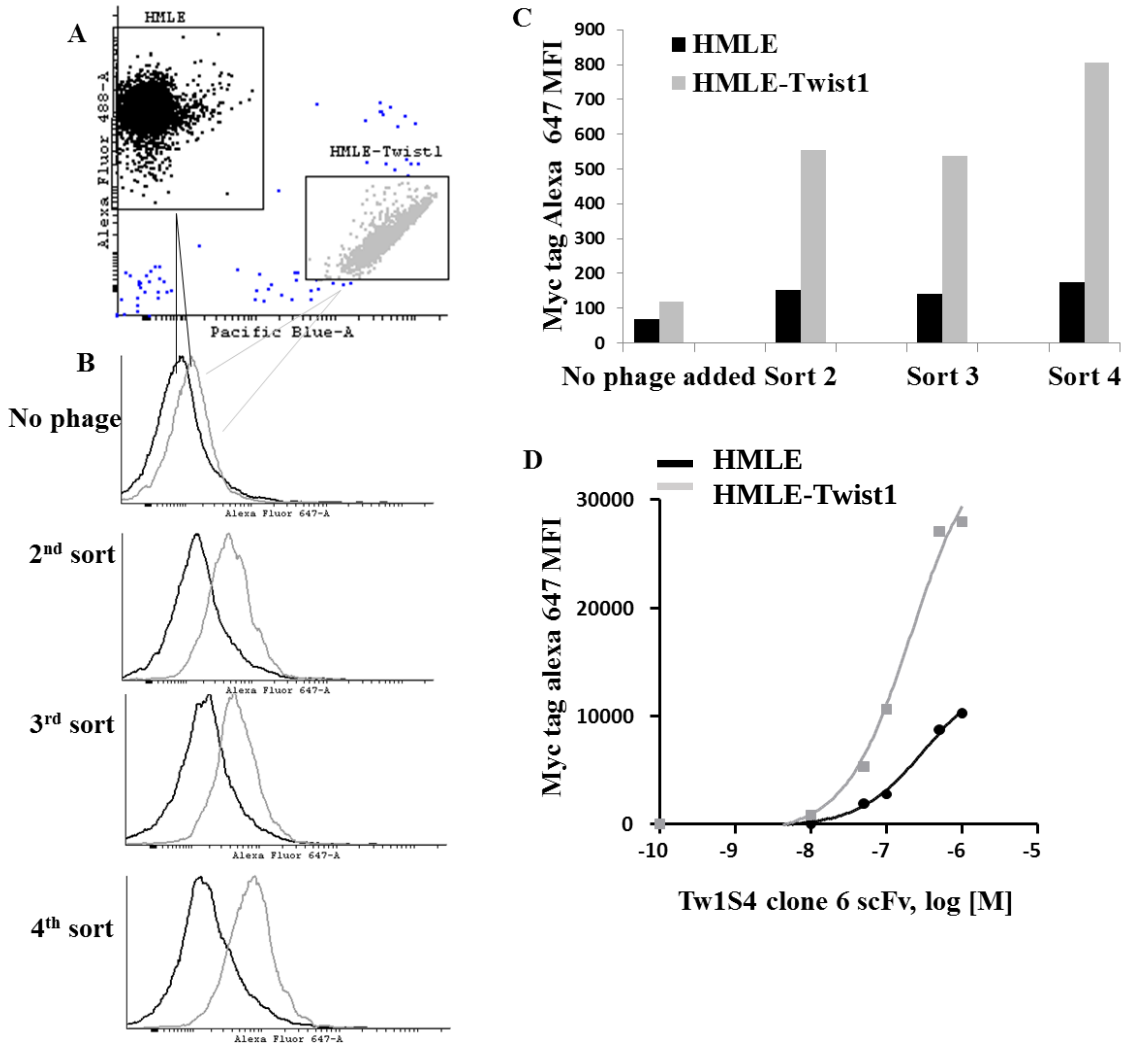

Figure 2. Phage display-based competitive cell panning. (A) Representative dot plot of phage enrichment experiment. HMLE cells were labeled with CFSE green fluorescent viability dye while Twist1 cells were labeled with Calcein violet in separate tubes, washed, and mixed at a 1:1 ratio. 10^9 phage from sorted sub-libraries were added to the cell mixture and incubated with agitation for 30 min at 4 C. Cells were subsequently washed and labeled with an antibody recognizing the C-Myc epitope tag of phage displaying scFv, followed by secondary Alexa-fluor 647 conjugate. (B, panels 1-4) HMLE and Twist1 cells were discriminated based on fluorescent labeling scheme in A. Each cell population was subsequently analyzed for C-Myc-Alexa 647 fluorescence intensity to determine relative binding of polyclonal phage sub-libraries (C) Graphical depiction of data in B. (D) Clone

6 scFv was identified as selective binder to HMLE-Twist1 cells (squares) relative to HMLE (circles), hereafter referred to as Tw1S4_6.

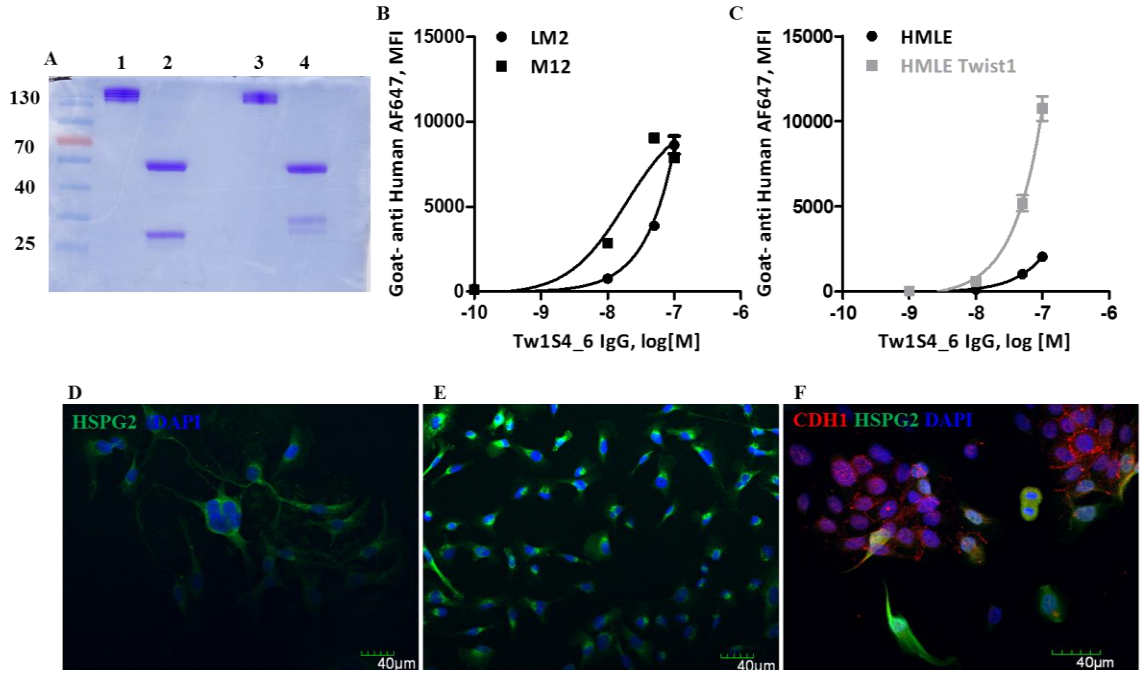

Figure 3. Tw1S4_6 scFv reformatting to human IgG (A) Coomassie stained acrylamide gel resolution. Variable regions of Tw1S4_6 scFv were subcloned into pFuse2ss vectors expressing constant regions of heavy and light chain human IgG1. The resulting heavy and light chain constructs were cotransfected into Expi293 suspension cells for recombinant antibody production. Lanes 1-2 represent isotype control human IgG1 under non-reducing (1) or reducing (2) conditions. Lanes 3-4 represent Tw1S4_6 reformatted IgG under non-reducing (3) or reducing (4) conditions. (B) Confirmation of Tw1S4_6 selective binding to HMLE-Twist1 cells is retained in IgG format. (C) Binding titration curves for Tw1S4_6 IgG to metastatic breast cancer cell line LM2, and melanoma cell line M12. (D-E) Immunofluorescence staining of LM2 and M12 cells, respectively, with commercial HSPG2 antibody A7L6. Scale bar = 40 µM. (F) Immunofluorescence staining of mixed phenotype HMLE cells with commercial HSPG2 antibody, and antibody recognizing E-Cadherin (CDH1).

Reformatting of Tw1S4_6 scFv to human IgG1 was accomplished via PCR amplification of V_H and V_L and subsequent sub-cloning of the variable domains into pFuse2ss vectors. The vector system consists of separate constructs expressing constant

domains of heavy and light chain. Following sequence verification, the full length heavy and light chain constructs representing humanized Tw1S4_6 IgG are co-transfected into Expi293 suspension adapted HEK cells. Subsequent affinity based purification yields a pure IgG product as determined by PAGE analysis (Figure 3A). To insure that the selective binding of Tw1S4_6, now in IgG format, is maintained, flow cytometry based analysis of binding to HMLE and HMLE-Twist1 cells was employed to confirm that IgG formatting retains selective binding capacity (Figure 3B). To elucidate the target cell surface antigen bound by Tw1S4_6, HMLE Twist1 cell lysates were passed over immobilized Tw1S4_6, in scFv format. Acryalmide gel resolution of heat denatured scFv-antigen complex revealed a single, high molecular weight antigen co-eluting with Tw1S4_6 scFv (Figure 4A – target band). Trypic digestion of the excised antigen band, followed by MS/MS based peptide identification identified two separate peptides that correspond to sequence within Heparan sulfate proteoglycan 2 (Figure 4B).

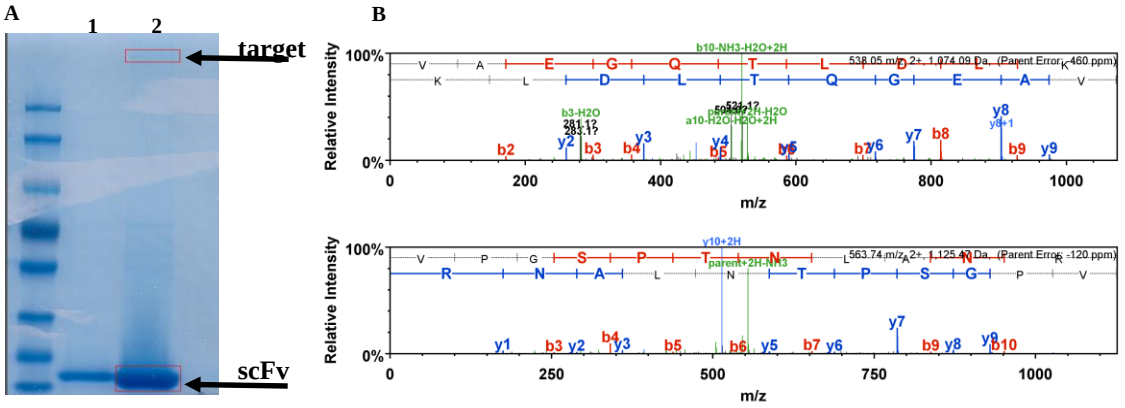

Figure 4. Tw1S4_6 scFv target deconvolution (A) Coomassie staining of acrylamide gel resolved antigen pull down. Tw1S4_6 was immobilized on IMAC resin. Solubilized HMLE-Twist1 cell lysate was applied to Tw1S4_6 scFv and washed extensively in PBS containing 20 mM imidazole. Lane 1 represents an aliquot of final wash fraction. Lane 2 represents elution fraction. (B) In gel tryptic digestion was performed prior to MS/MS. The

fragmentation pattern of two tryptic digest peptides from target band in (A) confirm HSPG2 as cognate target of Tw1S4_6 scFv.

HSPG2 consists of five distinct domains, each bearing unique structural features including several interspersed glycosylation sites. Linear epitope mapping was employed to further elucidate the binding region of Tw1S4_6 in IgG format, to HSPG2. The epitope mapping approach used linear HSPG2 amino acid sequence in 20 mer peptide fragments, each having an overlap of 16 amino acids. Tw1S4_6 binding was observed above background levels throughout linearized HSPG2, indicating that the epitope recognized by Tw1S4_6 is likely discontinuous, or represented by a unique glycosylation profile that linear epitope mapping fails to capture (Figure 5A). In the epitope mapping experiment, several pockets of concentrated binding were observed at N-terminal residues <500, and C-terminal residues >3800. These regions contain the first and fifth domains of HSPG2, respectively, and are sites known to contain high molecular weight heparan sulfate modifications. Although the mapping of Tw1S4_6 binding to HSPG2 proved inconclusive, we chose to focus further on the relative extent of Tw1S4_6 binding within the first and fifth domains of HSPG2. Recombinant HSPG2 domain 1 (HSPG2D1) was expressed and purified as previously reported[46], with HSPG2D5 being available commercially. An indirect ELISA was used to determine Tw1S4_6 IgG binding to HSPG2D1 relative to an isotype human IgG, thus demonstrating a specific binding event occurring within HSPG2D1 (Figure 5B). The same ELISA experiment comparing equimolar Tw1S4_6 IgG binding to immobilized HSPG2D1 and D5 provides further evidence that the epitope appears to be contained within domain 1 (Figure 5C).

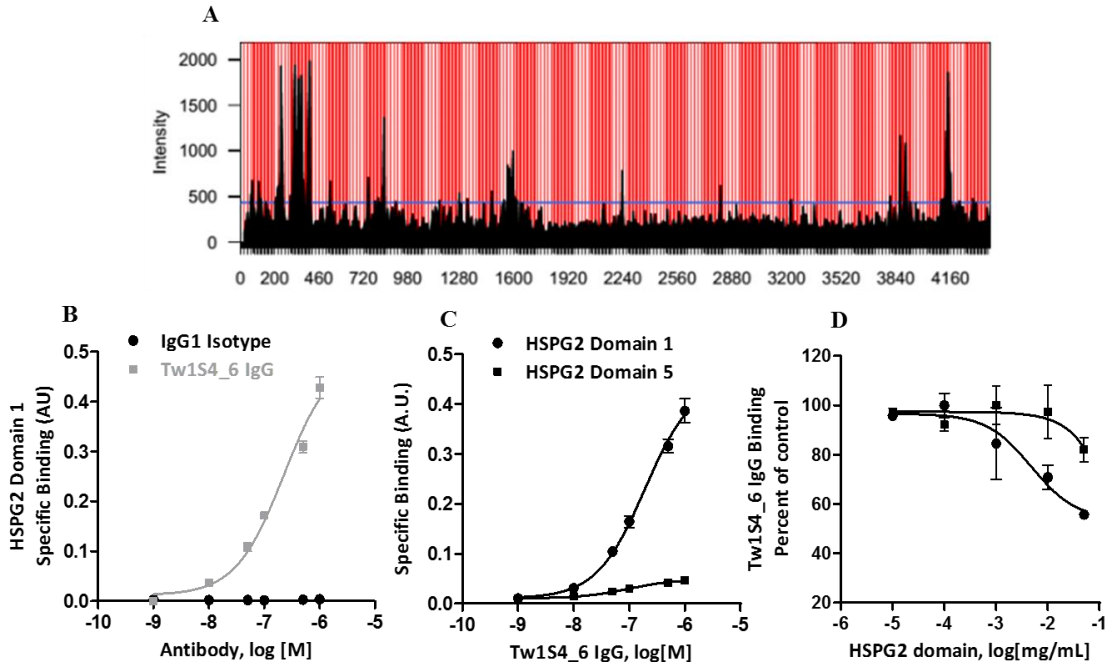

Figure 5 Tw1S4_6 Epitope mapping. (A) A linear epitope mapping strategy was employed. The epitope mapping used linear HSPG2 amino acid sequence in 20-mer peptide fragments, each having an overlap of 16 amino acids. Tw1S4_6 binding site was identified in a high-throughput ELISA format. (B) ELISA showing Tw1S4_6 IgG binds to an epitope contained within the first 247 amino acids of HSPG2. N-terminal HSPG2 (HSPG2 Domain 1) was immobilized on ELISA plates and incubated with the indicated concentration of Tw1S4_6 IgG. Equimolar concentration of isotype human IgG1 was used as a control **(C)** ELISA demonstrating Tw1S4_6 IgG selectively binds HSPG2 domain 1, relative to domain 5. **(E)** Competitive inhibition of Tw1S4_6 IgG binding to LM2 cells with increasing concentrations of soluble HSPG2 domain 1 proteoglycan

Our initial extension to relevant *in vitro* models of cancer focused on cell lines bearing predisposition to invasion and metastasis. Binding titration curves for Tw1S4_6 IgG were generated for two metastatic cell lines; breast to lung metastatic LM2, and melanoma to brain metastatic M12 cell lines. LM2 is an MDA-MB-231 derivative that is derived from ex vivo expanded spontaneous lung metastases. LM2 cells are highly efficient at seeding lung metastasis[53]. M12 is a primary cell line derived from a melanoma brain metastasis.

The inclusion of metastatic melanoma cell line is based on previous studies implicating sulfated proteoglycans as melanoma tumor antigens. Examples include monoclonal antibody development via active immunization with melanoma cell lysates which led to the identification of chondroitin sulfate proteoglycan (CSPG) as a melanoma tumor antigen[54]. Also termed HMW-MAA, antibodies against CSPG have been used to detect melanoma patient CTCs[55,56]. HMW-MAA has also been identified as a marker of melanoma tumor initiating cells. Immunotherapy strategies employing adoptive transfer of T-cells expressing HMW-MAA targeted CARs results in sustained remission of melanoma in mouse models[57]. Regarding HSPG2 specifically, elevated expression has been observed in invasive melanomas, notably those displaying metastasis to brain[58], lending support to our inclusion of M12 cell line in the current study. Confirmation of HSPG2 expression in LM2 and M12 cells was dermined via immunocytochemistry using a commercially available HSPG2 antibody (Figure 3D-E). Dual staining of mixed phenotype HMLE cells with commercial antibodies recognizing E-Cadherin and HSPG2 confirm expression pattern of HSPG2 is confined to the mesenchymal, E-Cadherin negative cell population (Figure 3F). These results validate HSPG2 as a potential biomarker both of EMT transitioned, and metastatically predisposed carcinoma cell lines. Competitive inhibition of Tw1S4_6 IgG binding to LM2 cells with increasing soluble HSPG2D1 and D5 peptides confirms the presence of the antibody epitope within HSPG2D1, on the LM2 cell surface. Binding of Tw1S4_6 IgG to LM2 cells was impaired by approx. 40% at the highest HSPG2D1 concentration utilized (Figure 5D). These results suggest that a consensus

sequence pattern or glycosylation event that is contained within known glycosylation domains of HSPG2, is being recognized by Tw1S4_6.

We next established *in vivo* models to evaluate the utility of Tw1S4_6 IgG as an immunodetection reagent for EMT transitioned CTCs. Xenograft models of LM2 and M12 were generated in Balb/c nude mice and allowed to reach 500mm^3. Peripheral blood was collected at the study endpoint by cardiac puncture, and peripheral blood mononuclear cells (PBMCs) were isolated via ficoll density gradient centrifugation, followed by RBC lysis, prior to antibody staining. The murine monoclonal antibody VU-1D9, derived from a hybridoma clone against human EpCAM, was used as the EpCAM CTC detection antibody. This antibody is utilized in the Veridex CellSearch platform as part of the immunomagnetic enrichment step. The version VU-1D9 EpCAM antibody employed in this study was a pacific blue violet dye conjugate, owing to use of FACS cell sorting equipment to perform the fluidics function. A Dylight647 labelled Tw1S4_6 IgG was generated as described in the methods. Thus, direct dye conjugate antibodies targeting EpCAM and HSPG2 (Tw1S4_6 IgG) were employed to discriminate CTC populations. Also included in the staining panel was PE conjugated antibody against murine CD45. Equimolar concentration of EpCAM and Tw1S4_6 IgG (100nM) were incubated with PBMCs to insure consistency of fluorescence intensity within positively labelled cell populations. CD45+ events, representing murine leukocytes, are excluded from the populations analyzed for EpCAM and Tw1S4_6 staining, with PBMCs derived from non-tumor bearing mice of the same strain serving as negative controls. Negative control PBMCs co-stained with CD45, EpCAM, and Tw1S4_6 antibodies were used to establish

the cell sorting gates for EpCAM and Tw1S4_6 positive events within tumor bearing mice as follows; Within the $CD45^{low/-}$ events of PBMCs from non-tumor bearing mice (Figure 6C – poly 14 population), non specific staining events for EpCAM (Figure 6D, x-axis) or Tw1S4_6 (Figure 6D, y-axis) are displayed, and used subsequently to define potential positive cells in tumor bearing mice, thereby avoiding the potential sorting of false positives. Within PBMCs from LM2 tumor bearing mice (Figure 6E), events staining positive for both Tw1S4_6 and EpCAM were observed. Notably, populations were singly positive, indicating mutually exclusive marker expression. Also of note is the greater abundance of Tw1S4_6 positive events relative to EpCAM (98 vs. 7 per 10,000 events) In CTCs from LM2 tumors. CTCs from the M12 model were less numerous, yet distinct single positive CTCs were detectable (Figure 6F - 5 vs. 2 per 10,000 events).

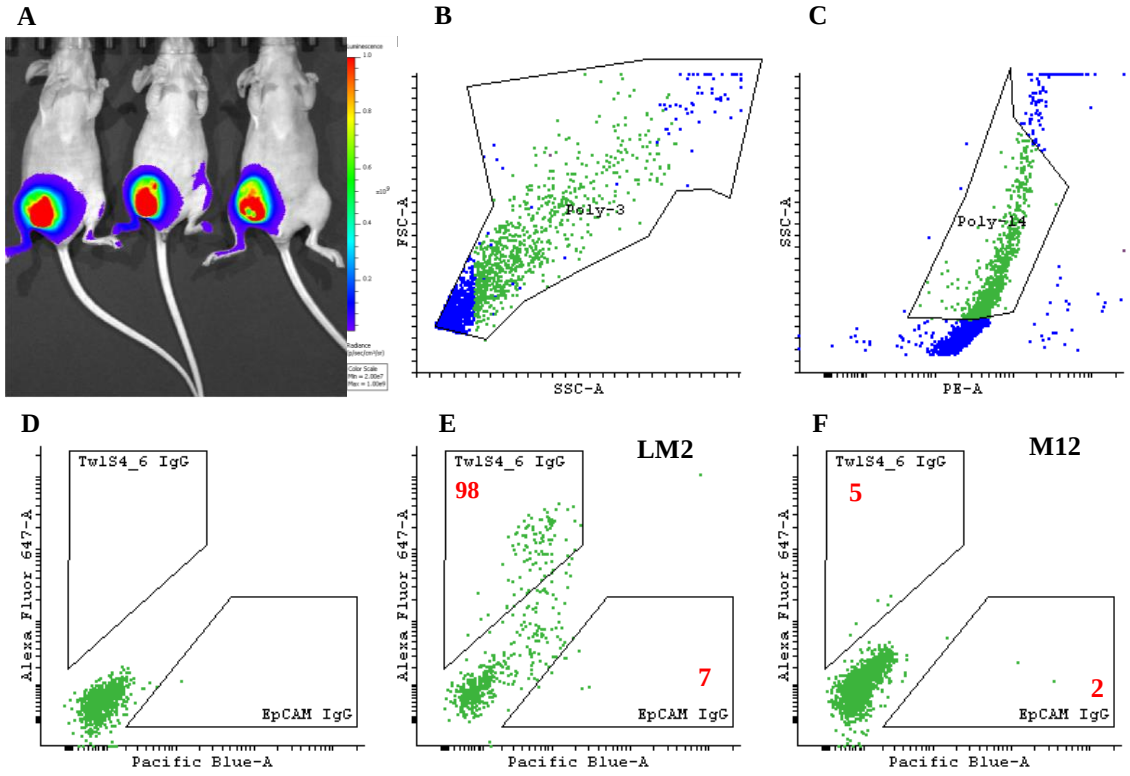

Figure 6 *in vivo* Circulating tumor cell model. (A) Bioluminescence imaging of orthotopic LM2 mammary tumor model. Cells were grafted orthotopically to the right flank mammary pad. Following 6 weeks of tumor growth, animals were sacrificed and whole peripheral blood was collected into EDTA vacutubes via cardiac puncture. Density gradient centrifugation over Ficoll paque was used to isolate PBMCs. Following RBC lysis, cells were stained with CD45–PE labeled antibody targeting mouse leukocytes, Pac blue labeled anti-EpCAM IgG, and Dylight 647 labeled Tw1S4_6 IgG. (B-C) FACS gating scheme. (D) PBMCs from non-tumor bearing mice were stained with CD45, EpCAM and TwtS4_6 antibodies. $CD45^{low}$ cells (gated population from panel C) are displayed on a secondary plot to discriminate EpCAM and Tw1S4_6 labelled cells. Panel D demonstrates the absence of false positive events in non-tumor bearing mice. (E) 10,000 events from CD45 low population of PBMCs from LM2 bearing mice and (F) M12 tumor bearing mice, stained for EpCAM and Tw1S4_6 antibodies.

To confirm the phenotype of these two populations, sorted CTCs from the LM2 tumor model were plated under adherent conditions, followed by immunofluorescence based detection of EpCAM presence in EpCAM sorted events, and corresponding absence of

HSPG2 (Figure 7 top panel). Tw1S4_6 positive CTCs displayed an absence of EpCAM expression, but were positive for HSPG2 as expected (Figure 7 bottom panel). Commercial HSPG2 antibody was used to determine expression in microscopy experiments, thus cross-validating HSPG2 as a relevant biomarker of EMT transitioned CTCs. The M12 tumor model did not yield a sufficient quantity of CTCs to perform post capture immunofluorescent characterization. We next utilized two breast cancer patient derived xenograft (PDX) models to evaluate the potential existence of Tw1S4_6 positive CTC events. These models are serially transplantable graft models taken directly from biopsied breast tumors that faithfully reproduce key aspects of tumorigenesis[59]. PBMCs from two PDX models were isolated as described for the LM2 and M12 xenograft models, and stained with the same panel of antibodies. Again non-tumor bearing mouse PBMCs were used to establish the EpCAM and Tw1S4_6 sorting gates within the $CD45^{low/-}$ population, and rule out false positive events (Figure 8B). PDX model TM91 displayed a roughly 10 fold elevated number of Tw1S4_6 labelled CTCs relative to EpCAM (Figure 8C - 34 vs. 3 per 10,000 events). PDX model TM96 had two-fold higher Tw1S4_6 labelled CTCs relative to EpCAM (Figure 8D – 12 vs. 6 CTCs per 10,000 events). Subsequent to cell sorting, sorted populations failed to adhere to microscopy slides, precluding the analysis of marker expression that was determined for the LM2 graft model.

EpCAM Captured CTCs

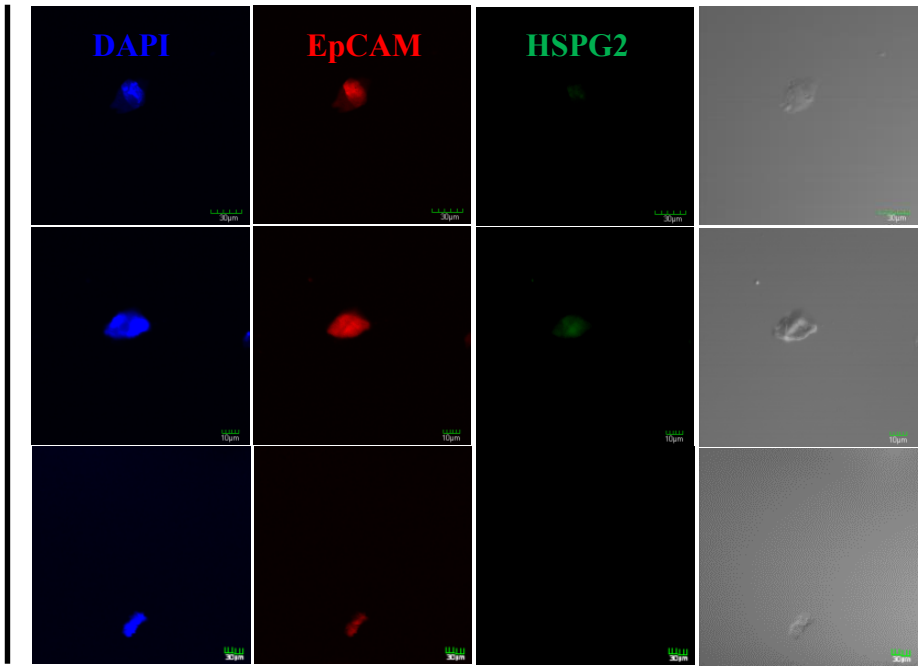

Tw1S4_6 Captured CTCs

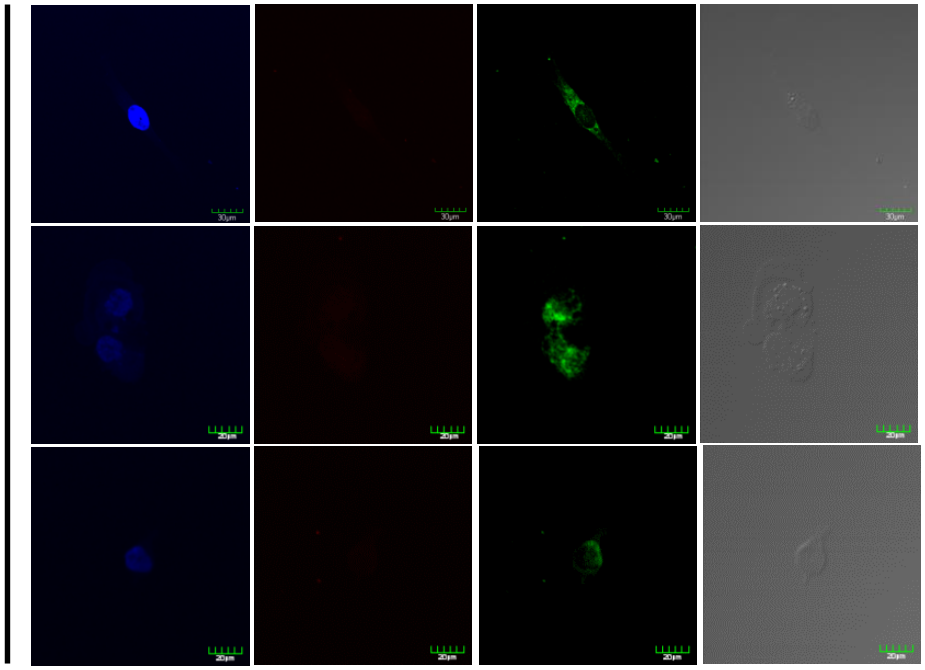

Figure 7 Immunofluorescence staining of sorted circulating tumor cells from LM2 tumors. Cells captured by EpCAM IgG (top panel) or Tw1S4 IgG (bottom panel) were assayed for coexpression of EpCAM and HSPG2 using commercial antibodies. Nuclear counterstaining was performed with DAPI. Images were acquired on an Olympus FluoView FV1000 upright confocal microscope under 40x oil immersion objective

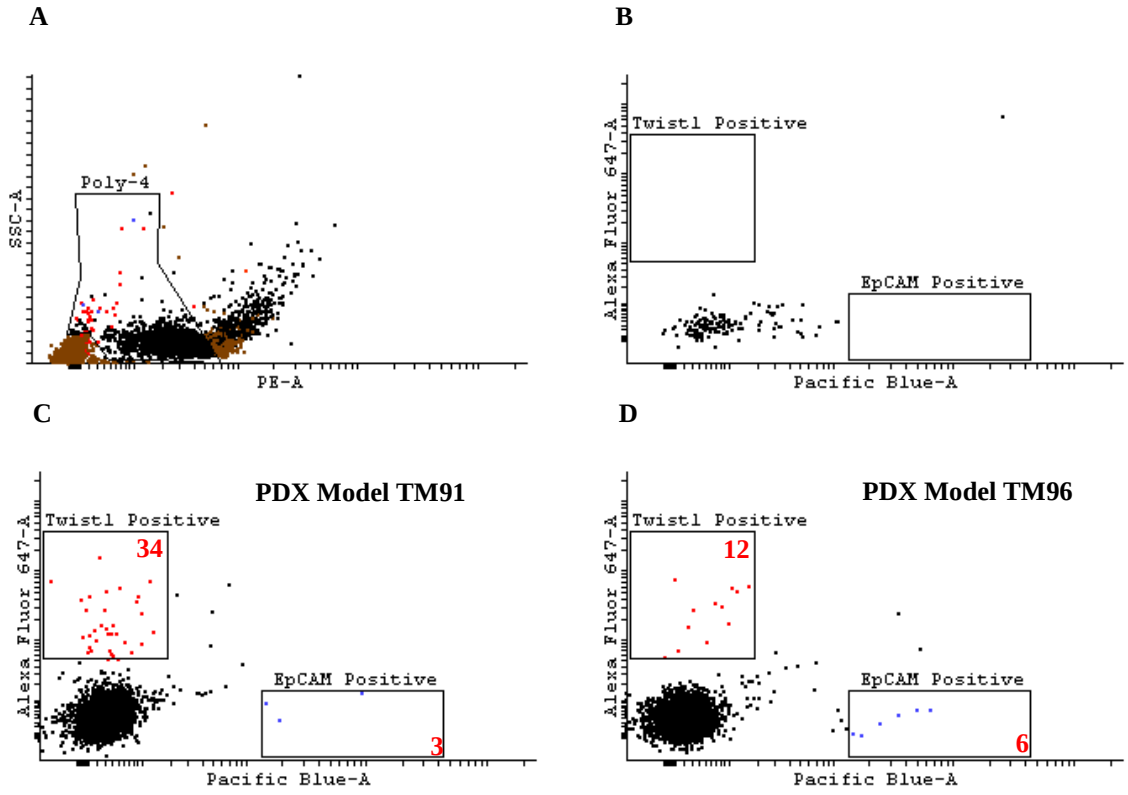

Figure 8 Patient derived tumor xenograft (PDX) models - circulating tumor cell analysis. (A-B) FACS gating scheme. (A) Mouse CD45-PE antibody was used to discriminate CD45 low cells. Poly 4 gate is displayed on a secondary plot to determine EpCAM and Tw1S4_6 positive cells within CD45 low events. (B) PBMCs from non-tumor bearing mice were stained with CD45, EpCAM and TwtS4_6 antibodies. Panel B confirms the absence of false positive events in non-tumor bearing mice. (E) 10,000 events from $CD45^{low}$ population of PBMCs from TM91 bearing mice (C) and TM96 tumor bearing mice (D), stained for EpCAM and Tw1S4_6 antibodies.

To this point, we have demonstrated the presence of HSPG2 within EMT transitioned CTCs from *in vivo* breast cancer and melanoma models, with detection occurring via a recombinant human antibody derived from a phage display based phenotype screening

approach. The results presented thus far suggest HSPG2 as a biomarker of cancer cell invasiveness. We next determined HSPG2 expression, as detected by Tw1S4_6 IgG, in tumor tissue array panels that capture both the primary tumor stage as well as metastases to determine whether HSPG2 persists as a metastatic biomarker beyond initial dissemination as CTCs. We first characterized the binding capacity of Tw1S4_6 IgG in breast tumor and melanoma biopsies by immunohistochemistry, using human cancer tissue array panels. An interesting trend in the localization of Tw1S4_6 staining in primary breast tumors was observed. Normal adjacent breast tissue stained positive exclusively in the stromal compartment, wheras stage 2 and 3 invasive breast carcinomas revealed a strong staining of malignant intraductal epithelium (Figure 9 B-C), and within cells invading the surrounding stroma (Figure 9C – Arrow). Lack of staining within the same tissue panel with an Isotype human IgG confirms that Tw1S4_6 staining owes to a specific binding event (Figure 9 D-F). The staining profile of Tw1S4_6 IgG in breast cancer derived liver, lung and lymphatic metastases is confined to the malignant cell surface (Figure 9 G-I), with some detectable stromal expression in the lymphatic metastasis (Figure 9 I). The expression profile of Tw1S4_6 IgG bound HSPG2 is somewhat distinct in melanoma, where stromal staining is observed in normal representative skin (Figure 10A), with pronounced cellular and stromal staining throughout malignant melanoma tissue (Figure 10B), and confined predominately to the malignant cells of melanoma derived brain metastases (Figure 10C).

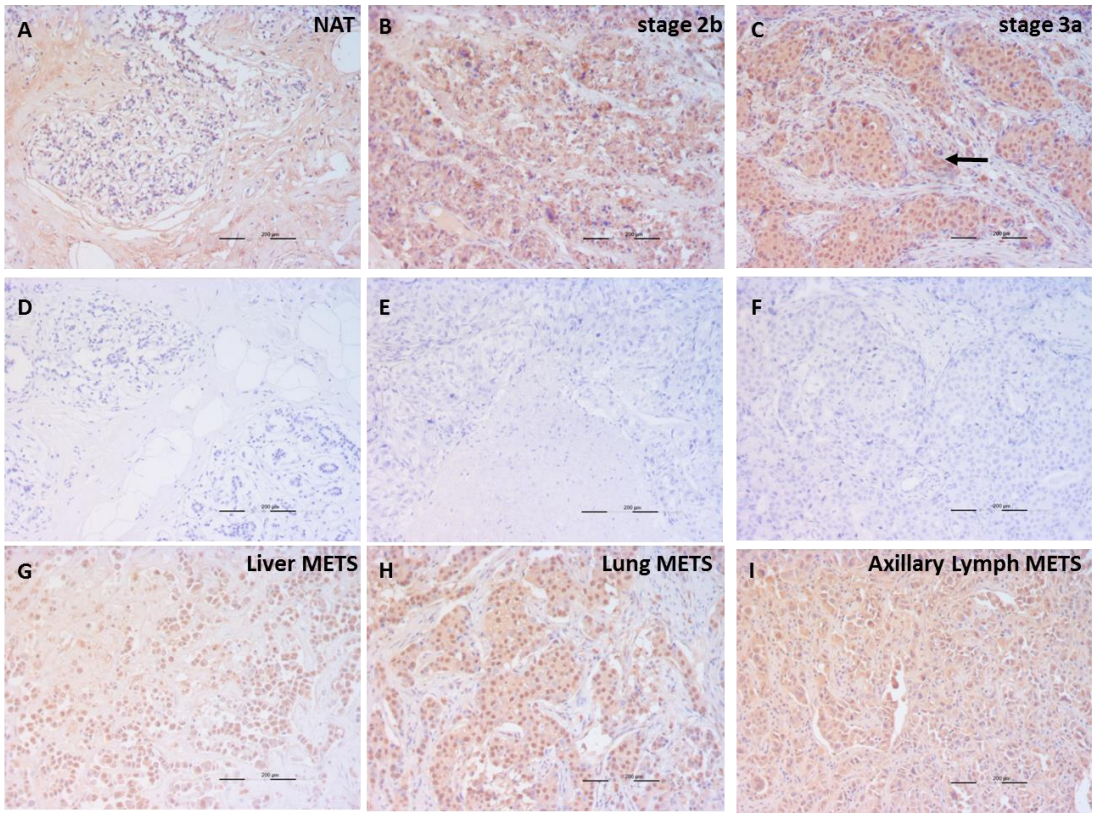

Figure 9 Immunohistochemistry staining of breast cancer tissue microarray. Tw1S4_6 and isotype IgG1 staining of breast tumor tissue array. (A-C) Staining profile of Tw1S4_6 IgG in (A) normal adjacent tissue, and (B-C) primary breast tumor biopsies at stages 2b and 3a, using TNM criteria. (D-F) Staining profile of isotype human IgG1 of the tumor biopsies in (A-C). (G-I) Breast cancer metastases to (G) liver, (H) lung, and (I) auxillary lymph node stain positive for Tw1S4_6 IgG. Scale bar = 100 μM

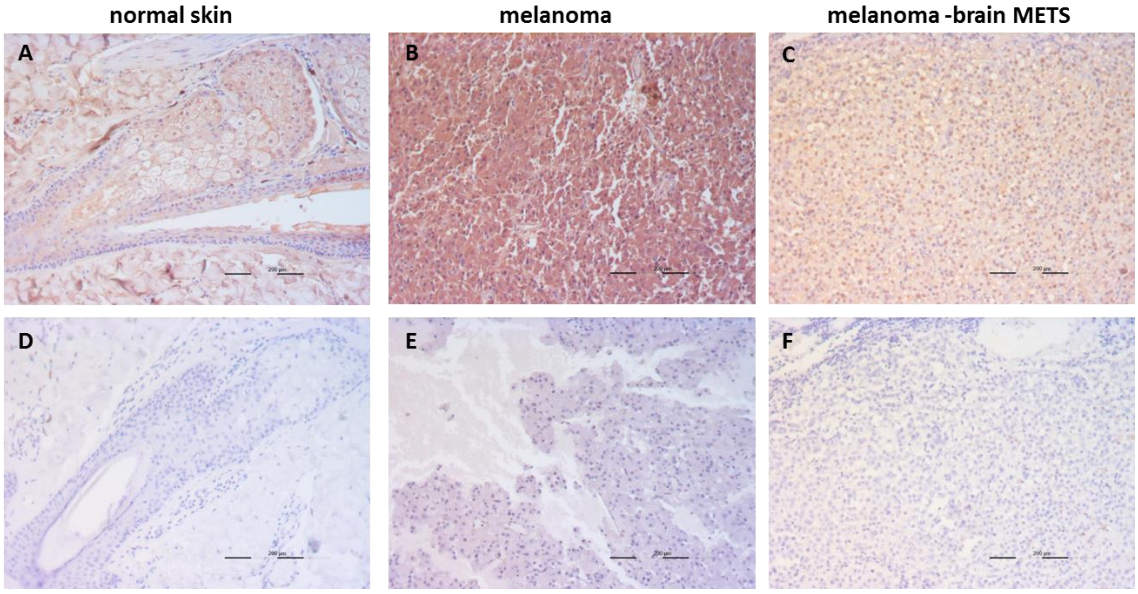

Figure 10. Immunohistochemistry staining of melanoma tissue microarray. (A-C) staining profile of Tw1S4_6 IgG in (A) normal skin tissue, (B) primary melanoma, and (C) metastasis to cerebrum. (D-F) Staining profile of Isotype human IgG1 of the tumor biopsies in (A-C). Scale bar = 100 μM

Discussion

EMT is established as rate limiting to cancer dissemination from the primary tumor. Being dictated by heterotypic signals from the primary tumor microenvironment, EMT has a transient influence on the metastatic cascade, to the point of blood borne dissemination. The working theory is that EMT transitioned cells would undergo the reverse mesenchymal to epithelial transition (MET) upon homing to distant tissue/lymph node, owing to loss of heterotypic, EMT inducing signals from the primary tumor[60]. The phenomena of EMT to MET plasticity has recently been observed in patient derived xenograft (PDX) models of breast cancer, where cells within micrometastatic lesions express markers of stemness, EMT and dormancy genes, while much larger, macrometastatic lesions express luminal

differentiation and proliferation genes[61]. Thus, the EMT phenotype harbors genes of metastatic virulence that exist transiently on both disseminating cancer cells in the cirulation as well as on extravasated cells within early micrometastatic lesions. Uncovering unique EMT cell antigens will lead to new avanues in the therapeutic management of metastasis.

The cell phenotype based screening approach outlined above demonstrates the ability to identify cell type specific antigens in the context of mixed phenotype cell populations. The inclusion of the HMLE isogenic cell line pair in the competition screen identified a unique and phenotype specific epitope within HSPG2. Importantly, the identification of a phenotype specific epitope, as outlined in this work, would not be possible using conventional target based screening approaches. The dramatic shift in HSPG2 localization from the stromal compartment in normal adjacent tissue, to the malignant cell compartment in invasive carcinoma raises interesting questions related to the role of HSPG2 in carcinoma progression. In pancreatic adenocarcinoma, progressive loss of stromal HSPG2 expression correlates to disease progression[62]. Similarly, stromal HSPG2 expression is detectable in ovarian tumors, yet is notably absent at the tumor invasive front[63]. In oral SCC, HSPG2 core protein levels increase in both differentiated and undifferentiated tumors, yet staining with antibodies specific to heparan sulfate chains does not reveal a corresponding increase[64], suggesting extensive enzymatic processing of the heparan sulfate chains is occurring within the tumor microenvironment. Enzymatic processing of proteoglycans within the tumor microenvironment has a well established role in cancer progression[65]. Heparanase (HSPE), found in secreted form and affiliated with the

malignant epithelial cell surface, is known to facilitate invasion and metastatic capacity of melanoma cell lines[66]. The causal role for HSPE in invasion/metastasis lies in its ability to cleave heparan sulfate chains from matrix and cell surface proteoglycans, liberating growth factors previously tethered to the glycosylation domains to participate in paracrine signaling. Indeed, the confined intraductal epithelial expression profile of HSPE in breast cancers that have been previously reported mirror that of HSPG2 expression detected by Tw1S4_6 IgG in the current study[67]. HSPE expression is also confined to malignant cells within pancreatic cancer derived metastatic lesions, and absent in the surrounding stroma[68]. Finally, HSPE has been used previously as a biomarker within a multi-parameter cell sorting protocol, to isolate CTCs from breast cancer patients that are competent to seed brain metastases[26]. We therefore hypothesize, on the basis of the current data set and previous literature precedent, that the epitope recognized by Tw1S4_6 IgG within HSPG2 domain 1 is likely revealed following HSPE dependent enzymatic processing on the surface of disseminating cancer cells.

Although advances in targeted therapy options have been made recently for the management of metastatic breast cancer, the primary treatment goal remains palliative care. Elucidating stage specific molecular markers of cancer dissemination will both aid in diagnosis, and serve as starting points for the development of new therapy options, in metastatic cancer. The identification of HSPG2 as a unique EMT cell antigen represents a potential new point of focus in the circulating tumor cell diagnostic field, given the need to precisely identify the full phenotypic complement of CTCs within patients. From a therapeutic perspective, the development of fully human antibodies that can selectively

discriminate the EMT phenotype has the potential to target cancer cells at the invasive front of primary tumors as well as cells contained within early micrometastatic lesions, two critical nodes of the metastatic cascade.

SECTION 1: DIAGNOSTIC ANTIBODY DEVELOPMENT

CHAPTER 3

DEVELOPMENT OF DIABODIES FROM PHAGE DISPLAY BASED PHENOTYPE SCREENS; APPLICATION TO THE DETECTION OF EpCAM NEGATIVE CIRCULATING TUMOR CELLS

Summary

Circulating tumor cell detection has emerged as an important biomarker of cancer dissemination that can aid in diagnosis. The future of CTC detection as a routine diagnostic platform hinges on the ability to use patient specific information, derived from such tools, to inform patient management. Molecular and functional characterization of circulating tumor cells (CTCs) isolated over the course of therapy can be used to predict drug susceptibility in an individual patient as the tumors acquire new mutations and develop resistance. Since CTCs are obtained through a routine blood draw, these cells may thus serve as an easily accessible source of markers for monitoring treatment effectiveness and for guiding treatment decisions. Currently available CTC detection systems fail to capture and/or distinguish a subset of CTCs that may be more metastatically virulent. We report here the development of bivalent scFv, termed diabodies, that are capable of identifying this important sub-population of CTCs that are EpCAM negative. The utility of diabodies in CTC detection lies in the potential to circumvent non-specific capture of unwanted cell types from patient blood samples that arises due to immune cell interaction with the antibody Fc domain. The absence of Fc domain in diabodies provides a potentially

advantageous route to avoiding false positive events being enumerated in existing CTC detection platforms.

Introduction

Circulating tumor cell (CTC) detection has emerged in recent years as a potential point of care technology for detecting disseminating tumor cells in real time. Meta-analysis of clinical datasets employing existing technologies to enumerate CTCs has confirmed the poor prognosis that is conferred upon patients with evidence of CTCs in the systemic circulation[69]. CellSearch [JP1]is the only current device approved by the FDA for CTC enumeration. Cell Search is not, however, currently recommended for use as a molecular marker in any form of solid tumor by either the American Society of Clinical Oncology (ASCO) or the National Comprehensive Cancer Network (NCCN)[70,71]. The current utility of CellSearch is to aid in prognosis of metastatic breast, colon and prostate cancer patients[72], and is used sporadically at the discretion of the clinician. The overarching goal of the CTC enumeration field, and a prerequisite for its recommendation for use, is to extend the utility of this technology beyond prognosis and into informing patient management. In the context of solid tumor metastasis, rapid decision making in terms of therapy management is critical. Thus, the capture and subsequent characterization of CTCs will represent a critical diagnostic criterion in cancer patient management in the near future. Further refinement of existing technologies like CellSearch to include parameters such as cell phenotype will be critical.

The major point of concern regarding CellSearch methodology is the dependence on immunomagnetic capture of epithelial cells via antibody-based recognition of Epithelial

cell adhesion molecule (EpCAM) expression by CTCs. The presence of phenotypic plasticity within disseminating cancer cells, which manifests as a loss of epithelial surface antigen expression has emerged recently as an important finding that calls the Cell Search methodology in to question[73]. As a result, a plethora of novel fluidics and immunomagnetic CTC capture platforms have emerged to attempt to circumvent this issue[74]. A recurring theme within emerging CTC capture platforms is the presence of leukocyte contamination within captured cell populations, which can restrict downstream molecular analysis of CTCs, notably phenotyping and genetic analysis[75,76]. Regarding gene expression profiling of CTCs in particular, multiplex RT-PCR methods have demonstrated the ability to detect epithelial and cancer associated genes within CellSearch captured CTCs[77]. The aforementioned study, in particular, effectively captures the promise and challenges in the CTC enumeration field, with the salient observations that can be drawn from it as follows. First, the presence of leukocytes as the predominant cell type recovered from a CTC capture device does not preclude CTC gene detection; CTCs are detectable when present at >1,000 fold dilution relative to leukocytes, owing to the specificity of PCR. Second, and of critical importance to the future viability of CTC capture platforms as a clinically relevant tool, is that gene expression or sequencing information derived from a population averaging approach will fail to capture gene expression and sequencing variability that is present at the single cell level.

The analysis of individual CTCs has subsequently proven of enormous value in revealing underlying causes of therapy resistance in cancer patients. For example, the antigen independent CTC capture platform known as CTC ichip, developed by Toner and

colleagues, has successfully identified androgen receptor splice variants from single CTC-RNA sequencing data as being over-represented in castration resistant prostate cancer patients[78]. The same ichip has been used in metastatic breast cancer patients, to isolate and expand captured CTCs ex vivo. RNA sequencing information was used to generate a gene candidate list that was used to inform, and successfully predict the in vitro efficacy of drug candidates on individual patient cultured CTCs[79].

The CTC ichip technology, and emerging fluidics platforms are expected to capture a substantial share of the projected 12 billion USD CTC diagnostic market. Importantly, evidence of epithelial to mesenchymal transition within captured CTCs is expected to play a large role in predicting disease recurrence, as EMT transitioned CTCs likely contain the more metastatically virulent population of cancer cells in the circulation[80]. Thus, a need for phenotypic characterization of captured CTCs exists, and such characterization methods will likely coalesce with the single cell molecular analysis afforded by the CTC ichip. The implementation of novel fluidics platforms as point of care technologies poses its own unique set of logistical challenges and associated costs. Many, if not all, research hospitals have flow cytometry core facilities for clinical immunology that could in theory circumvent the need to implement new CTC capture platforms. Fluorescence activated cell sorting (FACS) equipment is currently readily available, and offers the advantages of robust cell throughput, multi-color analysis capacity for immunophenotyping, cell size/morphology information, and most importantly, the ability to individually sort viable cells for downstream molecular characterization[81]. Immunodetection of epithelial CTCs has been established through the CellSearch platform. What is currently lacking is an effective

immunocapture reagent for those CTCs that have shed epithelial characteristics. Such an approach could replace the fluidics functionality of CTC ichip and CellSearch. Downstream single cell characterization could then be performed on distinct subsets of CTCs to better inform patient management.

We report here the development of an engineered, bivalent scFv as being capable of discriminating EMT-like CTCs from epithelial CTCs derived from an *in vivo* model of breast cancer metastasis. The cell surface binding partner of our scFv, termed Tw1S4_6, is HSPG2 and was described in detail in Chapter Two. The use of FACS equipment to enumerate both epithelial and mesenchymal like CTCs has the potential to provide a more comprehensive information set than existing CTC capture platforms. Given the ability of FACS analysis to sort cells individually, this approach will offer the advantage of single cell molecular characterization in the future, while offering the potential to avoid unwanted leukocyte contamination due to lack of Fc domain in diabodies.

Methods

Chemicals, reagents and cell lines

Rabbit monoclonal antibodies targeting human E-Cadherin (clone 24E10) and human Vimentin (clone D21H3) were purchased from Cell signaling technologies. Anti-rabbit Fab Alexa Fluor 555 conjugated secondary antibody was used for immunofluorescence detection. Cell lines were fixed in 4% paraformaldehyde, followed by permeabilization with 0.1% Triton-X100. 1000 fold antibody dilutions were used to stain cells according to the manufacturer's protocol. A Zeiss Axiovert 40 CFL fluorescent microscope equipped

with DAPI and Rhodamine (Alexa Fluor 555) emission filters was used for fluorescent microscope image acquisition.

Human mammary epithelial cell lines HMLE, and HMLE stably expressing Twist1 were a generous gift from the lab of Dr. Bob Weinberg. For stable knockdown of HSPG2 (Perlecan) in the HMLE-Twist1 cell line, lentiviral particles expressing shRNA targeting HSPG2, along with lentiviral particles expressing a scramble control shRNA, were purchased from Santa Cruz biotechnology. Viral transduction was performed according to the manufacturer protocol. Stable transformants were selected with 1µg/mL Puromycin for 5 days, and expanded for subsequent experiments. Confirmation of HSPG2 knockdown was determined by flow cytometry. A Biotinylated anti-human HSPG2 antibody was used for cell surface detection, followed streptavidin APC secondary staining.

ScFv linker length engineering

A candidate scFv with the identifier Tw1S4_6, identified previously as being capable of discriminating EMT transitioned mammary epithelial cells, was used as a template for non-covalent dimerization. Tw1S4_6 scFv was identified via a novel cell based biopanning procedure. The scFv sequence was shuttled into pET22b(+) vector as previously described. A panel of PCR primers designed to delete triplicate codons within the $(G_4S)_3$ scFv linker beginning at the second glycine codon within the final (G_4S) repeat, then moving towards N terminus in triplicate codon increments. A total of five linker length reduced constructs were generated. The forward primer hybridized to the N terminal codon of V_L, with reverse orientation primers hybridizing within the linker to generate the appropriate deletion of unwanted sequence. A deletion PCR protocol was then performed using the Phusion high

fidelity site directed mutagenesis kit, according to the manufacturer's protocol (Thermo Fisher). PCR primers are given below:

Tw1S4_6 Forward primer: ACGGACATCCAGATGACCCAGTCT

Tw1S4_6 Reverse Linker 8: ACCTCCGCCTGAACCGCC

Tw1S4_6 Reverse Linker 9: GCCACCTCCGCCTGAACC

Tw1S4_6 Reverse Linker 10: GCTGCCACCTCCGCCTGA

Tw1S4_6 Reverse Linker 11: GCCGCTGCCACCTCCGCC

Tw1S4_6 Reverse Linker 12: ACCGCCGCTGCCACCTCC

PCR cycling conditions consisted of an initial template denaturation at 98°C 30 sec, followed by 25 cycles: 98°C for 5 seconds, 65°C 10 seconds, 72°C 1:30 seconds.

Ligation was performed with vendor supplied T4 DNA ligase according to recommended protocol. Final product was transformed into chemically competent TG1 (Zymo research). DNA sequencing was used to confirm the appropriate linker deletion was present in each construct. Following sequencing, DNA constructs were transformed into BL21(DE3) competent E coli (Promega corp) for soluble production, according to the manufacturer's protocol. The wild-type, full 15 amino acid linker length Tw1S4_6 scFv was transformed into BL21(DE3) previously.

Diabody production

Tw1S4_6 full length scFv, and Tw1S4_6 bearing linker lengths of between 8-12 amino acids were cultured to log phase in 2xTY medium supplemented with 100µg/mL ampicillin, and 1% glucose with shaking at 180rpm, 37C. When the optical density reached 0.4, bacteria were pelleted at 4,000 rpm for 30 minutes, and resuspended in 2xTY medium

containing 100 µg/mL ampicillin and 0.2% glucose. Cultures were incubated with shaking at 30°C until the temperature stabilized. At this point, 0.4 mM IPTG was added to the cultures, with continued shaking for 3 hours at 30°C. After induction, bacteria were pelleted at 4,000 rpm for 30 minutes. Periplasmic extraction and immobilized metal affinity resin were used to purify the resulting product, according to the methods reported in Chapter two.

In vivo circulating tumor cell model

LM2 cells were grafted orthotopically in Balb/c nude mice. Four weeks after tumor induction, mice were euthanized, and blood collected by cardiac puncture. Following density gradient centrifugation to isolate mononuclear cells (PBMCs) and potential circulating tumor cells, erythrocytes were lysed, and samples from animals bearing LM2 tumors were pooled and divided into three equal fractions for labeling with 50 nM Alexa-647 labeled diabody or Pacific blue labeled IgG EpCAM antibody. Non-tumor bearing mouse blood was collected for use as controls.

Results

The method for generation of EMT targeted scFv was detailed in Chapter Two. Fluorescent viability dyes were employed to sort HMLE-Twist1 target cells from mixed populations containing HMLE cells. Following incubation with phage library, HMLE-Twist1 cells were sorted from the mixed cell population, and target bound phage were eluted by trypsin cleavage. This procedure led to the identification of a lead candidate scFv, termed Tw1S4_6 scFv that was capable of selective binding to HMLE-Twist1 cells relative to the isogenic control HMLE. This isogenic cell line pair was characterized by

immunofluorescence microscopy for expression of epithelial marker E-Cadherin and Vimentin in chapter one.

The monovalent binding affinity of Tw1S4_6 was deemed insufficient to proceed with subsequent experiments. To improve the apparent binding affinity of scFv, one strategy frequently employed is to facilitate non-covalent dimerization via reducing the linker length such that the scFv cannot form the appropriate variable domain fold. Reduced linker length scFv undergo a phenomena known as 'domain swapping', in which the scFv homo-dimerizes with an equivalent scFv monomer to form a dimer, termed a diabody. Higher order scFv multimers can form as a direct function of linker length. Previous work was undertaken to give a precise definition of linker length influence on scFv multimerization[82]. However given this work is solely based upon the NC10 anti-neuraminidase scFv, it is more useful in providing a theoretical guidance when constructing multivalent scFvs. These reports and others suggest that linker lengths greater than 12 amino acids facilitate the natural formation of a monovalent variable domain, whereas reducing the linker length to less than 12 will result in some degree of multimerization, with the precise transition between multimers being dependent on the individual scFv under investigation[83]. The introduction of cysteine residues into the linker can promote disulfide linkage of scFv monomers to generate covalent diabodies that offer the further advantage of site specific conjugation to facilitate prolonged circulation half-life (PEGylation) or delivery of radiocontrast/fluorescent probes[84], thus providing a useful antibody scaffold for preclinical imaging, diagnostics, and therapeutic development. We developed a deletion PCR protocol to engineer the linker length of Tw1S4_6 scFv. Our initial hypothesis was that linker

lengths of between 8 and 12 amino acids should capture the monomer to dimer transition for our candidate scFv. Primer pairs were designed to flank the linker region to be deleted (Figure 1A). The parent scFv, and linker reduced constructs were confirmed by sequencing, and subsequently produced under identical conditions to the original scFv. IMAC purification and acrylamide gel resolution revealed the monomer to dimer transition for Tw1S4_6 scFv as occurring between 8 and 11 amino acid linker lengths. Linkers 8 through 10 gave substantial dimer formation, whereas linker 11 was predominately monomer, as revealed by acrylamide gel resolution (Figure 1B).

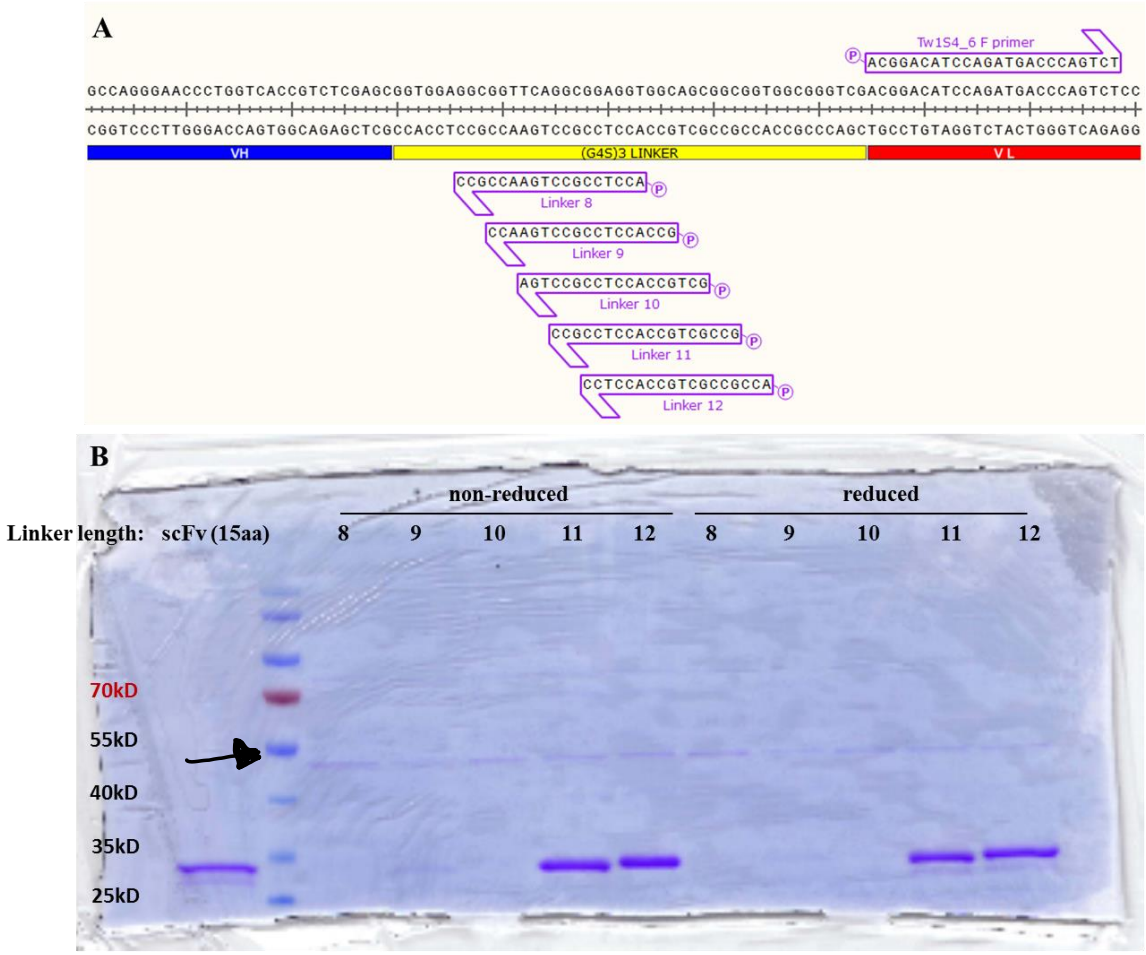

Figure 1 - Diabody production by linker length engineering – (A) schematic for deletion

PCR based protocol for linker length reduction in single amino acid increments. A universal forward primer hybridizing adjacent to the final codon contained by the linker. Reverse primer hybridation pattern reflects the resulting linker length, with linker residues C-terminal to the primer being deleted. (B) Acrylamide gel resolution was employed to determine the degree of dimerization for each of the constructs outlined in (A) Dimer band is present at the indicated arrow.

As reported previously, the binding partner of Tw1S4_6 scFv was determined to be cell surface HSPG2. Knockdown of HSPG2 in HMLE-Twist1 cells was accomplished with commercially available lentiviral particles encoding shRNA targeting HSPG2. Following puromycin selection, determination of Tw1S4_6 scFv binding to HSPG2 knockdown cells, as well as HSPG2 knockdown efficiency, was assessed by flow cytometry. Biotinylated HSPG2 antibody, and streptavidin APC dye conjugate were used to assess cell surface knockdown of HSPG2. Relative to control shRNA lentivirus transduced cells, cell surface expression of HSPG2 was reduced approx. 60% in target shRNA transduced HMLE-Twist1 cells (Figure 2A). The binding affinity of Tw1S4_6 scFv was assessed next. A reduction in binding of scFv to target shRNA transduced cells relative to shRNA control cells was confirmed (Figure 2B), and mirrored HSPG2 cell surface level reduction observed (Figure 2A). Thus, we provide cell line based evidence in support of HSPG2 as the candidate cell surface binding partner of Tw1S4_6 scFv. The Tw1S4_6 diabody with a linker length of 8 was chosen as the initial candidate for characterization.

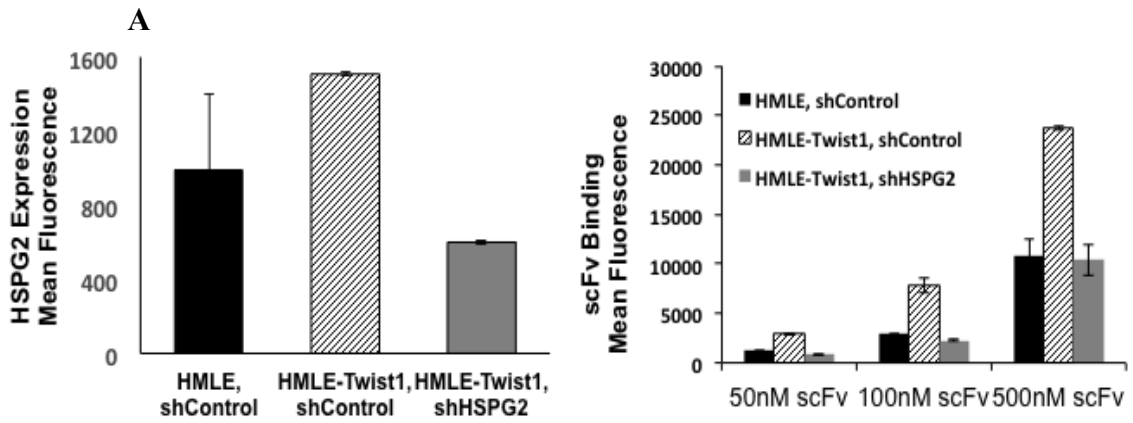

Figure 2. Confirmation of scFv binding partner HSPG2 target knockdown, and influence on scFv binding. (A) Lentiviral particles expressing either control shRNA or shRNA targeting HSPG2 were used to transduce HMLE and HMLE-Twist1 cells. Following stable selection in puromycin, cell surface HSPG2 expression was determined by flow cytometry using a commercial antibody recognizing a C-terminal epitope of HSPG2. Greater than 60% knockdown efficiency was observed compared to HMLE-Twist1 shControl cells. **(B)** Assessment of the relative binding of clone 6 scFv to HMLE-Twist1 cells after HSPG2 knockdown. Stable knockdown of HSPG2 reverts clone 6 scFv binding to the levels observed for HMLE control cells

An in vivo model for circulating tumor cell detection was generated. The xenograft model employed an MDA-MB-231 derivative cell line, termed LM2, which is predisposed to lung metastasis. The choice of the LM2 model was based on its derivation from spontaneous lung metastases of MDA-MB-231 orthotopic xenograft. Efficient lung colonization relative to the parent cell line would promote the existence of hematogenous dissemination of cells from the primary graft. Given that a prerequisite to this approach is confirmation of Tw1S4_6 scFv target expression on the surface of LM2 cells, we first determined HSPG2 cell surface expression in LM2 cells using commercially available HSPG2 antibody (Figure 3A). Greater than 90% of LM2 express surface HSPG2, indicating the model system is appropriate for diabody based immunocapture of CTCs. An improvement in apparent binding affinity for Tw1S4_6 diabody relative to scFv was

observed at equimolar concentration to target cell line LM2, indicating bivalent functionalization improved the binding affinity of monovalent scFv (Figure 3B). MFI values for the diabody approached values observed for commercial EpCAM IgG, establishing the utility of our subsequent dual labeling approach wherein PBMCs containing potential CTCs are stained with equimolar concentration of Tw1S4_6 diabody and EpCAM IgG.

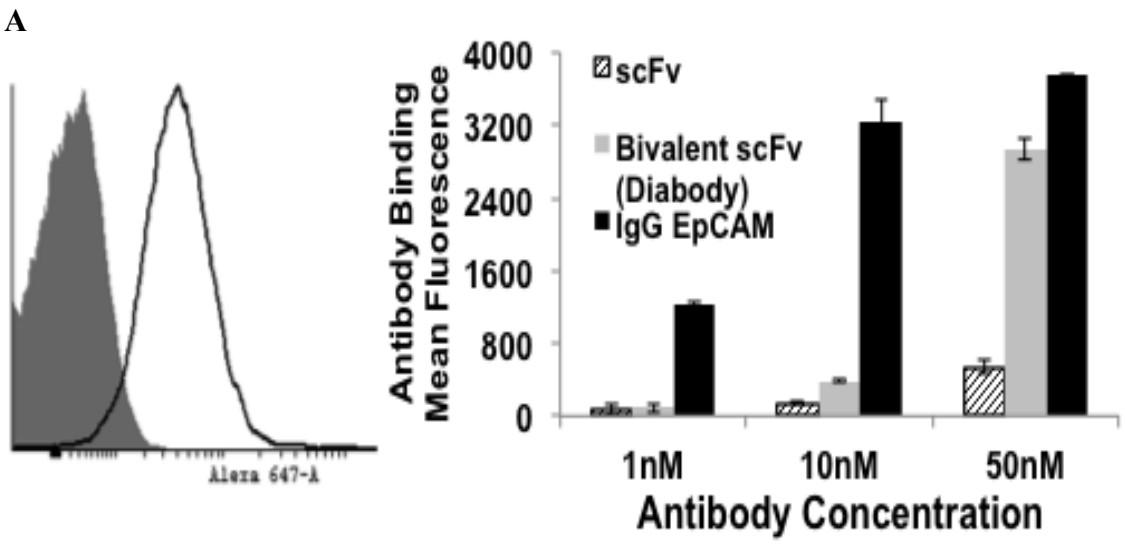

Figure 3 HSPG2 expression and assessment of diabody binding to lung metastatic LM2 cells (A) HSPG2 expression in MDA-MB-231 LM2 cells. Shaded histogram represents isotype control staining. Black histogram represents HSPG2 expression. (B) Relative LM2 cell surface binding of clone 6 scFv, diabody, and commercial IgG EpCAM antibodies, at equimolar concentration

In vivo LM2 grafts were implanted orthotopically to the hind limb mammary pad, and allowed to reach a volume 400-500mm^3 as determined by digital caliper measurements. Animals were sacrificed when the tumors reached the indicated volume, and peripheral blood was collected post euthanasia via cardiac puncture. PBMC isolation was performed

by passing whole blood over ficoll paque density gradient. Following red blood cell lysis and washing, total PBMCs were incubated with 50 nM of dylight 647-conjugated Tw1S4_6 diabody, and commercial EpCAM antibody conjugated to pacific blue. The LM2 cell line was stably transduced with a dual Luciferase-GFP reporter by Massague and colleagues[53], permitting green fluorescence as an initial gate on the FACS instrument. Initial establishment of GFP gate was performed on non-tumor bearing mouse PBMCs (Figure 4A). LM2 cells spiked into non-tumor bearing mouse PBMCs enables the P1 gate indicated on the figure to discriminate LM2 cells from PBMCs on the basis of GFP fluorescence (Figure 4B). PBMCs from tumor bearing animals were pooled and subsequently labeled singly with either dye-conjugated Tw1S4_6 diabody (Figure 4C), EpCAM IgG (Figure 4D), or both (Figure 4E). Within the PBMC population stained with both antibodies, distinct events staining positive for either antibody were observed, indicating mutually exclusive antigen expression. This is of critical importance, and indicates the existence of a large population of CTCs that are not positive for EpCAM in this in vivo graft model of breast to lung metastasis (Figure 4E).

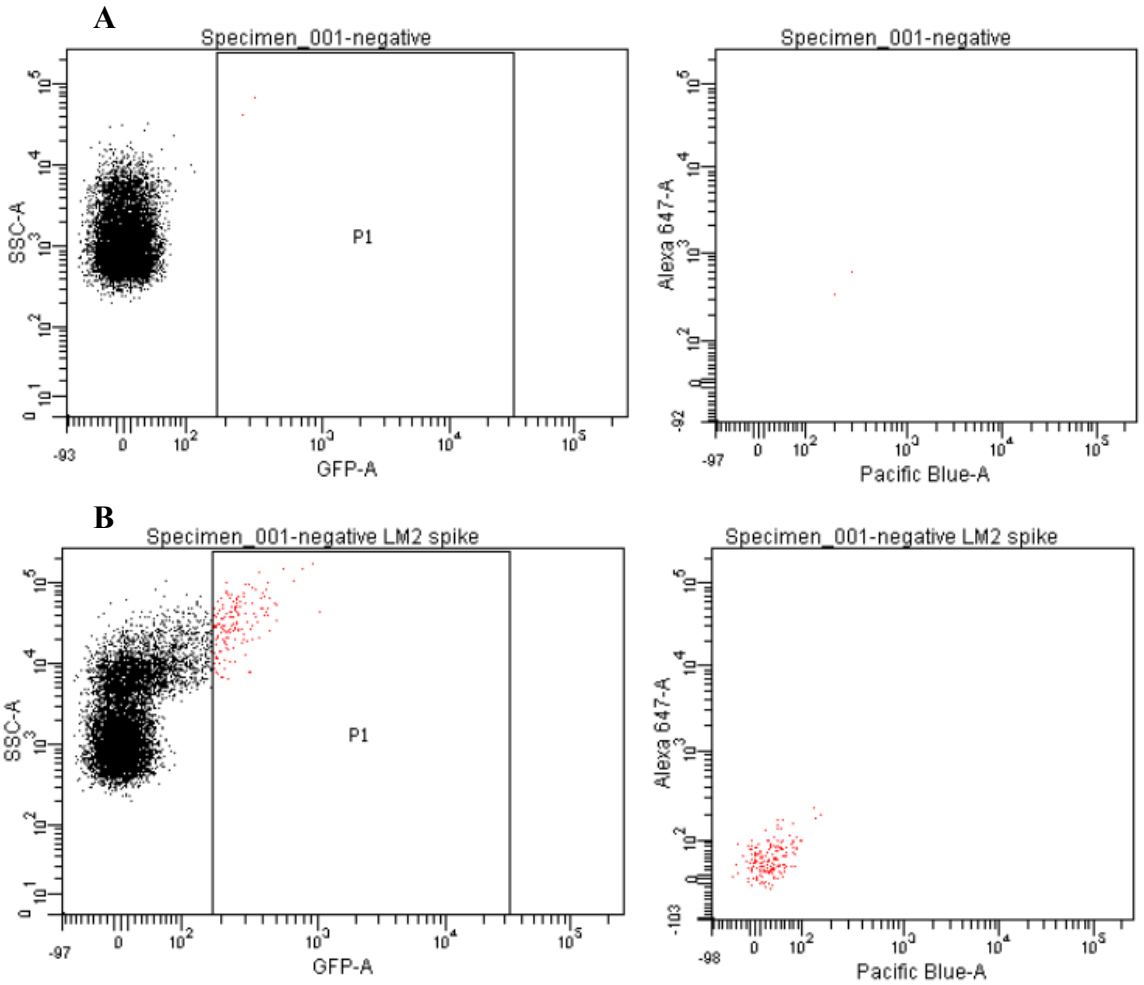

Figure 4 in vivo CTC detection with Tw1S4_6 diabody LM2 cells were grafted orthotopically in Balb/c nude mice. Four weeks after tumor induction, mice were euthanized, and blood collected by cardiac puncture. Following density gradient centrifugation to isolate mononuclear cells (PBMCs) and potential Circulating tumor cells, erythrocytes were lysed, and samples from animals bearing LM2 tumors were pooled and divided into three equal fractions for labelling with 50 nM Alexa-647 labelled Diabody or Pacific blue labelled IgG EpCAM antibody. Non-tumor bearing mouse blood was collected for use as controls (A) Control PBMCs from non-tumor bearing mice were used to establish fluorescent gating parameters. Population P1 is defined in the left panel as green fluorescent positive events. Note that LM2 cells are GFP stable. The right panel analyzes Pac-Blue EpCAM on the X-axis and Alexa-647 Diabody on the Y-Axis, in P1 gated events (B) LM2 cells spiked into control PBMCs immediately prior to analysis are used to establish population P1 based on GFP expression

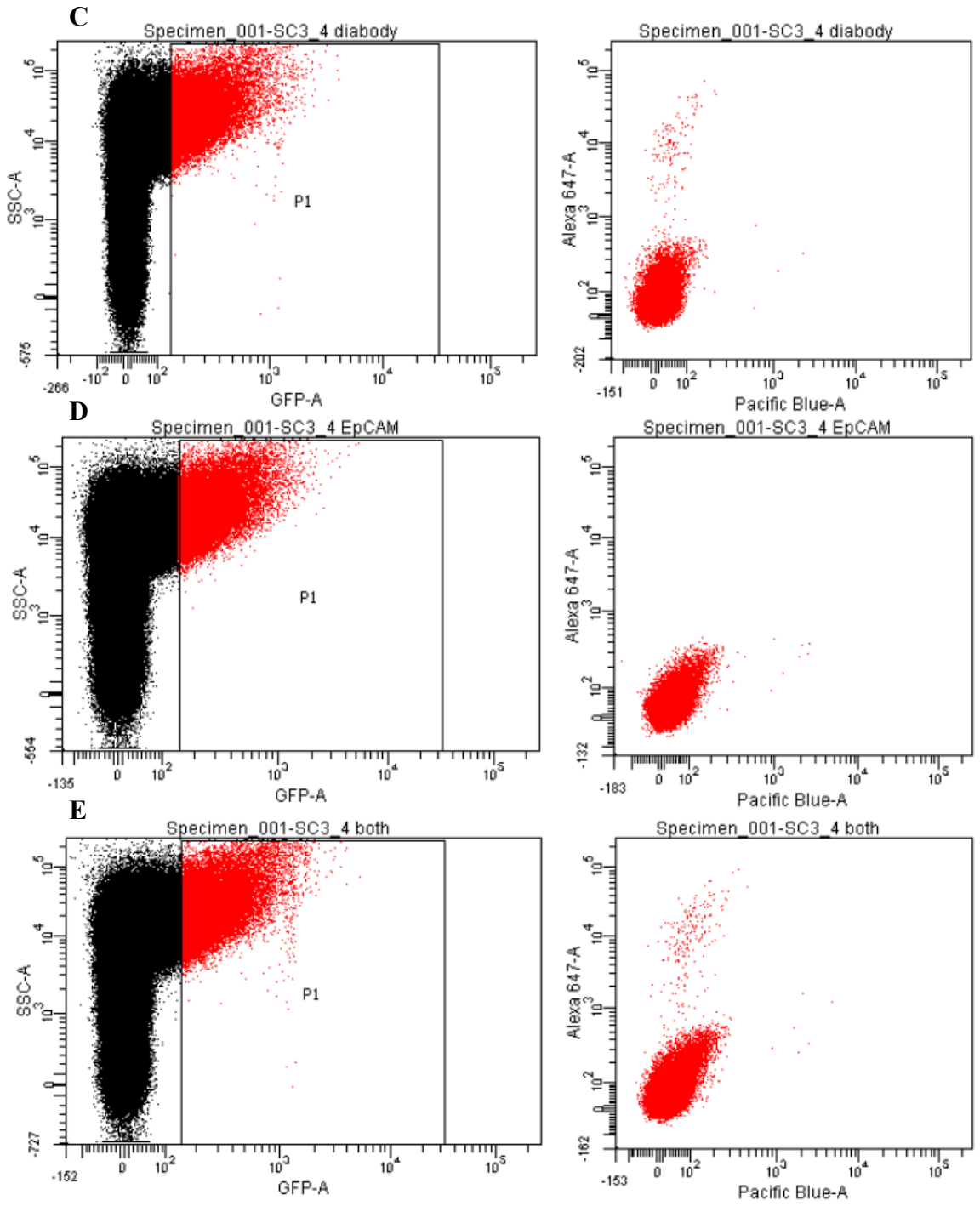

Figure 4, Continued (C) tumor bearing mouse GFP positive PBMCs singly stained for EpCAM Pacific blue. (D) tumor bearing mouse PBMCs single staining for Alexa-647 Diabody (E) tumor bearing mouse PBMCs double staining for EpCAM and Diabody

Discussion

Lack of recommendations from clinical governing bodies concerning implementation of CellSearch is the result of there being no current demonstration, via clinical trial, of CellSearch being an effective tool to inform patient management. The Southwest Oncology Group (SWOG) S0500 trial was designed to evaluate the utility of CellSearch in determining whether metastatic breast cancer patients with elevated CTC counts at first follow-up, would benefit from changing therapy regimen. The results failed to demonstrate that switching therapy regimen at first follow up was aided by CellSearch CTC enumeration[85]. CTC analysis by CellSearch was found not to be a good molecular indicator in determining whether therapy adjustments would benefit the patient. While the results of the SWOG trial predict a tenuous future for CellSearch, the emergence of capture platforms such as the CTC ichip have already provided evidence, based on single cell molecular profiling of captured CTCs, for drug resistance and disease recurrence in cancer patients.

Phage and other surface display libraries exist at the forefront of therapeutic and diagnostic antibody discovery. Through recombinant DNA techniques, fully human IgG antibodies can now be generated from phage display scFv. Examples include discovery and refinement of broadly neutralizing antiviral antibodies,[86,87] vascular compartment homing peptide identification via *in vivo* phage display,[88,89] and intracellular expression of antibody libraries in mammalian cell lines for agonist/antagonist antibody discovery[90].

Full-length IgG development, outlined in the previous chapter, represents the gold standard in biologic drug development owing to a number of highly favorable

physiological attributes that derive from their origins within the immune repertoire. These features include prolonged circulation half-life, highly specific targeting of disease relevant antigen, and recruitment of immune effector cell function. When focusing on the diagnostic utility of both full length IgG's and smaller antibody domains, antigen specificity is preserved in scFv, while the functionality that lies outside of the variable domain, within Fc domain of IgG, is removed from scFv, thus avoiding Fc receptor expressing immune cell interactions and its accompanying effects. Regarding CTC capture specifically, mono and multi-valent scFv possess the ability to avoid FcγR expressing immune cells, thereby avoiding potentially unwanted leukocyte contamination. Although not explicitly explored, this attribute could be evaluated in the future via biophysical characterization techniques such as SPR. It would be expected that Tw1S4_6 scFv and diabody would not bind to recombinant, immobilized human or mouse IgG FcγR. This would represent a favorable attribute of Tw1S4_6 diabody, which would enable avoidance of unwanted leukocyte contamination when sorting CTCs from patient samples.

The results presented in this chapter provide further evidence to support the results from the previous chapter, namely the CTC populations having shed epithelial characteristics during the process of solid tumor dissemination express a potentially EMT specific cell surface marker, HSPG2, that is bound by Tw1S4_6. Although capable of binding to HSPG2 expressing cell lines, the binding affinity of the monovalent scFv was deemed insufficient to proceed further. The generation of bivalent diabodies represents an alternative version of Tw1S4_6 when compared to the human IgG form outlined in the previous chapter. The functional attributes of each binder (scFv, diabody, and IgG) could

be taken into consideration for future projects whose aim is detecting EM transitioned CTCs.

Stable knockdown of HSPG2 via lentiviral delivered shRNA in HMLE cell lines was not as efficient as would be required to effectively characterize the phenotypic consequence of HSPG2 loss, as the remaining HSPG2 would confound the interpretation. This could relate to slow turnover of existing cell surface HSPG2. This could also be due to the primary mRNA transcript being sufficiently long to cause shRNA knockdown to fail at suppressing translation of the entire HSPG2, which could result in a functional, truncated HSPG2 on the cell surface, following shRNA knockdown. Nevertheless, the degree of HSPG2 knockdown was well correlated to loss of Tw1S4_6 scFv, indicating that HSPG2 is the putative target of Tw1S4_6.

The use of GFP expression within LM2 cells as an initial FACS gating strategy for CTC sorting was, in retrospect, less than ideal. This is owing to the weak signal, and large degree of variability of GFP expression within LM2 cells present in the circulation. This could indicate progressive loss of transgene expression due to *in vitro* passaging prior to initiating xenograft studies, or could be due to harsh conditions like shear stress, nutrient deprivation, and the induction of autophagy[140] within LM2 CTCs following detachment from the tumor matrix. Autophagy is a process known to result in catabolism of cellular biomacromolecules, which could include reporter proteins like GFP and luciferase. Low GFP fluorescence in LM2 cells, along with autofluorescence within PBMCs, likely representing doublet/multiplet cells that escaped the initial scatter gating, forced the GFP gate (Figure 4, population P1) to be placed less stringently than would be required for a

rigorous clinical flow cytometry protocol. The result of this low stringency fluorescent gate is the potential inclusion of PBMCs in the immunophenotyping plots (Figure 4C-E). This can lead to false positives when analyzing large numbers of events ($>10^7$) from a single sample. Taking into consideration the above mentioned issues with methodology, the presence of singly stained CTC's for EpCAM and Tw1S4_6 diabody provides corroborating evidence to what was observed in the previous chapter. Namely, the Tw1S4_6 binds to a distinct, EpCAM negative CTC population. Perhaps most importantly, this population is more numerous than EpCAM positive CTCs, and suggests that a large proportion of CTCs will fail to be enumerated by EpCAM immunodiagnostic reagents. This chapter confirms the ability to capture EpCAM negative CTCs using a bivalent form of EMT targeted scFv.

SECTION 2: THERAPEUTIC ANTIBODY DEVELOPMENT

CHAPTER 4

A PHARMACOKINETIC MODEL TO DETERMINE INFLUENCE OF ANTIBODY AFFINITY ON TARGETED DISTRIBUTION TO PRIMARY TUMOR AND MICROMETASTASES

Summary

While antibody based therapeutics possess very favorable pharmacokinetic profiles, physiological barriers to efficient antibody penetration of tumors can impede uniform concentrations being achieved, leading to inadequate response, and the emergence of acquired resistance. Within the class of antibody extrinsic barriers to penetration, heterogeneity of target antigen expression within the tumor can play an important role in non-uniform antibody concentrations. Antibody intrinsic properties can also impede uniform distribution, most notably their high molecular weight, leading to poor rates of diffusion through tumor. Antibody diffusion is slowed considerably when an antigen binding event occurs, thus compounding the problem. This phenomenon, termed the binding site barrier (BSB), suggests that improvements to antibody affinity can counteract diffusion through tumor, resulting in restricted localization of antibody to the tumor periphery. The importance of antibody affinity as a key parameter to uniform antibody distribution to tumor and micrometastases is interrogated in this chapter with the use of pharmacokinetic modeling. The BSB suggests that trade-offs in affinity must be made to promote efficient antibody diffusion and uniform concentrations throughout malignant mass. Pharmacokinetic modeling of the binding site barrier can, in theory, aid in the

identification of an ‘affinity sweet spot’, wherein antibody binding and pharmacodynamic effects are maximized while simultaneously minimizing losses to antibody diffusion that occur as a consequence of antibody binding and internalization. A pharmacokinetic model was developed in the software program STELLA in an attempt to interrogate the BSB. The parameters employed in this model are easily manipulated such that any therapeutic antibody-antigen pair could be optimized for targeting via fine tuning of the antibody binding affinity. This can be accomplished experimentally via affinity maturation protocols, which will be outlined in chapter five, to produce an optimized antibody for the targeting of antigens found in primary tumor or metastatic sites. The results of the model simulation suggest that targeting of high abundance tumor antigens may only require modest affinity antibodies.

Introduction

As of 2012, twelve antibody-based therapies were approved for use in humans for the management of solid tumors and hematological cancers. These encompass both ‘naked’ antibodies, and antibody-drug conjugates[92]. Antibodies represent a unique class of therapeutic biomolecules owing to several key features that include an active receptor mediated recycling mechanism that allows prolonged circulation half-life, selective binding affinity for a particular disease-associated antigen, and immune effector cell recruitment following the binding event. This unique repertoire of properties endows antibodies with the potential to satisfy the Ehrlich ‘magic-bullet’ theory, and explains the large investment on the part of pharmaceutical companies to develop antibodies, despite the astronomical costs associated with their production.

The pharmacokinetic model constructed here is an attempt to model the distribution of an i.v. bolus dose of therapeutic IgG to an arbitrary solid tumor and matched micrometastasis in lung. The primary tumor is a sub-cutaneous xenograft model in immunocompromised mice of undefined type. A single bolus dose of 20 mg/kg IgG is input into the central compartment, with relevant volume and flow parameters to lung and tumor supplied from the literature. In order for the administered antibody to reach target cells in the respective malignant cell masses, they must overcome three primary resistances: (1) transcapillary flux into the interstitial space, (2) diffusive transport through the interstitium, and (3) saturable binding to a cell surface receptor and subsequent internalization. Antibody internalization, also called target mediated disposition (TMDD), is the principle pharmacodynamics effect for antibodies targeting cell surface receptors. TMDD, by removing antibody from the pool available for diffusion further into the malignant mass, is considered as a clearance process. As a result, we consider TMDD as one of the primary resistances to uniform antibody distribution. It is important to note however that TMDD, being the principle effect component of this antibody class, is still critical to achieving a therapeutic response.

Model Part A: Antibody convective and diffusive transport across the capillary wall

Previous studies employing physiology based pharmacokinetic models to determine rate and extent of IgG penetration into tumor xenografts describe a ‘two pore’ capillary model, where large pores (~250 angstroms) permit antibody extravasation via convection on the arterial end, while small pores (40 angstrom) that exist on the venous return end of the capillary do not permit antibody extravasation by either diffusion or

convection.[93] Transcapillary flux of antibody is thus likely to occur via convective transport, with additional contribution given by fluid phase pinocytosis across vascular endothelial cells. This flux can be described by a modified form of the Starling equation:

$$P_s = \frac{J_s}{S\Delta C} = P_d\left[\frac{Pe'}{(e^{Pe'}-1)}\right] + L_p(1-\sigma)(\Delta P - \sigma\,\Delta\pi)\,.$$ [94]

Here, P_s describes solute permeability across the capillary wall. Key parameters are: Pe'clet number (Pe^t) which describes how much of the net flux is due to convection or diffusion. Hydraulic conductivity (L_p) is a coefficient describing vessel leakiness

Osmotic reflection coefficient (δ), varies from 0 to 1 and describes the likelihood that antibody approaching a vessel pore will be 'reflected' away from the pore and remains in the vessel.

The complexity of the Starling equation makes a numerical solution tedious. As a result, various experimental approaches have been employed to determine effective permeabilities (P_{eff}), which represent a practical estimate of both convective and diffusive transports. P_{eff} estimates for IgG in normal (granulation/connective) and malignant tissues are based on intravital microscopic analysis of vascular extravasation using FITC dextran of 150 kD molecular weight.[95] These P_{eff} values are included as parameters in the model. In order to normalize effective permeability values by tissue type, the parameter S/V is included. S/V represents the vascular surface area per unit tissue volume, values of which have been estimated in tumor grafts via colloidal carbon vascular tracer injection, and subsequent manual measurements on fixed tissue cross-sections.[96] Similar estimates for S/V in 'normal' tissue have been reported, and are included in the model. The model

assumes 20:1 ratio of lung to tumor vascular perfusion (1.9 vs. 0.1 mL/min flow rates). Transcapillary flux of antibody (J_{Ab}) is therefore modeled according to the equation:

$$\mathbf{J_{Ab} = (S/V)*P_{eff}*[Ab_{vascular}]}$$

We assume no net solute recirculation, and thus a uni-directional solute flux. This assumption is based on osmotic reflection coefficients for small pores (venous return) for large macromolecules being essentially equal to one. Osmotic reflection coefficients for large macromolecule intravasation into a lymphatic vessel, however, are small. This enables lymphatic drainage of antibody back to the central compartment. The existence of lymphatic recirculation of solutes in tumors seems counterintuitive to conventional wisdom. However, owing to a net pressure gradient that falls with distance from the tumor core, the result is in an outwardly directed interstitial fluid velocity that counteracts antibody diffusion from peripheral vessels into the tumor, and can result in an 'oozing' effect, whereby peripherally extravasated macromolecules, such as antibodies, can drain into the central compartment via normal tissue lymphatics.[97] The existence of lymphatic drainage in the normal tissue compartment harboring micrometastases has not been perturbed, and is thus of greater magnitude than tumor lymphatic drainage. Lymphatic recirculation flows for tumor and normal tissue have been previously estimated, and are included as parameters in the model (parameter references are provided in tables). A separate means by which antibody can extravasate from the central compartment is pinocytosis into vascular endothelial cells, followed by trafficking across the endothelial cell for distribution into the extravascular space. When estimating the relative magnitude of capillary flux due to pinocytosis, it has been suggested that the FcRN mediated

trafficking predominates.[98] Acidification of endosomes enables IgG interaction with salvage receptor FcRN. Subsequent bi-directional transport of antibody to interstitial space or back into circulation plays a major role in the pharmacokinetics of antibodies. A PBPK model incorporating pinocytosis, IgG-FcRN interaction, and IgG catabolism of unbound IgG in endothelium has been reported.[99] Sensitivity analysis of the model parameters indicated that pinocytosis uptake clearance, and IgG-FcRN affinity constants have equivalent to slightly higher influence on plasma AUC when compared to vascular reflection coefficient δ. Thus, both transcapillary flux and endothelial cell pinocytosis influence antibody distribution, with influence of roughly equal magnitude on distribution. In addition, alterations in IgG-FcRN interaction kinetics via antibody Fc domain engineering can have a dramatic influence on circulation half-life of therapeutic antibodies by exploiting the known interaction of IgGs with FcRN.[100]

The current pharmacokinetic model in Stella does not incorporate IgG-FcRN interaction, and thus provides a conservative estimate to antibody extravasation. A first order rate constant for clearance from the central compartment of 0.0055 hr^{-1} is included in the model. This is a rate of catabolism term for tissue sites in rapid equilibrium with the central compartment, principally vascular endothelium.[101]

Parameter	Lung (normal)	Tumor	Reference
Flow rate ($ml*min^{-1}$)	1.9	0.1	102
Vascular volume (mL)	0.019	0.033	102
S/V (cm^{-1})	70	200	103
Peff ($cm*s^{-1}$)	$7.3*10^{-8}$	$5.7*10^{-7}$	103
Lymphatic flow ($ml*min^{-1}$)	$1*10^{-4}$	$7*10^{-5}$	102
Interstitial volume (mL)	0.057	0.258	102
k CL central (hr^{-1})	0.0055		101

Table 1 Model parameters for antibody transcapillary flux

Model Part B: Antibody diffusion within the malignant mass compartment

The interstitium of most tissue types, including tumor masses, are composed of two phases; a fluid phase and a gel-like phase. Antibody transport through the interstitial space will be due to convection (interstitial fluid velocity) and diffusion. For the sake of simplicity, the current model in Stella assumes both the primary tumor and micrometastasis are prevascular, having a contiguous capillary network on the surface, supplied from the host tissue, available for antibody extravasation. This assumption is required to eliminate the need to model for pressure gradient differences that would exist for an exchange capillary enveloped by malignant cells within the tumor (chord model). Transport through the tumor in this scenario would be due to a combination of outward radially directed interstitial fluid velocity (convection) and diffusion. Previous modeling of antibody percolation through well vascularized tumors treat the system as a cylindrical model, with the center of the cylinder being a tumor exchange capillary surrounded by tumor cells and interstitium. Radial diffusion and convection from a central capillary to the periphery is governed by partial derivatives relating concentration and pressure gradients to antibody distance travelled from the capillary. Simulations with this model suggest that modest affinity antibodies (100 nM-10 nM K_D) are predicted to yield maximal average concentration and specificity ratios while maintaining a uniform percolation.[104] A major complication to these types of dimensional modeling analyses however is non-uniform distribution of antigen within a malignant mass. Owing to the mathematical complexity of modeling vascularized tumor transport described above, we will model antibody

distribution into the malignant mass as a diffusive process, moving from the surface of a sphere inwards via diffusion.

As stated above, we will assume that both malignant masses are spheres, having a contiguous capillary network available for solute exchange. Antibody distribution into the malignant mass will be due to diffusion. To model the diffusive process of transport into the tumor, we will use an analytical approximation of Fick's law of diffusion,[105] which states that the time required for antibody concentration at the center of the sphere to reach the concentration at the surface is related to the square of the radius over the diffusion coefficient of the antibody. We consider this as the saturation time. This relationship will be true for antibodies in the absence of antigen binding.

$$t_{sat} = R^2/D_{eff} \quad [105]$$

Measured diffusion coefficients in the fluid phase of interstitium for antibodies are much smaller in magnitude than their values in physiological buffer. Antibody diffusion coefficients in tumor tissue (D_{eff}) however, are greater in magnitude than their value in 'normal' tissue. These effective diffusion coefficients were determined experimentally via intravital microscopic analysis using methods similar to those described for capillary permeability determination. Given the discrepancy in D_{eff} values for antibody in normal and tumor tissue, this would seem counterintuitive. A likely explanation for enhanced diffusion of IgGs in tumor tissue is due to reduced levels of macromolecules normally present in the interstitial fluid phase. Notable among these macromolecules are polysaccharides that can impose both physical and electrostatic resistance to antibody diffusion. Given that polysaccharide components are reduced in

tumor via elevated lytic enzyme activity, this can help to explain the D_{eff} value discrepancies, when comparing those observed in normal and malignant tissue. The different forces governing the hindrance provided by the interstitial space to diffusion in normal vs. tumor will be explicitly taken into account by use of experimentally derived D_{eff} values. To summarize, while the insoluble phase of tumor interstitium (collagen, laminin, etc) is likely to be elevated, both the void space (Ɛ), and the molecular composition of the fluid phase of tumors are altered. These two parameters likely explain the greater effective diffusion of antibody in tumor relative to normal tissue. One important note regarding the model simulations in STELLA is that we will not be able to account for the heterogeneous distribution of antigen within the malignant cell mass. As a result, we have to make the assumption of homogenous antigen distribution available for binding.

When binding occurs, saturation time is slowed considerably. The saturation time equation is then modified to take into account an antibody – antigen binding event as follows:

$$t_{sat} = \frac{R^2}{D} \frac{[Ag]/\varepsilon}{6[Ab]_{surf}} \quad 105$$

where [Ag] represents that antigen concentration (mg/mL), Ɛ is the void space available for diffusion, and $[Ab]_{surf}$ is the antibody concentration at the surface of the malignant mass. The factor 6 is a spherical geometry factor. Since $[Ab]_{surf}$ will be much less than the antigen density, we can see that the process of binding will slow the saturation time considerably. The parameters R^2, Ɛ, and [Ag] represent intrinsic features of tumor physiology and as a result lie outside the realm of experimental intervention. Although

antigen concentration is an intrinsic feature of the solid tumor, the process of antibody generation requires thoughtful selection of the antigen to be targeted. Attention should be paid to localization, as well as homogeneity of target antigen expression, in order to achieve a therapeutic response. Differences in target antigen expression are taken into account by simulating a range of cell surface expression levels. Generally, tumor antigens targeted by antibodies are expressed in high abundance, with cell surface receptor antigens typically on the order 10^5-10^6 receptors/cell. Parameters in the above equation that are available for experimental manipulation are D_{eff} and $[Ab]_{surface}$. For diffusion coefficients, these are inversely proportional to molecular size, which would conceivably result in better diffusion of antibody fragments within the tumor sphere relative to full length IgG's. This idea will be discussed in the next section in the context of the binding site barrier. $[Ab]_{surface}$ could be altered via dose manipulation (increased dose, dosing interval), or via Fc domain engineering to effect endothelial cell transcytosis.

Parameter	Lung (normal)	Tumor	Reference
R^2 (cm)	0.045	0.13	estimated
Malignant mass cell volume (mL)	0.04	0.181	[102]
Malignant mass cell density (cells*mL^{-1})	4*10^8	4*10^8	[106]
EGFR $Ag_{membrane}$ (mg*mL^{-1}) = B_{MAX}	0.043	0.043	calculated
Cell volume (L*cell^{-1})	4*10^{-10}	4*10^{-10}	[107]
D_{eff} (cm^2*s^{-1})	2.4*10^{-9}	1.3*10^{-8}	[108]

Table 2 Model parameters for antibody diffusion through malignant cell mass

Model Part C: Saturable binding to tumor cells and observation of the Binding site barrier

To this point, we have observed that effective targeting of therapeutic antibodies to malignant cancer lesions involves transcapillary flux to present the antibody to the malignant sphere surface, followed by diffusion from the surface to the center of the sphere. Saturation times for poor affinity antibodies will be rapid, owing to the absence of a saturable binding mechanism, whereas antibodies with very low K_d will be immobilized by the first antigen presented within the malignant sphere. In the context of antibodies targeting cell surface receptors, frequently reported mechanisms of action relate to the internalization of the receptor, causing the receptor to be unavailable for participation in ligand mediated signaling events. This phenomenon is termed 'down-regulation' and can be a critical aspect to antibody pharmacodynamics. Saturable binding of antibody to cell surface antigen in the STELLA model is described by the following equation:

$$[\text{Ab-Ag}]_{\text{complex}} = \frac{[B_{max}]*[\text{Ab}]_{\text{surface}}}{K_D + [\text{Ab}]_{\text{surface}}}$$

One might reason that the most efficacious antibody therapies would be those displaying the highest affinity binding towards antigen. This is not the case, however, as the now well-established phenomena termed the binding site barrier (BSB), has consistently demonstrated that high affinity antibodies are bound and sequestered at the rim of tumor spheres.[109] The BSB has also been observed in antibody distribution within micrometastases.[110] This affinity based barrier to homogenous distribution has also been

observed to be independent of antibody size, as single chain Fv antibody fragments encounter the same barrier.[111] The BSB is thus a fundamental consequence of antigen binding and internalization rates being much more rapid than diffusion rates; If the rate of dissociation of antibody from cell surface antigen is sufficiently slow, then receptor internalization will act as a clearance, defeating diffusive transport further into the center of the sphere.

The goal of the STELLA model is to observe the BSB in the context of antibody distribution to a primary tumor and lung metastasis. In theory, such a model could be used to guide antibody engineering and optimization based on knowledge of the antigen to be targeted, and the equilibrium dissociation constant of the antibody for the antigen. The BSB suggests that trade-offs in affinity vs. diffusive tumor penetration must be made. This type of modeling could aid in the identification of an 'affinity sweet spot'. Identification of K_D values that maximize binding (effect compartment), while minimizing the sequestration of antibody at the periphery of the tumor sphere that occurs as a consequence of binding (BSB), would make this type of simulation highly practical. The two parameters that will be varied via sensitivity analysis are the K_D and [Ag].

Parameter	Lung (normal)	Tumor	Reference
k_{on} $[nM]^{-1}*hr^{-1}$	5.82	5.82	107
k_{off} hr^{-1}	14.4	14.4	107
$k_{degrade}$ hr^{-1}	15	15	107
$k_{internalize}$ hr^{-1}	1	1	estimated

Table 3 Model paramers for saturable binding and TMDD

Model Simulations

The initial simulation depicted in figure one varies the K_D from 1 μM to 100 pM, with each increment representing one order of magnitude improvement in affinity. 1 μM affinity represents a very weak binding IgG, while 100 pM represents the lower limit of IgG affinity currently achievable. As a simplified measure of antibody pharmacodynamic effect, the time integral of the bound antibody within the malignant sphere (AUC bound) is a rough estimate of effect. STELLA treats compartments as 'well stirred', which is not an appropriate assumption. The critical information that is lacking is, spatially, is where the simulated concentrations exist in the malignant sphere. Subsequent simulations will attempt to offer some insight into the concentrations observed in the bound compartment, relative to the saturation compartment, which arise as a result of diffusion. As seen in figure 1, AUCs in both binding compartments plateau at 1nM K_D values. This observation is consistent with previous reports modeling antibody penetration into tumor spheres.[112] We can assume that no appreciable difference in therapeutic effect would be observed beyond 1 nM K_D when the antigen targeted is expressed at 10^5 receptors/cell.

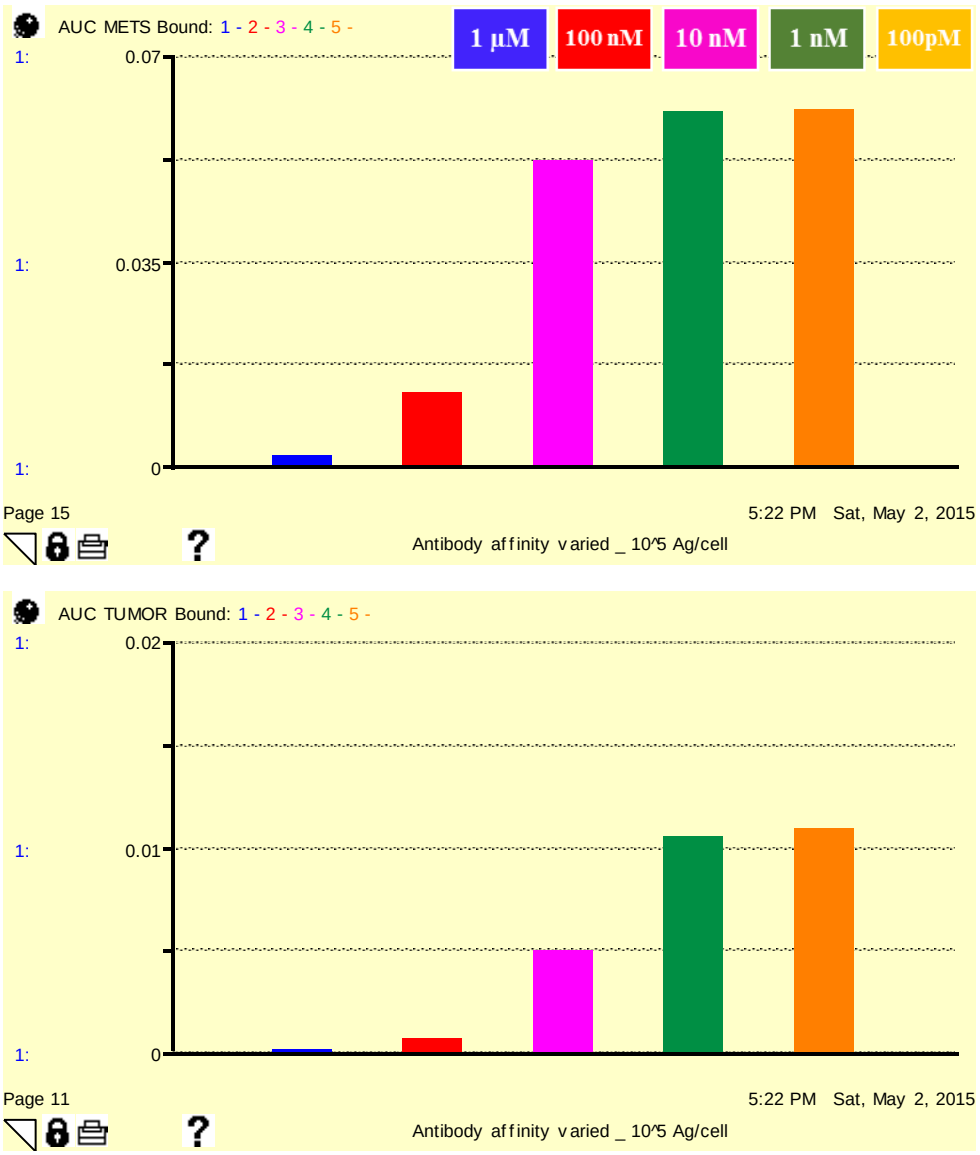

Figure 1 Sensitivity analysis of the influence of antibody K_D towards model tumor antigen EGFR expressed at 10^5 receptors/cell, on the targeted distribution to primary tumor and lung metastasis. AUC units are ($mg*mL^{-1}*hr$). Top panel represents AUC in the lung metastasis compartment. Bottom panel represents AUC in the primary tumor compartment.

The second set of simulations (figure 2) depicts AUCs in both binding compartments at higher antigen density (10^6 receptors/cell). As would be expected in the

context of the binding site barrier, higher antigen density would bind and sequester a greater extent of antibody made available for diffusion. In this scenario, we would not expect appreciable differences in therapeutic effect with K_D values better than 10 nM for the tumor bound compartment. Interestingly, 100 nM affinity is sufficient to approach the AUC plateau in the METS compartment. If this observation were reflective of reality, this would indicate that only modest affinity IgGs would be required to target a high density receptor in micrometastatic lesions.

As stated above, STELLA treats compartments as well-stirred, which is an inaccurate representation of the process of antibody diffusion through a malignant sphere. The model also fails to consider heterogeneous antigen distribution throughout the sphere. Nevertheless, we can draw some conclusions from the simulations depicted in figure 3 regarding our ability to observe the BSB. Figure 3 depicts concentration vs time profiles in the METS bound compartment, along with the METS saturation compartment for 10^5 receptors/cell. For K_D = 1 μM, the saturation compartment, and thus the antibody diffusion through the malignant sphere, is maximal (Figure 3 – top panel). Saturation time is likely only limited by the effective diffusion coefficient in the respective tissue. There is minimal antibody accumulation in the binding compartment, indicating that at K_D of 1 μM, saturation of the malignant sphere is occurring due to the absence of binding, and thus no effect will be observed.

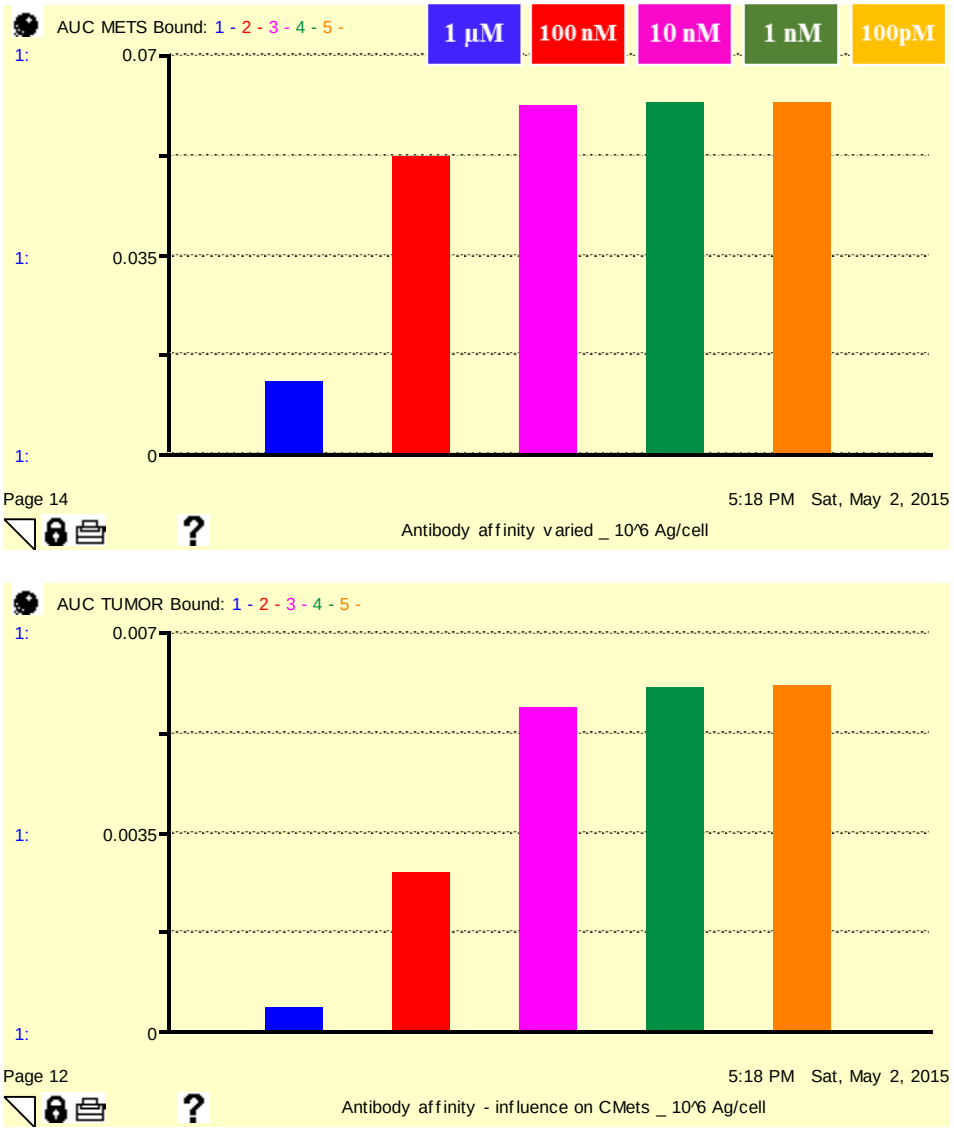

Figure 2 Sensitivity analysis of the influence of antibody K_D towards model tumor antigen EGFR, expressed at 10^6 receptors/cell, on the targeted distribution to primary tumor and lung metastasis. AUC units are ($mg*mL^{-1}*hr$). Top panel represents AUC in the lung metastasis compartment. Bottom panel represents AUC in the primary tumor compartment.

For very high affinity antibodies (Figure 3, 100 pM K_D), a much higher C_{max} is observed along with earlier t_{max}. We observed in figure 1 (top panel), that under these simulation conditions, a plateau in AUC is observed at 1 nM K_D. Considering that no

appreciable difference in exposure of the METS compartment to antibody will occur when using a 1 nM or 100 pM affinity antibody, we look to the concentration time profiles in the saturation and bound compartment under these simulation conditions (figure 3) to see that while we will sacrifice maximum concentration achieved in the METS bound compartment at 1 nM K_D vs. 100 pM K_D, we would expect better saturation of the sphere with the lower affinity (1 nM K_D) antibody. Arguably, this is the closest the current STELLA model will come to elucidating the BSB.

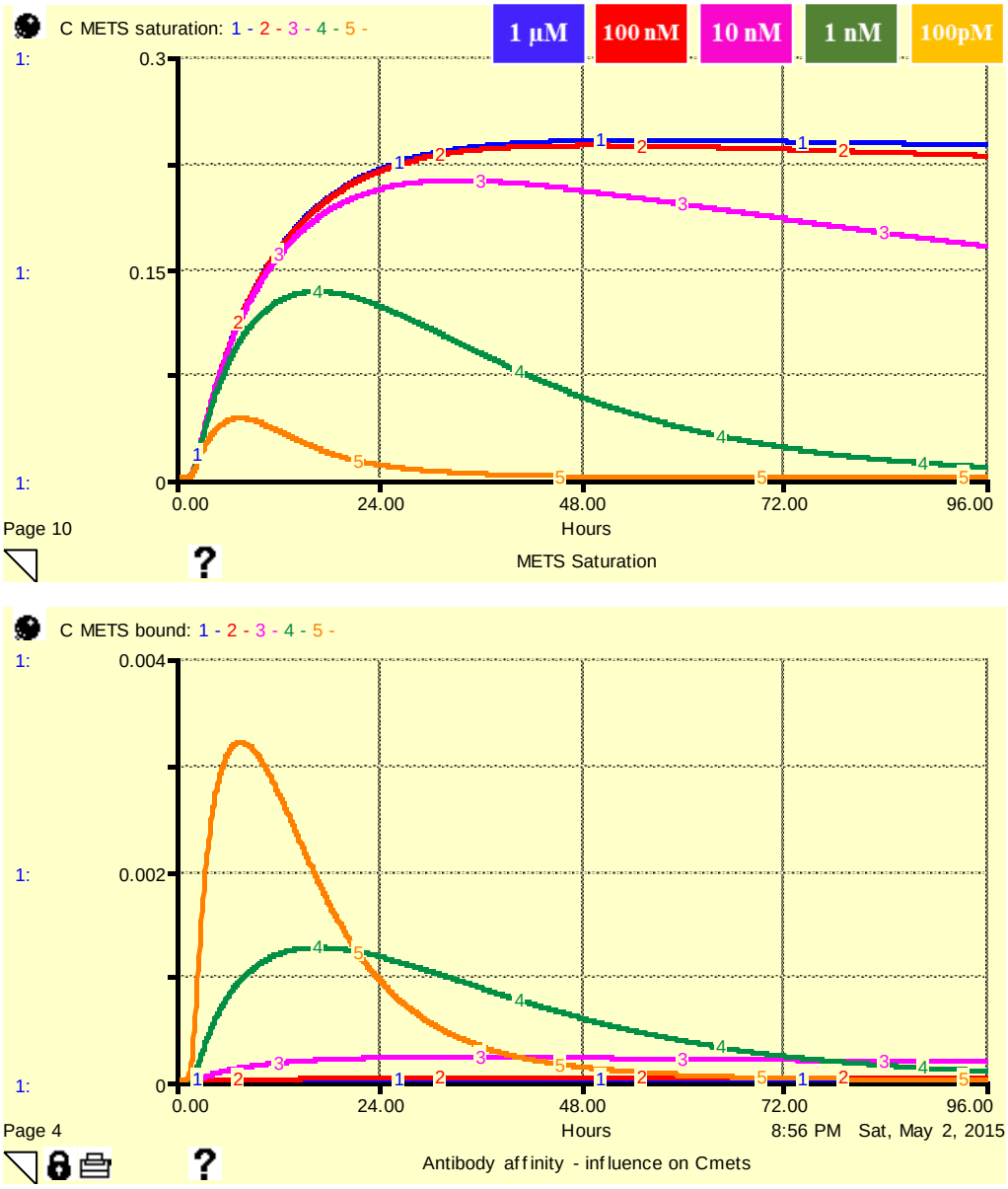

Figure 3 Sensitivity analysis of K_D on concentration time profiles in the METS saturation compartment (top panel) and METS bound compartment (bottom panel).

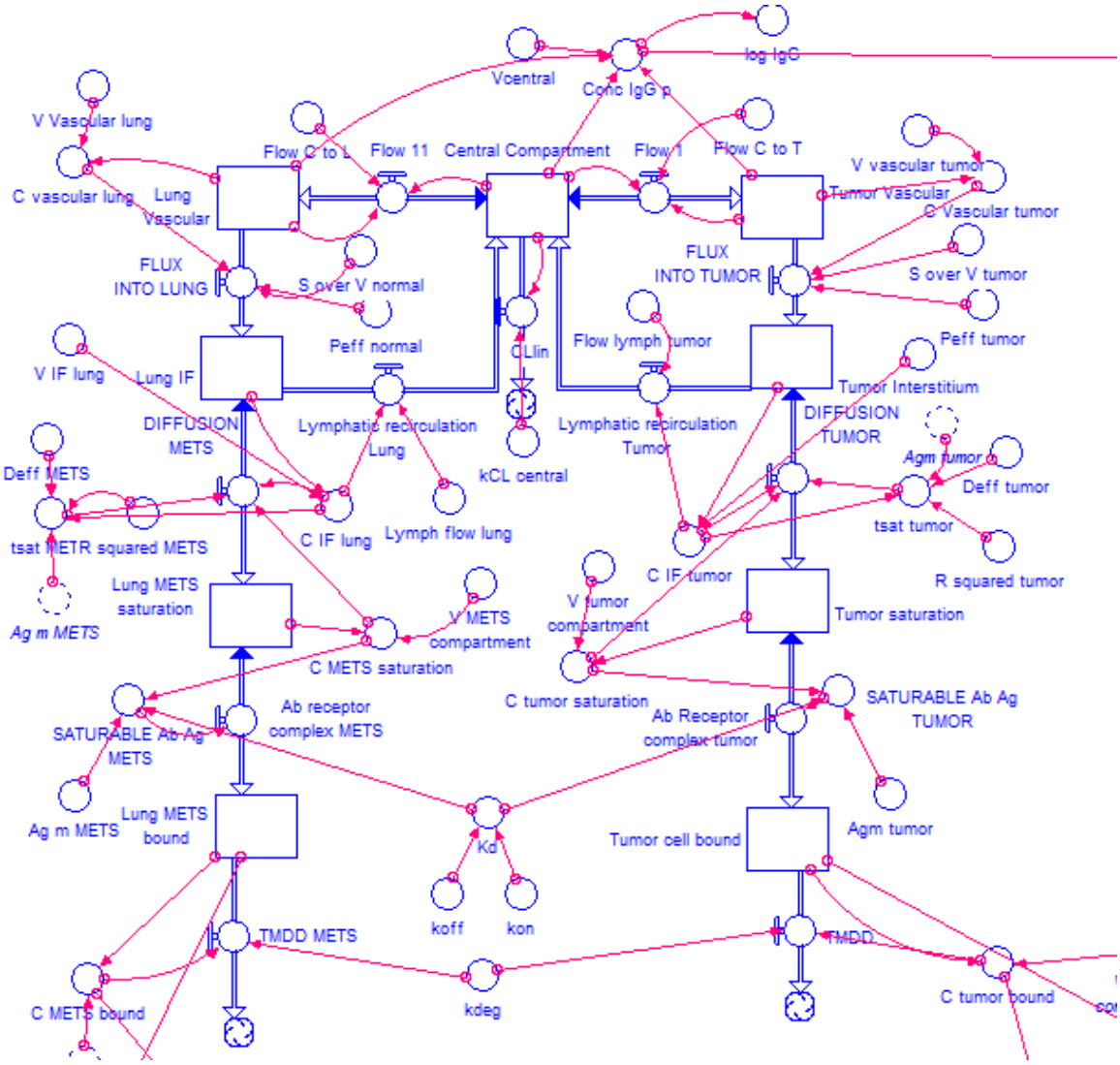

Figure 4 Schematic of Pharmacokinetic model in STELLA

Discussion

Although sufficient information is lacking to draw the following conclusion, it could be argued that tumor dimensionality, lacking in the current model, can still be considered as a thought experiment, by comparing both panels of figure 3 simultaneously. If one were to reason that the Cmax observed in the bound cell compartment for high affinity antibody (100 pM K_D), occurs when concentrations are far below the non-binding scenario in the saturation compartment (K_D = 1 μM), then this would suggest that locally high concentrations of antibody occur on the tumor periphery, which would be the definition of the binding site barrier. In conclusion, antigen density and antibody affinity play critical roles in the use of therapeutic antibodies in oncology. Antibodies targeting high density antigens would only require modest affinity antibodies to prevent sequestration at the sphere surface, resulting in insufficient distribution (Figure 2). Antibodies targeting antigens with more modest expression level require improved affinity to achieve maximal targeting (Figure 1). Based on an AUC plateau modeling strategy to predict efficacy, the BSB would suggest to us to choose the affinity that approaches the AUC plateau but occurs before the plateau is reached. This will maximize binding in the effect compartment, without considerable sacrifices to diffusion through the saturation compartment. Ultimately, each antibody – antigen pair will have its own unique parameters.

The parameters employed in this model are easily manipulated such that any therapeutic antibody could be fine tuned via affinity maturation protocols to produce an optimized antibody for the targeting of antigens found in metastatic sites. There are

numerous aspects of therapeutic antibody pharmacokinetics, mentioned briefly in the introduction to this chapter, the current model fails to capture. These include fluid pressure gradients within the tumor, heterogeneity in antigen expression, the influence of FcRN mediated receptor recycling and extravascular distribution, and distribution to non-target sites. Also of note is the assumption within this model of equal abundance of tumor antigen at both primary tumor and metastatic sites. The now accepted theory for the existence of metastasis virulence genes suggests that a number of tumor antigens confer a selective advantage upon disseminated cancer cells that have reached a foreign tissue microenvironment.[113] Antibodies developed against such antigens could be affinity optimized with the above pharmacokinetic model to facilitate the selective targeting of therapeutic antibody to metastatic sites.

SECTION 2: THERAPEUTIC ANTIBODY DEVELOPMENT

CHAPTER 5

AFFINITY MATURATION, IN VITRO RESPONSE, AND IN VIVO EFFICACY OF HUMANIZED ANTIBODIES TARGETING PERLECAN

Summary

Cell surface affiliated perlecan is a known participant in ligand-receptor interactions, acting as a low affinity growth factor co-receptor to mediate receptor signal transduction. Antibodies targeting cell surface affiliated perlecan were previously developed from phage display based phenotype screening to identify metastatically virulent subsets of tumor cells. Given the known promiscuity of perlecan towards a diversity of cancer relevant growth factors, we hypothesized that these antibodies could elicit therapeutic responses. The initial candidate antibody was affinity matured with the goal of improving the binding capacity and specificity towards perlecan. The two antibodies were first evaluated in a series of *in vitro* assays to determine their pharmacologic effects. Next, in vivo efficacy was determined using subcutaneous xenograft model. The results suggest that perlecan-targeted IgGs could represent a potentially novel class of targeted antibody therapeutics.

Introduction

Heparan sulfate proteoglycans are ubiquitous constituents of extracellular matrix and vascular basement membranes. Perlecan (HSPG2) is the primary HSPG within tissue and vascular basement membranes (BM) and has also been observed to be affiliated with

the surface of malignant cells, and abundant in tumor stroma. Tumor cells as well as stromal cells, including fibroblasts, endothelial and smooth muscle cells produce and secrete perlecan[114]. Functional roles of perlecan are diverse, and include participation in the scaffolding function of ECM, along with collagens, laminins and fibronectin. This promotes cell-matrix interaction and tissue integrity both within ECM and tissue/vascular basement membranes. HSPGs also provide a reservoir of immobilized growth factors (GF) within ECM and in pericellular spaces via electrostatic interactions of heparin sulfates with GFs. This GF interaction is of particular importance to cancer, as HSPGs in pericellular space or directly affiliated with the cell membrane can act as co-receptors in ligand-receptor mediated signaling events[65].

Cell surface affiliated perlecan has a diversity of known interactions with GFs that include members of the FGF family, VEGF and PDGF, among others[115,116]. HSPG - GF interactions are based on the negative charge density imparted by heparan sulfate chains, enabling electrostatic interactions with positively charged residues present within shallow grooves on the GF surface, known as Cardin-Weintraub motifs[117]. Thus, perlecan is likely functioning as a promiscuous participant in growth factor receptor-mediated signaling, via tethering the ligand close to the cell surface. Importantly, antibody mediated targeting of perlecan to impede the GF coreceptor function may represent a relevant therapeutic strategy in cancer.

As described above, several cancer relevant ligand–receptor systems depend on HSPG glycosylation dependent tethering of the ligand in proximity to the cell surface to mediate signal transduction from the receptor. The FGFR family is the best studied receptor

system requiring heparin sulfate interactions with FGF to mediate mitogenic signaling in breast cancer cell lines[118,119]. Crystal structures of HS – FGF – FGFR ternary complexes suggest that an octamer of fully sulfated heparin is required for FGF – FGFR interaction[120]. The working hypothesis is that Tw1S4 antibodies binding within domain 1 of HSPG2 will disrupt the coreceptor function of the HSPG, leading to impaired signal transduction/receptor activation.

GF receptors represent the predominant therapeutic target of monoclonal antibodies in cancer. Antibodies targeting members of the HER receptor family are the best characterized, with FDA approved monoclonal antibodies targeting the extracellular ligand binding domain of members of this receptor family now in widespread use for solid tumor management. EGFR targeted antibodies invariably produce cytostatic effects on cancer cell lines *in vitro.* These effects are characterized by cell cycle arrest in G1 phase, induction of cyclin dependent kinase inhibitors, and activation of the intrinsic apoptotic pathway[121]. The cytostatic effects of HER targeted antibodies have been demonstrated to act synergistically with radiation and chemotherapy to prevent tumor cell repopulation between dosing intervals[122]. Notable among this antibody class is the EGFR targeting chimeric antibody cetuximab, which was the first FDA approved antibody targeting a cancer growth factor receptor. It is used in combination with radiation therapy for head/neck and metastatic colorectal cancer. Additional examples include the humanized antibody panitumumab – also approved for metastatic colorectal cancer, and the HER2 targeting antibody Trastuzumab, which is approved for use in HER2 positive breast cancer.

With the initial demonstration of clinical success came evidence of both intrinsic and acquired resistance to HER targeted antibodies. HER targeted antibodies are most effective when coupled to clinical diagnostics, which are used to evaluate HER gene amplification/expression and K-Ras mutation, to identify likely responders[123]. Acquired resistance to HER targeted therapy has been attributed to several mechanisms, including HER2 and HER3 compensatory activation in the case of cetuximab[124], a phenomena that is not restricted to antibody mediated targeting, as the small molecule TKI gefitinib exerts the same HER3 transactivation mechanism in resistant cell lines[125]. As a result, the development of combination approaches to HER receptor targeting is active in preclinical development. These approaches include combination anti-HER antibodies with small molecule inhibitors[126], and multiple anti-HER antibody cocktails labeled as Pan-HER antibodies[127]. These strategies are proving more effective than single agent HER receptor targeting by enhancing receptor blockade and preventing heterodimerization of different HER isoforms. It is likely that antibodies recognizing domain 1 of HSPG2 will act to impair the GF coreceptor function, thereby producing pharmacologic responses similar to Pan-HER antibody cocktails. Given the promiscuity of HS chains in sequestering GFs, it is likely that antibodies recognizing cell surface localized HSPG2 will impair signal transduction across an even greater array of receptor systems, given that known GF interactions encompass a plethora of cancer relevant processes that include EGF, FGF, PDGF, and potential bystander effects on tumor endothelium via impairing VEGF - VEGFR mediated angiogenesis.

A reasonable assumption in therapeutic antibody development is that the most efficacious antibody therapies would be those displaying the highest affinity binding towards antigen. This however is not the case, as the now well established binding site barrier (BSB), outlined by a pharmacokinetic model in the previous chapter, has consistently demonstrated that high affinity antibodies are bound and sequestered at the rim of tumor spheres[128], and micrometastases.[129] To interrogate this phenomena we chose to empirically characterize the influence of antibody-antigen binding affinity and its role in the binding site barrier using Tw1S4_6 IgG, and an affinity matured variant, Tw1S4_AM6 IgG, using in vitro tools to assess the pharmacologic effects of perlecan targeted antibodies, and finally in vivo efficacy using subcutaneous xenograft models to monitor tumor growth post- antibody treatment.

Methods

scFv affinity maturation

Affinity maturation of scFv was accomplished via a targeted mutagenesis approach in which 7 amino acids comprising CDR3 of the light chain were mutagenized with a primer containing NNB degenerate codons. The procedure involves two sequential steps. The initial step employs the mutagenic primer, which hybridizes to CDR3 of V_L, along with LMB3 primer to amplify the full scFv gene and introduce directed mutagenesis. The second PCR employs the same LMB3 primer, as well as a forward primer that contains the remaining C terminal scFv residues, which were lost during the first PCR amplification.

The primers used were as follows:

1. LMB3 primer: CAGGAAACAGCTATGAC

2. V_L CDR3 mutagenic primer:

   CCCTCCGCCGAACACCCAACCNNBNNBNNBNNBNNBNNBNNBCTGGCAGTA

   ATAATCAGCCTC

Vent (exo -) DNA polymerase with deficient 3' – 5' proofreading activity was used for mutagenesis (NE biolabs). Mutagenic PCR thermal cycling conditions were: 94^{o}C for 5 minutes followed by 30 cycles of: 42^o C 1 minute, 72^{o}C for 2 minutes. The mutagenized scFv template was gel purified on a 1% agarose gel. Gel extraction was accomplished with QIAquick PCR purification kit (Qiagen) according to the manufacturer-supplied protocol.

scFv reformatting to human IgG1

PCR primers were designed to append restriction enzyme sites to the final PCR amplicon, such that subsequent restriction enzyme digest would produce a variable domain that was compatible with the recipient vector. A detailed protocol for scFv reformatting to human IgG1 using pFUSE constant domain vector pair is detailed in chapter 2.

Biolayer Interferometry (BLITZ)

Ni-NTA biosensors were hydrated for 10 minutes in phosphate buffered saline. Following hydration, a 30 second baseline was established, followed by a 10 minute loading of the biosensor with 10 µg/mL HSPG2 domain 1 protein. The biosensor was then placed in PBS to establish baseline for 30 seconds. A two-step antibody association – dissociation cycle of 5 minutes was then used to determine the kinetic association (k_a) and dissociation (k_d) rate constants. The equilibrium dissociation constant (K_D) was calculated as $K_D = k_d/k_a$

Flow cytometry antibody binding curves

LM2 and M12 cells were trypsinized and aliquoted to 10^5 cells in PBS (volume?). Cells were incubated with a range of antibody concentrations for 60 minutes at 4^0C on a rotating

shaker. Flow cytometry staining buffer used was PBS, 0.5% w/v BSA, 2 mM EDTA. Following two wash steps, a goat anti-human Dylight 647 conjugate antibody was used to determine the extent of antibody binding to cells. A BD LSR2 was used to analyze cells for fluorescence.

Inhibition of cell growth by MTS

Cells were seeded at 2,500/well in 96 well plates, and allowed to adhere overnight. The following day, cells were treated with the indicated concentration of antibodies. After 48 hours, the media was discarded, the cells were washed once in PBS, and MTS reagent was added to the wells according to manufacturer protocol. The colorimetric MTS assay assesses the number of viable cells. The assay employs the intracellular redox enzyme substrate MTS, which is converted to a color product in viable cells. Colorimetric detection of viable cells was determined on a UV/Vis plate reader with at 490 nM filter.

Cell cycle analysis

Propidium iodide is a red shifted fluorescent DNA intercalating dye (ex 633nm, em 650 nm) used frequently to assess the DNA content in cells by flow cytometry[130]. Following treatment of LM2 and M12 cells with Tw1S4_6 and Tw1S4_AM6 IgGs at the indicated concentrations above, cells were detached from solid support with trypsin. Following wash steps, harvested cells are washed in PBS. 2. Fixation s performed in ice-cold 70% ethanol by adding with a Pasteur pipette on a vortex. After additional washes, 50 µl RNAse (100 µg/ml Sigma) was added and cells were incubated at RT for 15 mins. Propidium iodide (10 nM Invitrogen) was added and the cells were immediately analyzed by flow cytometry, collecting 25,000 events per sample. FSC and SSC were used to generate the initial cell gate, which was subsequently displayed on an AF647 area vs. AF647 width plot for

singlet/doublet discrimination. The singlet population was finally displayed on an AF647 histogram plot, where G1, S and G2/M phase be discriminated.

Assessment of apoptotic index

Following treatment of LM2 and M12 cells with Tw1S4_6 and Tw1S4_AM6 at the indicated times/concentrations, induction of apoptosis was determined using the FITC Annexin, PI co-staining procedure. A common feature of the onset of apoptosis is the loss of cell membrane asymmetry, which is detected when inner membrane phosphatidyl serine is detectable on the cell surface. A FITC conjugated form of the phospholipid binding protein Annexin is used to detect early apoptosis. Late stage apoptosis is characterized by loss of membrane integrity. This step is detected with cell impermeant fluorescent dyes like PI. Cells were stained with FITC-Annexin and PI according to manufacturer's protocol.

In vivo tumor growth inhibition

Balb/c homozygous nude mice were used for the in vivo tumor growth inhibition study. LM2 cells were dissociated from tissue culture plate with trypsin, centrifuged, and washed twice with PBS. Cells were resuspended in PBS such that 50 µL contained 10^6 cells. Cell suspensions were diluted with an equal volume of matrigel (BD Bioscience). The cell suspension was grafted subcutaneously to the right flank corresponding to mammary pad. Tumor volumes were measured daily with an electronic caliper. Tumor volumes were calculated from the ellipsoid sphere equation $V = (L^2 * W)/2$. Additionally, tumor growth kinetics was monitored via non-invasive live animal bioluminescence imaging. An IVIS Spectrum in vivo imager, housed in the University of Minnesota Imaging Center, was used.

Results

Prior to initiating specific aim 2, the binding affinity of Tw1S4_6 scFv was matured. The rationale behind this is to generate an affinity range of antibodies that, when used in *in vivo* biodistribution and targeting experiments, could identify an optimal affinity for targeting metastatic lesions, in a preclinical setting. The affinity maturation approach was reliant upon mutagenesis of key residues within complementarity determining regions of Tw1S4_6 scFv. This approach is meant to simulate the process of somatic hypermutation that occurs in the latter stages of B-cell maturation in vivo[131]. In brief, CDR3 of Tw1S4_6 scFv light chain was mutagenized at seven amino acid residues with a primer containing degenerate codons. A second PCR on the resulting mutagenized template is performed to add the remaining 3' terminal sequence that includes the Not1 restriction site for restriction digestion and re-insertion into pHEN phagemid vector (Figure 1). This process resulted in the generation of a new surface display library comprised entirely of mutagenized Tw1S4_6 scFv. Critical to this approach is the generation of a large amount of sequence diversity, estimated by dilution plate titering of the initial bacterial transformation. The estimated diversity of the new Tw1S4_6 scFv affinity matured library (AFFMAT) was $2.5*10^6$. It is suggested that $>10^7$ transformants should be obtained prior to initiating a new panning procedure. Given our lack of access to electroporation equipment, which can dramatically improve bacterial transformation efficiency, the new AFFMAT library was deemed sufficiently diverse to start a new round of cell based panning experiments.

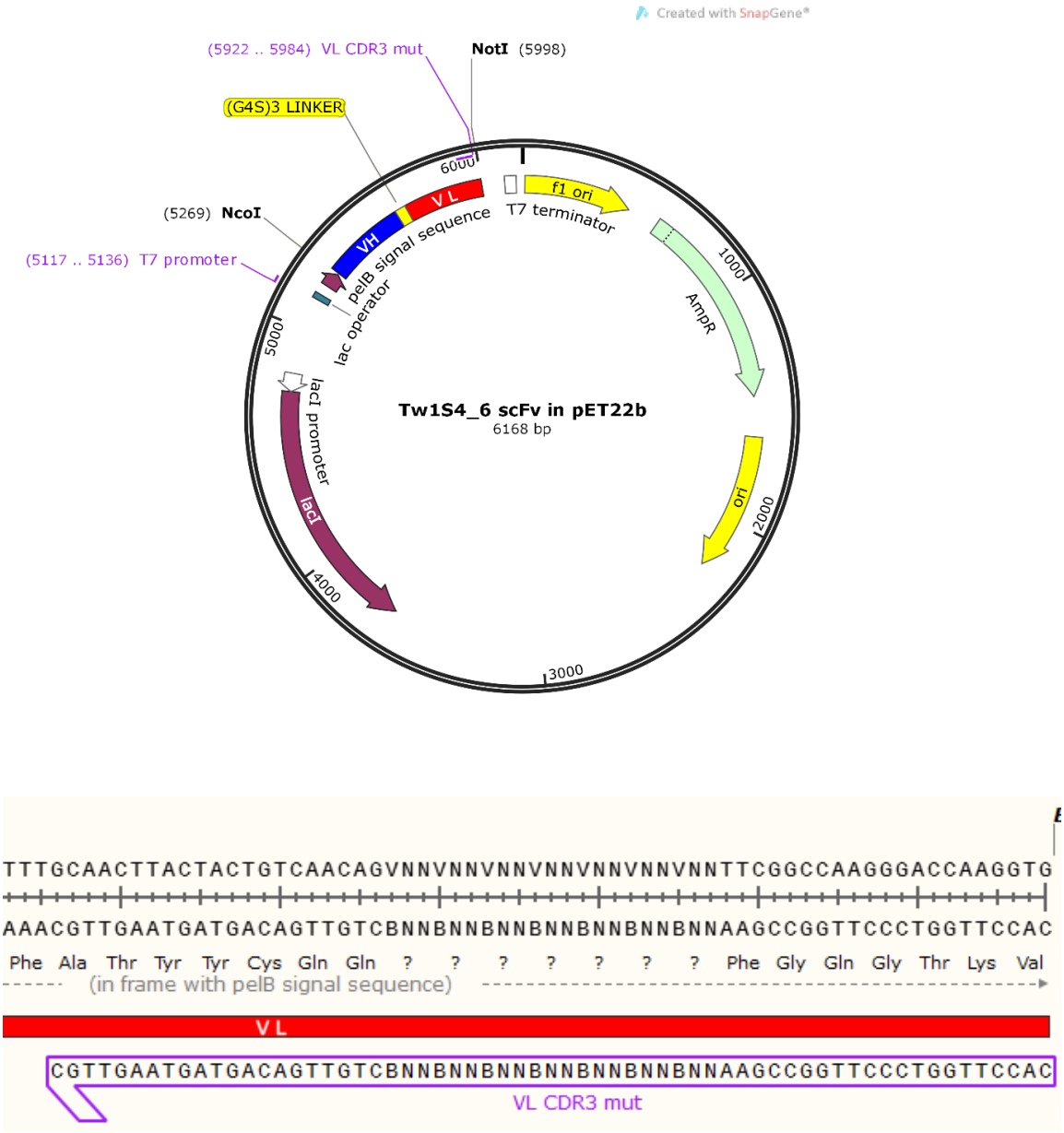

Figure 1 – Tw1S4_ scFv affinity maturation schematic. The third complementarity determining region of the light chain from Tw1S4_6 scFv is used as a template for affinity maturation. Seven amino acids within VL CDR3 are subjected to random mutagenesis using a primer containing a degenerate primer at the site where sequence diversity is introduced.

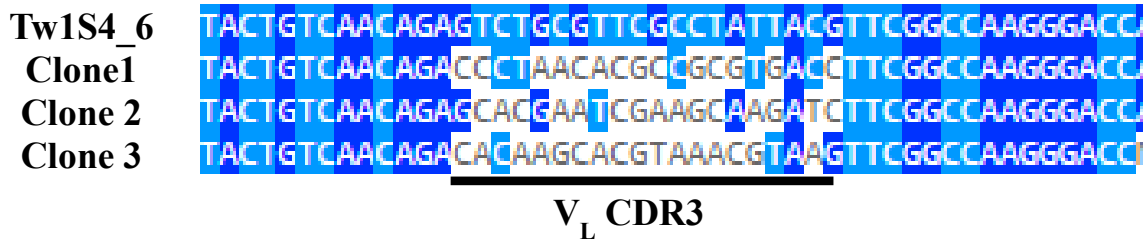

Figure 2 Confirmation of sequence diversity introduced into V_L CDR3. Following bacterial transformation, Three random colonies were picked for plasmid preparation and subsequent DNA sequencing. Sequence alignment with the original Tw1S4_6 scFv confirms the mutagenesis strategy was focused within V_LCDR3

Sequencing of three random clones from the AFFMAT library was used to confirm the successful introduction of diversity (Figure 2). A cell sorting procedure was used to select for phage displaying increased binding to LM2 cells from the AFFMAT library. Bound phage were detected using fluorescent mouse IgG recognizing the Myc tag. Following the cell sorting procedure, screening of candidate affmat clones led to the identification of Tw1S4_AM6, which was subsequently formatted to IgG as outlined in chapter 2 (data not shown). Tw1S4_AM6 demonstrated a substantial improvement in the apparent binding affinity, with an apparent Kd estimated from flow cytometric staining of target cell lines LM2 and M12 of 10 nM. The parent antibody, Tw1S4_6, displays an apparent Kd between 125 to 275 nM by flow cytometry (Figure 3 A-D). An important note on flow cytometry based titration curves is the potential for avidity affects to contribute to binding. Avidity represents the cumulative affects of multiple monovalent interactions, resulting in a net reduction in kinetic dissociation rates, which can lead to an overestimation of the true equilibrium dissociation constant, K_d. Biophysical techniques are most often employed to generate the true equilibrium K_d value. We chose biolayer interferometry as a means of assessing the kinetics of our antibody–antigen pair. HSPG2_D1 was

immobilized via Ni_NTA biosensor, and incubated with concentration ranges of our two candidate antibodies designed to capture the true K_d. Surprisingly, the parent antibody Tw1S4_6 returned a very modest K_d value in the µM range (Figure 4). Affinity matured Tw1S4_AM6 demonstrated substantial monovalent affinity improvement to HSPG2_D1, having a K_d value of 80 nM (Figure 4).

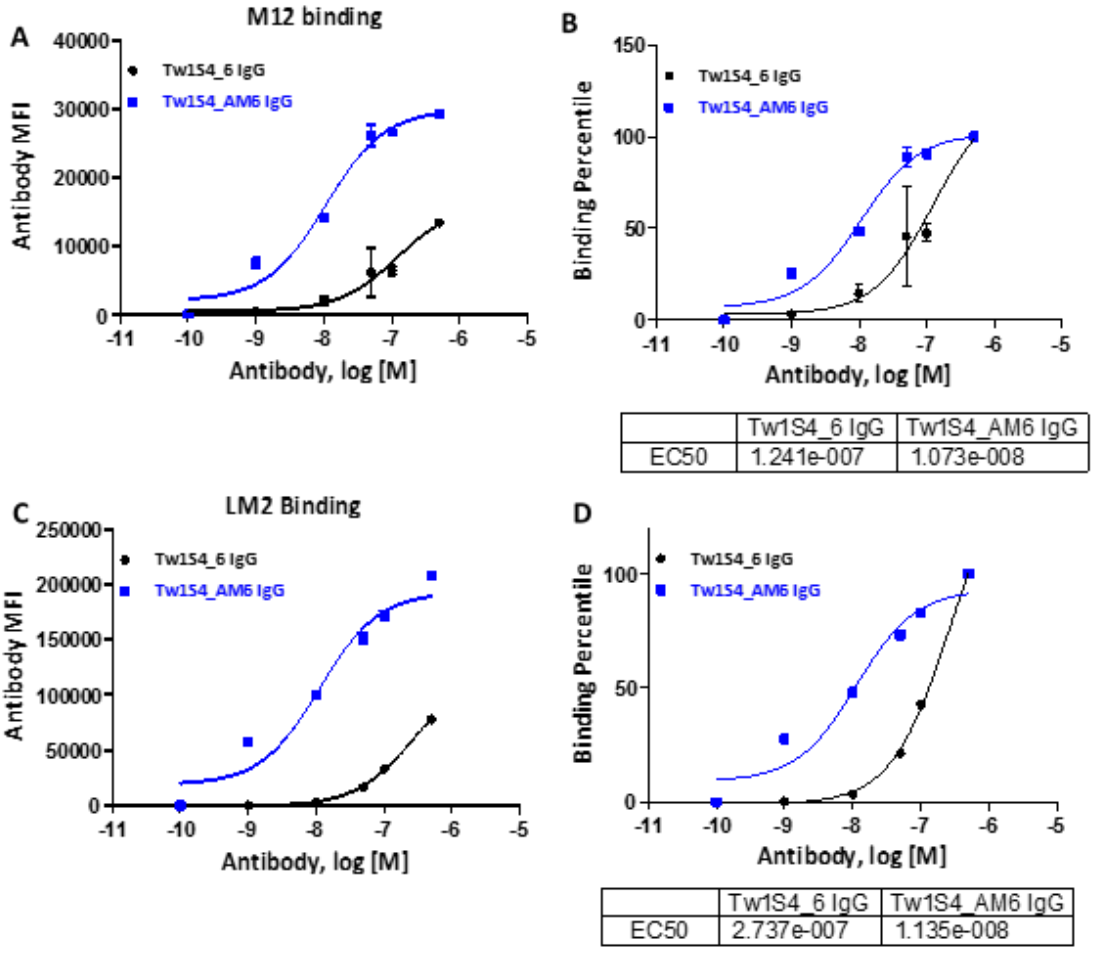

	Tw1S4_6 IgG	Tw1S4_AM6 IgG
EC50	1.241e-007	1.073e-008

	Tw1S4_6 IgG	Tw1S4_AM6 IgG
EC50	2.737e-007	1.135e-008

Figure 3 Tw1S4_6 and Tw1S4_AM6 IgG cell binding (A,C) flow cytometry determination of relative binding affinities ofTw1S4_6 and Tw1S4_AM6 IgG to (A) M12 cells and (C) LM2 cells at the indicated concentration range. IgG binding was detected with a goat-anti human IgG Dylight 647 conjugate and is presented as raw signal intensity. (B,D) Percentile normalization of raw signal intensity data from (A) and (C) is presented to observe a shift in apparent affinity. EC50 values represent molar antibody concentrations

at which 50% of maximal binding is achieved, and are representative of "apparent Kd" values

A

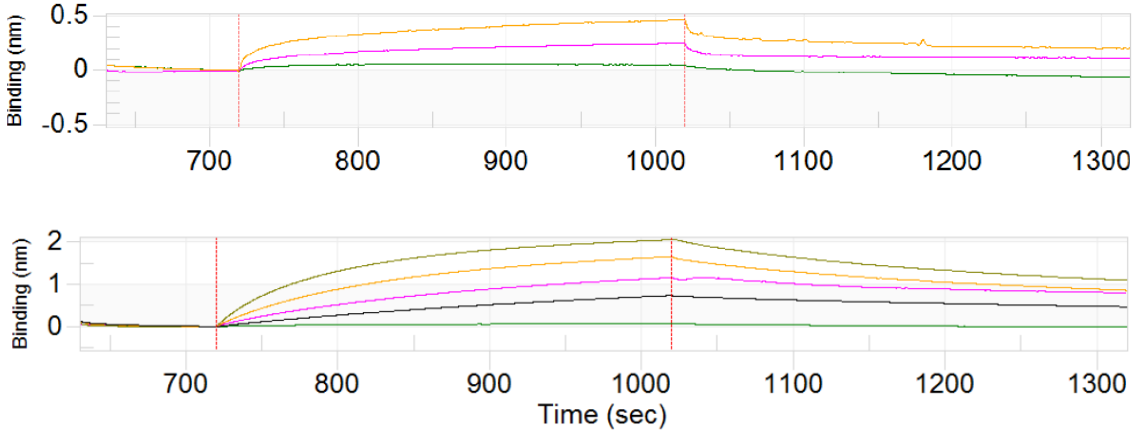

B

Antibody	k_{on} $M^{-1}*s^{-1}$	k_{off} s^{-1}	Kd (M)
Tw1S4_6 IgG	6.14e3	1.09e-2	**1.79e-6**
Tw1S4_AM6 IgG	2.84e4	2.25e-3	**7.93e-8**

Figure 4 – Biolayer Interferometry - Tw1S4 antibody binding to HSPG2 domain 1

We next explored the *in vitro* influence of HSPG2 targeted antibodies on the behavior of our metastatically predisposed cell lines, LM2 and M12. We first assessed the antibodies' ability to influence the proliferation of target cell lines. Our hypothesis was based on previous observations indicating the influence of heparan sulfate side chains as low affinity growth factor coreceptors, a number of which have been implicated in aberrant signaling patterns in cancer.[132] As predicted, a dose dependent cytostatic effect was observed for both the initial and affinity matured antibodies in target cell lines LM2 and M12 at 48 hours post treatment (Figure 5). Simultaneous analysis of apoptotic index using Annexin-FITC and propidium iodide costaining of antibody treated cells did not reveal an

increase in either early (Figure 6 – lower right quadrants) or late (Figure 6 – upper left quadrants) stage apoptotic cells.

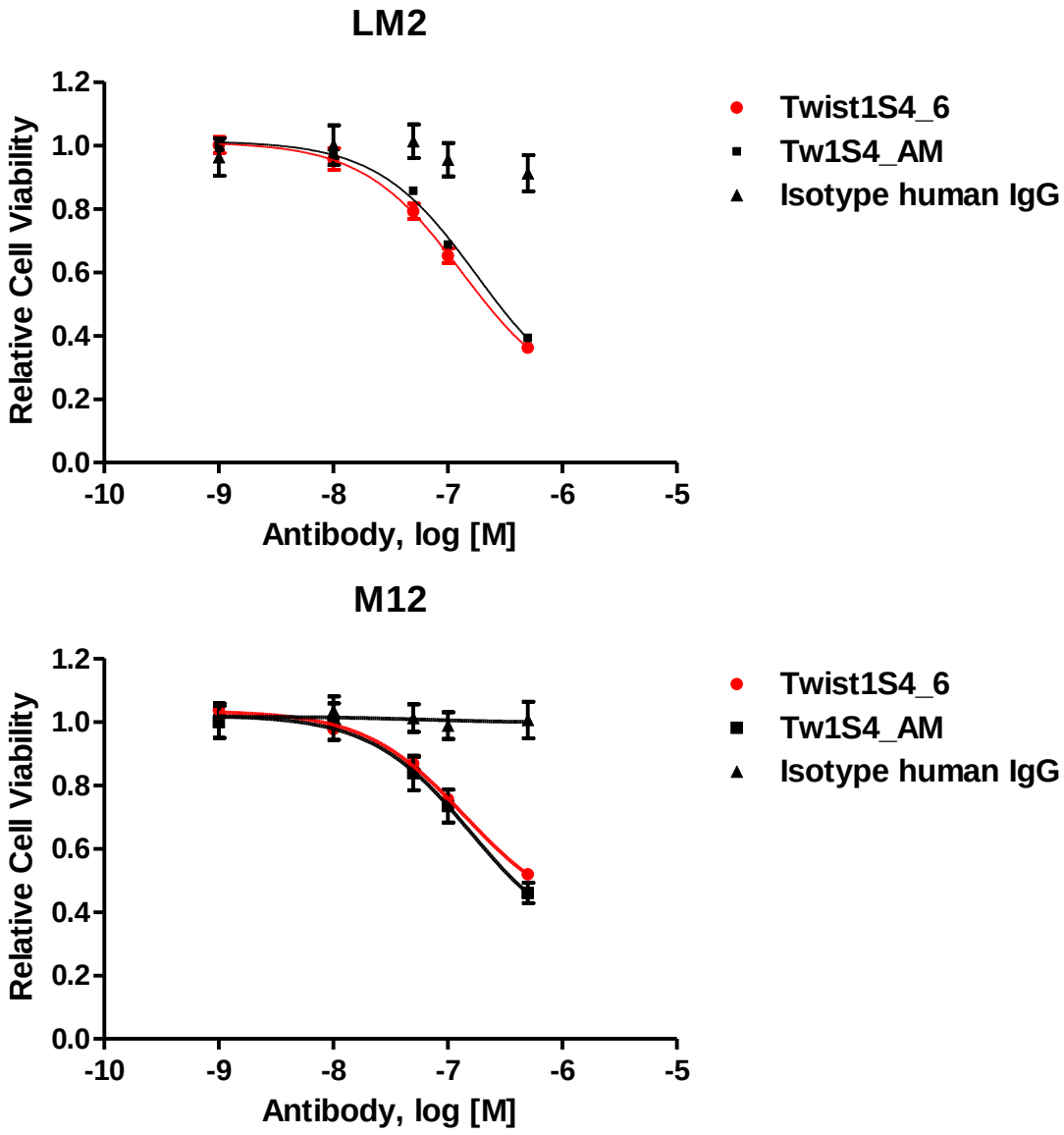

Figure 5 – Cytostatic effects of Tw1S46 and Tw1S4_AM6 in target cell lines. A dose dependent inhibition of LM2 cell proliferation (Top Panel) 48 hours post-treatment was observed for both therapeutic antibodies. Isotype human IgG1 was used as a positive control. (Bottom Panel) a similar cytostatic effect was observed in M12 cells 48 hours post-treatment.

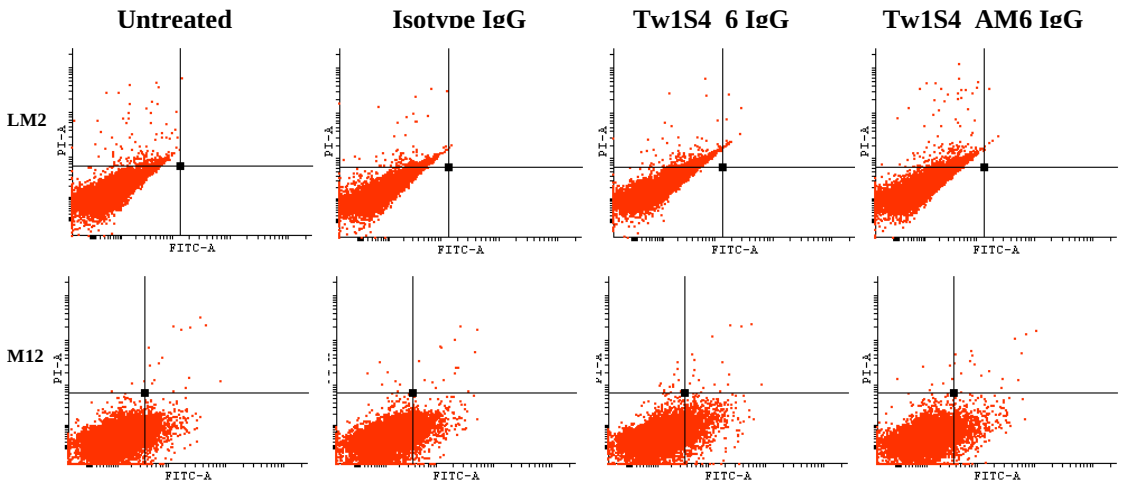

Figure 6 – assessment of Tw1S4 antibody treatment on apoptosis in target cell lines. Cell lines were treated for 48 hours with 100nM of the indicated antibody, along with untreated control cells. X-axis represents FITC Annexin V positivity, an indicator of early stage apoptosis. Y-axis represents positive staining for viability dye propidium iodide. Moving counterclockwise from bottom right quadrant determines early to late stage apoptotic transition.

The preliminary results indicated a reduced rate of proliferation of cells treated with Tw1S4 antibodies, with no indication of induction of apoptosis. Cell cycle analysis revealed a prominent decrease in S phase percentage, with 19.8% of LM2 cells in S phase for isotype treated cells, while Tw1S4 and Tw1S4_AM6 had 11.8 and 12.5% respectively (Figure 7 and Table 1). An increase in G0/G1 percentage relative to isotype treated cells was observed, with isotype treated cells having 56.2% of cells in G0/G1, while Tw1S4 and and Tw1S4_AM6 treated cells had 69.9 and 69.7% of cells in G0/G1 respectively (Figure 7 and Table 1). Collectively, the preliminary *in vitro* characterization of Tw1S4 antibody treated cells reveals a cytostatic mechanism of action.

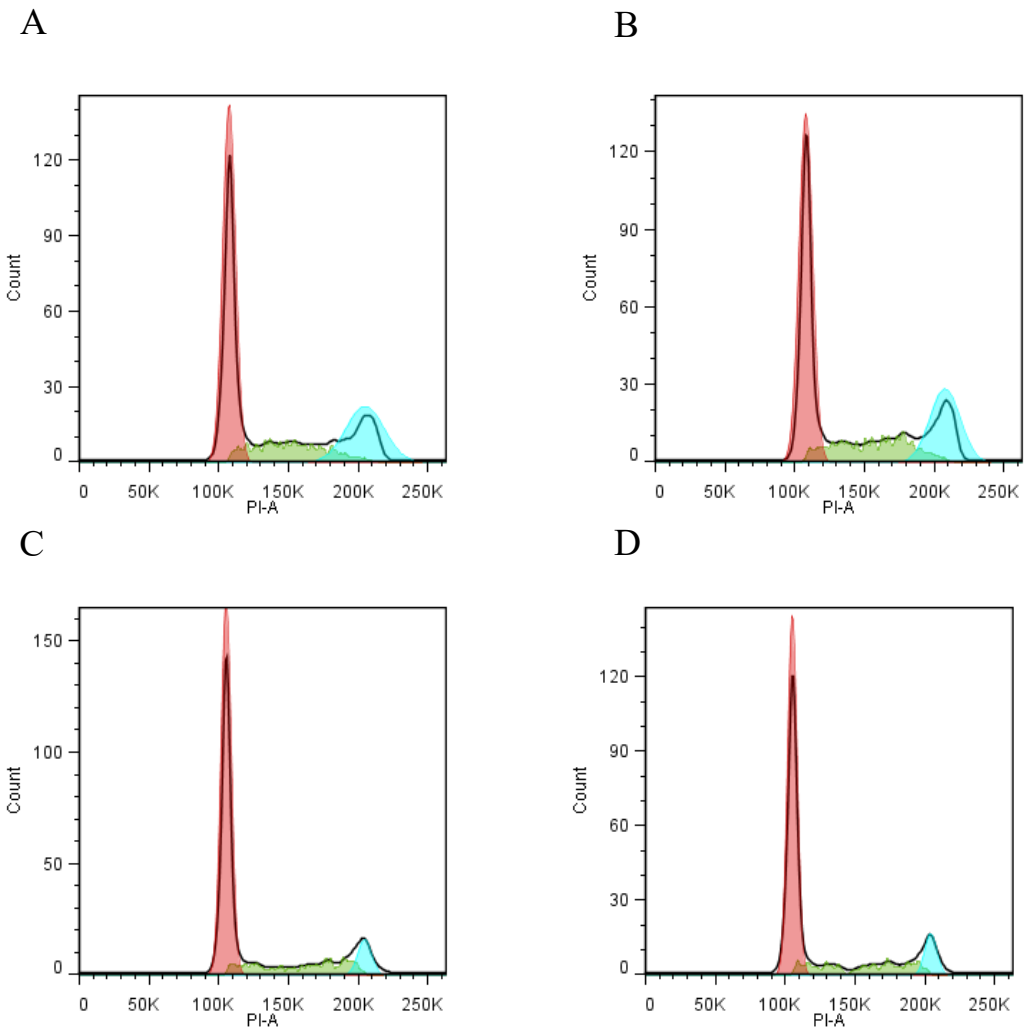

Figure 7 Cell cycle analysis of Tw1S4 antibody treated target cell line LM2. Cells were treated for 48 hours with 100nM of the indicated antibody, followed by fixation and permeabilization with 70% ethanol, and staining with PI. Shaded red histogram represents G1, shaded green represents S phase, and turquoise represents G2/M. (A) untreated cells, (B) 100nM isotype human IgG, (C) 100nM Tw1S4_6 and (D) 100nM Tw1S4_AM6 IgG

		LM2			M12	
	G1 %	S %	G2/M %	G1 %	S %	G2/M %
untreated	**61.1**	**18.6**	**20.3**	**40.8**	**14.3**	**44.8**
Std. Dev.	*1.9*	*0.3*	*1.5*	*1.9*	*0.4*	*1.5*
Isotype	**56.2**	**19.8**	**24**	**42.4**	**15.1**	**42.5**
Std. Dev.	*1.4*	*1.1*	*0.3*	*1.7*	*0.6*	*1.1*
Tw1S4_6	**69.9**	**11.8**	**18.3**	**50.7**	**16.5**	**32.7**
Std. Dev.	*0.9*	*0.2*	*1.1*	*1.6*	*1.9*	*1.3*
Tw1S4 AM6	69.7	**12.5**	**17.8**	**51.5**	**14.2**	**34.2**
Std. Dev.	*1.4*	*0.9*	*0.8*	*2.9*	*0.8*	*2.5*

Table 1 – Cell cycle analysis in antibody treated cell lines. The results from cell cycle analysis of antibody treated cell lines are presented as mean and standard deviation percent of total population. Cells were treated in duplicate. Data was analyzed with the FlowJo software version 7.6.5. using the Watson model for analysis.

We next established orthotopic xenografts of LM2 cells in nude mice to determine whether the *in vitro* cytostatic effects observed could be extended to an in vivo model of tumor growth inhibition. Three doses of antibody were administered systemically at 5 mg/kg. Isotype human IgG was used as a positive control, along with saline negative control (n=3 mice/group). Surprisingly, the original Tw1S4_6 IgG produced negligible tumor growth inhibition relative to the isotype control treated group (Figure 8). The affinity matured variant did however produce a pronounced inhibition of tumor growth, having mean tumor volumes of 500 mm^3 at day 22, relative to saline and isotype control groups, which had mean tumor volumes >1,500mm^3 at the same time point.

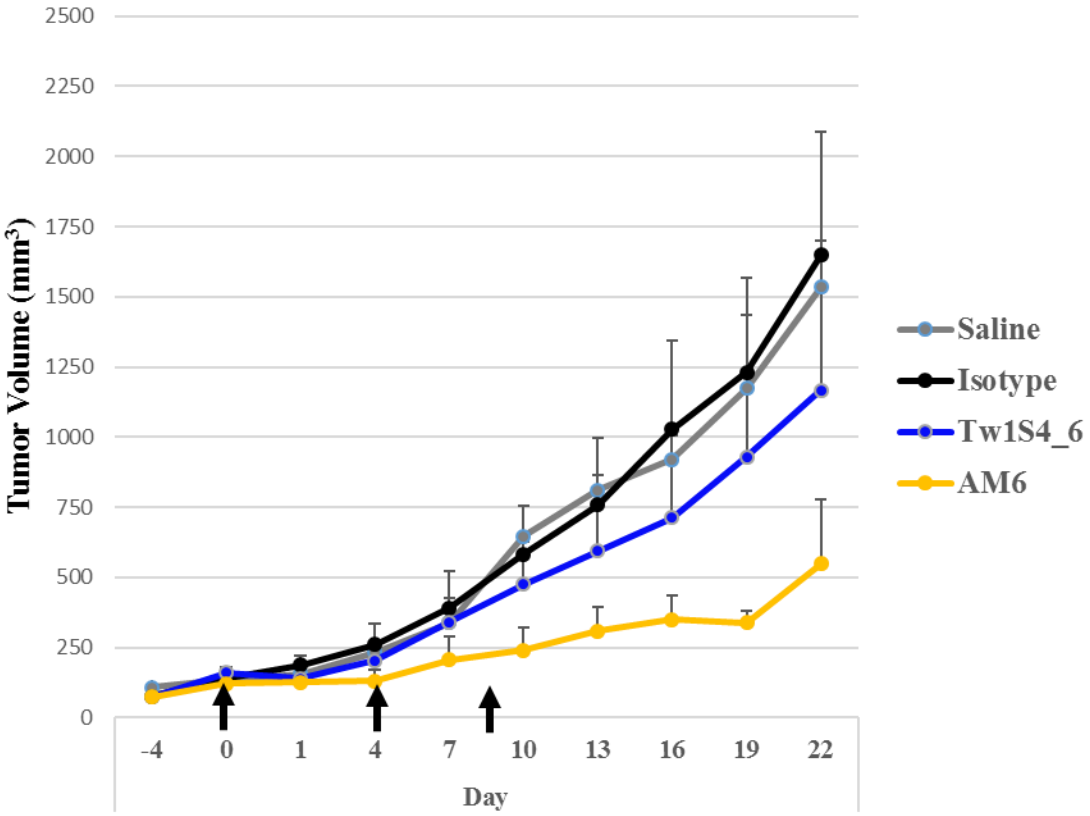

Figure 8 – **Therapeutic efficacy of perlecan (HSPG2) targeted antibodies.** LM2 cells were grafted orthotopically into mammary pad of nude mice. Once tumors reached 100mm^3, animals were randomized into 4 groups receiving saline, human IgG isotype, Tw1S4_6, or Tw1S4_AM6 IgG. Three doses every fourth day of 5mg/kg antibody was administered systemically (black arrows indicate dosing schedule). Tumor volumes were monitored longitudinally via a digital calipers.

Discussion

A two antibody panel spanning an order of magnitude in affinity towards perlecan has been developed from a phage display whole cell phenotype screening. A hard randomization approach for affinity maturation was employed to randomize light chain CDR3 of our initial candidate scFv, Tw1S4_6. Subsequent panning experiments led to the identification of an affinity matured variant, Tw1S4_AM6, whose K_d value, as revealed by biolayer techniques, was observed to be 80 nM against perlecan domain 1. This represents

a substantial affinity improvement from Tw1S4_6, which had K_d value in the μM range. This is a promising result in the context of previously reported affinity maturation procedures, which often work sequentially to mutagenize multiple CDRs, with lead candidates being selected as templates for subsequent rounds of mutagenesis.[133] These approaches, termed 'CDR walking', can lead to scFv displaying picomolar affinity to cell surface antigens, when used in conventional target based screening.[134] The affinity maturation approach for Tw1S4_6, relying solely on light chain CDR3 mutagenesis, should be considered as an incomplete or partial maturation protocol. Given the observed K_d value of 80 nM for the affinity matured Tw1S4_AM6, affinity improvements could certainly still be realized. This also suggests that further improvements in affinity of our perlecan targeted antibody panel should generate antibodies with even greater *in vivo* efficacy in the future. When considering the pharmacokinetic modeling of the previous chapter, an antibody affinity of 80 nM would not have reached the 'affinity sweet spot' of roughly 10 nM K_d, wherein maximal effect would be predicted prior to approaching the binding site barrier.

The preliminary *in vitro* pharmacological effects of our perlecan-targeted antibodies are consistent with the profile of growth factor receptor targeted antibodies. The *in vitro* effects reported previously for cetuximab, the first FDA approved EGFR targeted antibody,[135] closely mirror those observed for our perlecan targeted antibody panel. Of note, cetuximab treatment results in an almost identical cell cycle arrest profile to that observed for our perlecan targeted antibodies, with a 50% reduction in S phase, and corresponding increase in G0/G1, in squamous cell carcinoma.[136] Perlecan targeted

antibodies produced a pronounced cytostatic effect that is revealed by a reduction in cancer cell proliferation, and is coupled to the cell cycle arrest profile observed for Cetuximab. A lack of observed induction of apoptosis suggests that these antibodies may act via competitive inhibition or receptor downregulation mechanisms, to block the growth factor co-receptor function of cell surface affiliated perlecan and subsequent signal transduction.

The pilot *in vivo* efficacy experiments suggest that further refinement of the dosing schedule will be required to achieve durable responses. It is worth noting that antibody dosing of 5 mg/kg is low relative other anti-cancer antibodies. In rodent xenograft models, reported dosing range from 10 – 40 mg/kg for the EGFR targeted antibody Cetuximab for at least five doses.[137] A dosing schedule of thrice weekly for 10 weeks at 17 mg/kg of cetuximab lead to sustained remission of pancreatic carcinoma grafts.[138] Similar cetuximab dosing has been used effectively in preclinical breast cancer xenografts to overcome trastuzumab resistance.[139] Even with sub-optimal dosing, the observation that the affinity matured, perlecan-targeted IgG can dramatically impede tumor growth is a promising result.

CHAPTER 6: SUMMARY AND FUTURE DIRECTIONS

The goal of this thesis is focused on the development of diagnostic and therapeutic antibodies for MBC. In order to accomplish this goal, phage display scFv libraries were employed to derive antibody variable domains that can selectively discriminate EMT cells. Once a candidate scFv was identified, target deconvolution approaches were performed to identify the binding partner. This led to the identification of HSPG2, or perlecan, as the binding partner of the EMT selective antibody. Although the precise epitope recognized within HSPG2 is still unclear, it likely resides within the first domain of HSPG2, a site known to contain extensive glycosylation patterns. This suggests the potential for a unique glycosylation pattern within HSPG2 that is present on the surface of EMT cells, and could conceivably represent a novel tumor associated antigen. Future work will focus on providing a more rigorous mapping of the HSPG2 epitope recognized by the antibody.

Diagnostic antibody development for MBC was focused on the evaluation of EMT targeted antibodies for *in vivo* detection and characterization of CTCs. The initial approach focused on bivalent forms of antibody variable domains, termed diabodies, to capture EpCAM negative CTCs. This approach, outlined in chapter three, proved successful in identifying CTC subpopulations that are EpCAM negative. Owing to practical concerns, the focus shifted to humanized IgG forms of our candidate EMT targeted scFv in all subsequent work. The full length antibody provided a corroborating dataset to that of the diabody. EpCAM negative CTC populations were identified using *in vivo* xenograft models of breast cancer. This methodology will be extended to clinical patient samples in

the future to facilitate the inclusion of EMT targeted antibodies into existing immunomagnetic CTC capture platforms.

The second goal of this thesis was to develop therapeutic antibodies for MBC. The rationale behind this approach is based on the aforementioned ability to selectively target EMT cells with humanized antibodies. Affinity maturation proved essential to this goal, as our initial candidate antibody did not demonstrate sufficient *in vivo* tumor growth inhibition. The in vitro pharmacology of EMT targeted antibodies closely mirrors that of existing GF receptor targeted antibodies, cetuximab being a primary example. The effects observed were cytostatic. Reduction in the rate of cell proliferation was observed in the metastatically predisposed cell lines LM2 and M12. This was coupled to an arrest in the cell cycle dynamics of antibody treated cells. Future work will focus on covalent modification of the existing antibodies to generate drug conjugate forms. This could improve the efficacy substantially.

References

1. Cancer Facts and Figures 2016. 2016.
2. Pantel K, Müller V, Auer M, Nusser N, Harbeck N, Braun S. Detection and clinical implications of early systemic tumor cell dissemination in breast cancer. *Clin Cancer Res*. 2003;9(17):6326-6334.
3. Patani N, Mokbel K. Clinical significance of sentinel lymph node isolated tumour cells in breast cancer. *Breast Cancer Res Treat*. 2011;127(2):325-334.
4. Beslija S, Bonneterre J, Burstein H, et al. Second consensus on medical treatment of metastatic breast cancer. *Ann Oncol*. 2007;18(2):215-225.
5. Bonnomet A, Brysse A, Tachsidis A, et al. Epithelial-to-mesenchymal transitions and circulating tumor cells. *J Mammary Gland Biol Neoplasia*. 2010;15(2):261-273.
6. Malhotra GK, Zhao X, Band H, Band V. Histological, molecular and functional subtypes of breast cancers. *Cancer Biol Ther*. 2010;10(10):955-960.
7. Kalluri R, Zeisberg M. Fibroblasts in cancer. *Nat Rev Cancer*. 2006;6(5):392-401.
8. Kennecke H, Yerushalmi R, Woods R, et al. Metastatic behavior of breast cancer subtypes. *J Clin Oncol*. 2010;28(20):3271-3277.
9. Gaedcke J, Traub F, Milde S, et al. Predominance of the basal type and HER-2/neu type in brain metastasis from breast cancer. *Mod Pathol*. 2007;20(8):864-870.
10. Sarrió D, Rodriguez-Pinilla SM, Hardisson D, Cano A, Moreno-Bueno G, Palacios J. Epithelial-mesenchymal transition in breast cancer relates to the basal-like phenotype. *Cancer Res*. 2008;68(4):989-997.
11. Blick T, Widodo E, Hugo H, et al. Epithelial mesenchymal transition traits in human breast cancer cell lines. *Clin Exp Metastasis*. 2008;25(6):629-642.
12. Blick T, Hugo H, Widodo E, et al. Epithelial mesenchymal transition traits in human breast cancer cell lines parallel the CD44(hi/)CD24 (lo/-) stem cell phenotype in human breast cancer. *J Mammary Gland Biol Neoplasia*. 2010;15(2):235-252.
13. Braun S, Vogl FD, Naume B, et al. A pooled analysis of bone marrow

micrometastasis in breast cancer. *N Engl J Med*. 2005;353(8):793-802.

14. Cristofanilli M, Budd GT, Ellis MJ, et al. Circulating tumor cells, disease progression, and survival in metastatic breast cancer. *N Engl J Med*. 2004;351(8):781-791.
15. Hayes DF, Cristofanilli M, Budd GT, et al. Circulating tumor cells at each follow-up time point during therapy of metastatic breast cancer patients predict progression-free and overall survival. *Clin Cancer Res*. 2006;12(14 Pt 1):4218-4224.
16. Kallergi G, Papadaki MA, Politaki E, Mavroudis D, Georgoulias V, Agelaki S. Epithelial to mesenchymal transition markers expressed in circulating tumour cells of early and metastatic breast cancer patients. *Breast Cancer Res*. 2011;13(3):R59.
17. Mego M, Mani SA, Lee B-N, et al. Expression of epithelial-mesenchymal transition-inducing transcription factors in primary breast cancer: The effect of neoadjuvant therapy. *Int J cancer*. 2012;130(4):808-816.
18. Raimondi C, Gradilone A, Naso G, et al. Epithelial-mesenchymal transition and stemness features in circulating tumor cells from breast cancer patients. *Breast Cancer Res Treat*. 2011;130(2):449-455.
19. Polyak K, Weinberg RA. Transitions between epithelial and mesenchymal states: acquisition of malignant and stem cell traits. *Nat Rev Cancer*. 2009;9(4):265-273.
20. Tsuji T, Ibaragi S, Shima K, et al. Epithelial-mesenchymal transition induced by growth suppressor p12CDK2-AP1 promotes tumor cell local invasion but suppresses distant colony growth. *Cancer Res*. 2008;68(24):10377-10386.
21. Velasco-Velázquez MA, Popov VM, Lisanti MP, Pestell RG. The role of breast cancer stem cells in metastasis and therapeutic implications. *Am J Pathol*. 2011;179(1):2-11.
22. Smalley M, Ashworth A. Stem cells and breast cancer: A field in transit. *Nat Rev Cancer*. 2003;3(11):832-844.
23. Al-Hajj M, Wicha MS, Benito-Hernandez A, Morrison SJ, Clarke MF. Prospective identification of tumorigenic breast cancer cells. *Proc Natl Acad Sci U S A*. 2003;100(7):3983-3988.

24. Mani SA, Guo W, Liao M-J, et al. The epithelial-mesenchymal transition generates cells with properties of stem cells. *Cell*. 2008;133(4):704-715.
25. Brabletz T, Jung A, Spaderna S, Hlubek F, Kirchner T. Opinion: migrating cancer stem cells - an integrated concept of malignant tumour progression. *Nat Rev Cancer*. 2005;5(9):744-749.
26. Zhang L, Ridgway LD, Wetzel MD, et al. The identification and characterization of breast cancer CTCs competent for brain metastasis. *Sci Transl Med*. 2013;5(180):180ra48.
27. Baccelli I, Schneeweiss A, Riethdorf S, et al. Identification of a population of blood circulating tumor cells from breast cancer patients that initiates metastasis in a xenograft assay. *Nat Biotechnol*. 2013;31(6):539-544.
28. Slamon DJ, Leyland-Jones B, Shak S, et al. Use of chemotherapy plus a monoclonal antibody against HER2 for metastatic breast cancer that overexpresses HER2. *N Engl J Med*. 2001;344(11):783-792.
29. Swain SM, Baselga J, Kim S-B, et al. Pertuzumab, trastuzumab, and docetaxel in HER2-positive metastatic breast cancer. *N Engl J Med*. 2015;372(8):724-734.
30. Verma S, Miles D, Gianni L, et al. Trastuzumab emtansine for HER2-positive advanced breast cancer. *N Engl J Med*. 2012;367(19):1783-1791.
31. Targeted therapy for breast cancer. 2015.
32. Millner LM, Linder MW, Valdes RJ. Circulating Tumor Cells: A Review of Present Methods and the Need to Identify Heterogeneous Phenotypes. *Ann Clin Lab Sci*. 2013;43(3):295-304.
33. Yu M, Bardia A, Wittner BS, et al. Circulating breast tumor cells exhibit dynamic changes in epithelial and mesenchymal composition. *Science*. 2013;339(6119):580-584.
34. Sarioglu AF, Aceto N, Kojic N, et al. A microfluidic device for label-free, physical capture of circulating tumor cell clusters. *Nat Methods*. 2015;12(7):685-691.
35. Van Poznak C, Somerfield MR, Bast RC, et al. Use of Biomarkers to Guide Decisions on Systemic Therapy for Women With Metastatic Breast Cancer: American Society of Clinical Oncology Clinical Practice Guideline. *J Clin Oncol*.

2015;33(24):2695-2704.

36. Yu M, Bardia A, Aceto N, et al. Cancer therapy. Ex vivo culture of circulating breast tumor cells for individualized testing of drug susceptibility. *Science*. 2014;345(6193):216-220.
37. Rhim AD, Mirek ET, Aiello NM, et al. EMT and dissemination precede pancreatic tumor formation. *Cell*. 2012;148(1-2):349-361.
38. Armstrong AJ, Marengo MS, Oltean S, et al. Circulating tumor cells from patients with advanced prostate and breast cancer display both epithelial and mesenchymal markers. *Mol Cancer Res*. 2011;9(8):997-1007.
39. Lecharpentier A, Vielh P, Perez-Moreno P, Planchard D, Soria JC, Farace F. Detection of circulating tumour cells with a hybrid (epithelial/mesenchymal) phenotype in patients with metastatic non-small cell lung cancer. *Br J Cancer*. 2011;105(9):1338-1341.
40. Lim SHS, Becker TM, Chua W, Ng WL, de Souza P, Spring KJ. Circulating tumour cells and the epithelial mesenchymal transition in colorectal cancer. *J Clin Pathol*. 2014;67(10):848-853.
41. Zhang L, Ridgway LD, Wetzel MD, et al. The identification and characterization of breast cancer CTCs competent for brain metastasis. *Sci Transl Med*. 2013;5(180):180ra48.
42. Baccelli I, Schneeweiss A, Riethdorf S, et al. Identification of a population of blood circulating tumor cells from breast cancer patients that initiates metastasis in a xenograft assay. *Nat Biotechnol*. 2013;31(6):539-544.
43. Baccelli I, Trumpp A. The evolving concept of cancer and metastasis stem cells. *J Cell Biol*. 2012;198(3):281-293.
44. Lee J, Bogyo M. Target deconvolution techniques in modern phenotypic profiling. *Curr Opin Chem Biol*. 2013;17(1):118-126.
45. Swinney DC, Anthony J. How were new medicines discovered? *Nat Rev Drug Discov*. 2011;10(7):507-519.
46. Decarlo AA, Belousova M, Ellis AL, et al. Perlecan domain 1 recombinant proteoglycan augments BMP-2 activity and osteogenesis. *BMC Biotechnol*.

2012;12:60.

47. Elenbaas B. Human breast cancer cells generated by oncogenic transformation of primary mammary epithelial cells. *Genes Dev*. 2001;15(1):50-65.
48. Gupta PB, Onder TT, Jiang G, et al. Identification of selective inhibitors of cancer stem cells by high-throughput screening. *Cell*. 2009;138(4):645-659.
49. Taube JH, Herschkowitz JI, Komurov K, et al. Core epithelial-to-mesenchymal transition interactome gene-expression signature is associated with claudin-low and metaplastic breast cancer subtypes. *Proc Natl Acad Sci U S A*. 2010;107(35):15449-15454.
50. Yang J, Mani SA, Donaher JL, et al. Twist, a master regulator of morphogenesis, plays an essential role in tumor metastasis. *Cell*. 2004;117(7):927-939.
51. Mani SA, Guo W, Liao M-J, et al. The epithelial-mesenchymal transition generates cells with properties of stem cells. *Cell*. 2008;133(4):704-715.
52. Lee CMY, Iorno N, Sierro F, Christ D. Selection of human antibody fragments by phage display. *Nat Protoc*. 2007;2(11):3001-3008.
53. Minn AJ, Gupta GP, Siegel PM, et al. Genes that mediate breast cancer metastasis to lung. *Nature*. 2005;436(7050):518-524.
54. Bumol TF, Reisfeld RA. Unique glycoprotein-proteoglycan complex defined by monoclonal antibody on human melanoma cells. *Proc Natl Acad Sci U S A*. 1982;79(4):1245-1249.
55. Khoja L, Shenjere P, Hodgson C, et al. Prevalence and heterogeneity of circulating tumour cells in metastatic cutaneous melanoma. *Melanoma Res*. 2014;24(1):40-46.
56. Ulmer A. Immunomagnetic Enrichment, Genomic Characterization, and Prognostic Impact of Circulating Melanoma Cells. *Clin Cancer Res*. 2004;10(2):531-537.
57. Schmidt P, Kopecky C, Hombach A, Zigrino P, Mauch C, Abken H. Eradication of melanomas by targeted elimination of a minor subset of tumor cells. *Proc Natl Acad Sci U S A*. 2011;108(6):2474-2479.
58. Cohen IR, Murdoch AD, Naso MF, Marchetti D, Berd D, Iozzo R V. Abnormal expression of perlecan proteoglycan in metastatic melanomas. *Cancer Res*.

1994;54(22):5771-5774.

59. DeRose YS, Wang G, Lin Y-C, et al. Tumor grafts derived from women with breast cancer authentically reflect tumor pathology, growth, metastasis and disease outcomes. *Nat Med*. 2011;17(11):1514-1520.
60. Kalluri R, Weinberg RA. The basics of epithelial-mesenchymal transition. *J Clin Invest*. 2009;119(6):1420-1428.
61. Lawson DA, Bhakta NR, Kessenbrock K, et al. Single-cell analysis reveals a stem-cell program in human metastatic breast cancer cells. *Nature*. 2015;526(7571):131.
62. Wang ZH, Manabe T, Ohshio G, et al. Immunohistochemical study of heparan sulfate proteoglycan in adenocarcinomas of the pancreas. *Pancreas*. 1994;9(6):758-763.
63. Davies EJ, Blackhall FH, Shanks JH, et al. Distribution and clinical significance of heparan sulfate proteoglycans in ovarian cancer. *Clin Cancer Res*. 2004;10(15):5178-5186.
64. Ikarashi T, Ida-Yonemochi H, Ohshiro K, Cheng J, Saku T. Intraepithelial expression of perlecan, a basement membrane-type heparan sulfate proteoglycan reflects dysplastic changes of the oral mucosal epithelium. *J Oral Pathol Med*. 2004;33(2):87-95.
65. Hammond E, Khurana A, Shridhar V, Dredge K. The Role of Heparanase and Sulfatases in the Modification of Heparan Sulfate Proteoglycans within the Tumor Microenvironment and Opportunities for Novel Cancer Therapeutics. *Front Oncol*. 2014;4:195.
66. Nakajima M, Irimura T, Di Ferrante D, Di Ferrante N, Nicolson GL. Heparan sulfate degradation: relation to tumor invasive and metastatic properties of mouse B16 melanoma sublines. *Science*. 1983;220(4597):611-613.
67. Fernández-Vega I, García O, Crespo A, et al. Specific genes involved in synthesis and editing of heparan sulfate proteoglycans show altered expression patterns in breast cancer. *BMC Cancer*. 2013;13:24. doi:10.1186/1471-2407-13-24.
68. Koliopanos A, Friess H, Kleeff J, et al. Heparanase Expression in Primary and Metastatic Pancreatic Cancer. *Cancer Res*. 2001;61(12):4655-4659.

69. Zhang L, Riethdorf S, Wu G, et al. Meta-analysis of the prognostic value of circulating tumor cells in breast cancer. *Clin Cancer Res*. 2012;18(20):5701-5710.
70. Harris L, Fritsche H, Mennel R, et al. American Society of Clinical Oncology 2007 update of recommendations for the use of tumor markers in breast cancer. *J Clin Oncol*. 2007;25(33):5287-5312.
71. Febbo PG, Ladanyi M, Aldape KD, et al. NCCN Task Force report: Evaluating the clinical utility of tumor markers in oncology. *J Natl Compr Canc Netw*. 2011;9 Suppl 5:S1-S32; quiz S33.
72. Sinha G. Circulating tumor cells in early-stage breast cancer. *J Natl Cancer Inst*. 2012;104(22):1693-1694.
73. Bednarz-Knoll N, Alix-Panabières C, Pantel K. Plasticity of disseminating cancer cells in patients with epithelial malignancies. *Cancer Metastasis Rev*. 2012;31(3-4):673-687.
74. Millner LM, Linder MW, Valdes R. Circulating tumor cells: a review of present methods and the need to identify heterogeneous phenotypes. *Ann Clin Lab Sci*. 2013;43(3):295-304.
75. Talasaz AH, Powell AA, Huber DE, et al. Isolating highly enriched populations of circulating epithelial cells and other rare cells from blood using a magnetic sweeper device. *Proc Natl Acad Sci U S A*. 2009;106(10):3970-3975.
76. Etayash H, Jiang K, Azmi S, Thundat T, Kaur K. Real-time Detection of Breast Cancer Cells Using Peptide-functionalized Microcantilever Arrays. *Sci Rep*. 2015;5:13967.
77. Sieuwerts AM, Kraan J, Bolt-de Vries J, et al. Molecular characterization of circulating tumor cells in large quantities of contaminating leukocytes by a multiplex real-time PCR. *Breast Cancer Res Treat*. 2009;118(3):455-468.
78. Miyamoto DT, Zheng Y, Wittner BS, et al. RNA-Seq of single prostate CTCs implicates noncanonical Wnt signaling in antiandrogen resistance. *Science*. 2015;349(6254):1351-1356.
79. Yu M, Bardia A, Aceto N, et al. Cancer therapy. Ex vivo culture of circulating breast tumor cells for individualized testing of drug susceptibility. *Science*.

2014;345(6193):216-220.

80. Yu M, Bardia A, Wittner BS, et al. Circulating breast tumor cells exhibit dynamic changes in epithelial and mesenchymal composition. *Science*. 2013;339(6119):580-584.

81. Takao M, Takeda K. Enumeration, characterization, and collection of intact circulating tumor cells by cross contamination-free flow cytometry. *Cytometry A*. 2011;79(2):107-117.

82. Atwell JL, Breheney KA, Lawrence LJ, McCoy AJ, Kortt AA, Hudson PJ. scFv multimers of the anti-neuraminidase antibody NC10: length of the linker between VH and VL domains dictates precisely the transition between diabodies and triabodies. *Protein Eng*. 1999;12(7):597-604. http://www.ncbi.nlm.nih.gov/pubmed/10436086. Accessed June 21, 2016.

83. Kortt AA, Dolezal O, Power BE, Hudson PJ. Dimeric and trimeric antibodies: high avidity scFvs for cancer targeting. *Biomol Eng*. 2001;18(3):95-108.

84. Olafsen T, Cheung C-W, Yazaki PJ, et al. Covalent disulfide-linked anti-CEA diabody allows site-specific conjugation and radiolabeling for tumor targeting applications. *Protein Eng Des Sel*. 2004;17(1):21-27.

85. Smerage JB, Barlow WE, Hortobagyi GN, et al. Circulating tumor cells and response to chemotherapy in metastatic breast cancer: SWOG S0500. *J Clin Oncol*. 2014;32(31):3483-3489.

86. Barbas CF, Björling E, Chiodi F, et al. Recombinant human Fab fragments neutralize human type 1 immunodeficiency virus in vitro. *Proc Natl Acad Sci U S A*. 1992;89(19):9339-9343.

87. Giang E, Dorner M, Prentoe JC, et al. Human broadly neutralizing antibodies to the envelope glycoprotein complex of hepatitis C virus. *Proc Natl Acad Sci U S A*. 2012;109(16):6205-6210.

88. Rajotte D, Arap W, Hagedorn M, Koivunen E, Pasqualini R, Ruoslahti E. Molecular heterogeneity of the vascular endothelium revealed by in vivo phage display. *J Clin Invest*. 1998;102(2):430-437.

89. Joyce JA, Laakkonen P, Bernasconi M, Bergers G, Ruoslahti E, Hanahan D.

Stage-specific vascular markers revealed by phage display in a mouse model of pancreatic islet tumorigenesis. *Cancer Cell*. 2003;4(5):393-403.

90. Zhang H, Yea K, Xie J, Ruiz D, Wilson IA, Lerner RA. Selecting agonists from single cells infected with combinatorial antibody libraries. *Chem Biol*. 2013;20(5):734-741.
91. Ni H-M, Bockus A, Wozniak AL, et al. Dissecting the dynamic turnover of GFP-LC3 in the autolysosome. *Autophagy*. 2011;7(2):188-204.
92. Scott AM, Wolchok JD, Old LJ. Antibody therapy of cancer. *Nat Rev Cancer*. 2012;12(4):278-287.
93. Baxter LT, Zhu H, Mackensen DG, Jain RK. Physiologically based pharmacokinetic model for specific and nonspecific monoclonal antibodies and fragments in normal tissues and human tumor xenografts in nude mice. *Cancer Res*. 1994;54(6):1517-1528.
94. Scallan J, Huxley VH, Korthuis RJ. *Capillary Fluid Exchange*. Morgan & Claypool Life Sciences; 2010.
95. Sands H, Jones PL, Shah SA, Palme D, Vessella RL, Gallagher BM. Correlation of vascular permeability and blood flow with monoclonal antibody uptake by human Clouser and renal cell xenografts. *Cancer Res*. 1988;48(1):188-193.
96. Hilmas DE, Gillette EL. Morphometric analyses of the microvasculature of tumors during growth and after x-irradiation. *Cancer*. 1974;33(1):103-110.
97. Jain RK. Physiological barriers to delivery of monoclonal antibodies and other macromolecules in tumors. *Cancer Res*. 1990;50(3 Suppl):814s - 819s.
98. Lobo ED, Hansen RJ, Balthasar JP. Antibody pharmacokinetics and pharmacodynamics. *J Pharm Sci*. 2004;93(11):2645-2668.
99. Shah DK, Betts AM. Towards a platform PBPK model to characterize the plasma and tissue disposition of monoclonal antibodies in preclinical species and human. *J Pharmacokinet Pharmacodyn*. 2012;39(1):67-86.
100. Kaneko E, Niwa R. Optimizing therapeutic antibody function: progress with Fc domain engineering. *BioDrugs*. 2011;25(1):1-11.
101. Lammerts van Bueren JJ, Bleeker WK, Bøgh HO, et al. Effect of target dynamics

on pharmacokinetics of a novel therapeutic antibody against the epidermal growth factor receptor: implications for the mechanisms of action. *Cancer Res*. 2006;66(15):7630-7638.

102. Baxter LT, Zhu H, Mackensen DG, Butler WF, Jain RK. Biodistribution of monoclonal antibodies: scale-up from mouse to human using a physiologically based pharmacokinetic model. *Cancer Res*. 1995;55(20):4611-4622.
103. Baxter LT, Jain RK. Transport of fluid and macromolecules in tumors. I. Role of interstitial pressure and convection. *Microvasc Res*. 1989;37(1):77-104.
104. Fujimori K, Covell DG, Fletcher JE, Weinstein JN. Modeling analysis of the global and microscopic distribution of immunoglobulin G, F(ab')2, and Fab in tumors. *Cancer Res*. 1989;49(20):5656-5663.
105. Thurber GM, Schmidt MM, Wittrup KD. Antibody tumor penetration: transport opposed by systemic and antigen-mediated clearance. *Adv Drug Deliv Rev*. 2008;60(12):1421-1434.
106. Lyng H, Haraldseth O, Rofstad EK. Measurement of cell density and necrotic fraction in human melanoma xenografts by diffusion weighted magnetic resonance imaging. *Magn Reson Med*. 2000;43(6):828-836.
107. Krippendorff B-F, Kuester K, Kloft C, Huisinga W. Nonlinear pharmacokinetics of therapeutic proteins resulting from receptor mediated endocytosis. *J Pharmacokinet Pharmacodyn*. 2009;36(3):239-260.
108. Clauss MA, Jain RK. Interstitial transport of rabbit and sheep antibodies in normal and neoplastic tissues. *Cancer Res*. 1990;50(12):3487-3492.
109. Fujimori K, Covell DG, Fletcher JE, Weinstein JN. A modeling analysis of monoclonal antibody percolation through tumors: a binding-site barrier. *J Nucl Med*. 1990;31(7):1191-1198.
110. Saga T, Neumann RD, Heya T, et al. Targeting cancer micrometastases with monoclonal antibodies: a binding-site barrier. *Proc Natl Acad Sci U S A*. 1995;92(19):8999-9003.
111. Adams GP, Schier R, McCall AM, et al. High affinity restricts the localization and tumor penetration of single-chain fv antibody molecules. *Cancer Res*.

2001;61(12):4750-4755.

112. Graff CP, Wittrup KD. Theoretical analysis of antibody targeting of tumor spheroids: importance of dosage for penetration, and affinity for retention. *Cancer Res*. 2003;63(6):1288-1296.

113. Nguyen DX, Massagué J. Genetic determinants of cancer metastasis. *Nat Rev Genet*. 2007;8(5):341-352.

114. Jiang X, Couchman JR. Perlecan and tumor angiogenesis. *J Histochem Cytochem*. 2003;51(11):1393-1410.

115. Aviezer D, Hecht D, Safran M, Eisinger M, David G, Yayon A. Perlecan, basal lamina proteoglycan, promotes basic fibroblast growth factor-receptor binding, mitogenesis, and angiogenesis. *Cell*. 1994;79(6):1005-1013.

116. Gitay-Goren H, Soker S, Vlodavsky I, Neufeld G. The binding of vascular endothelial growth factor to its receptors is dependent on cell surface-associated heparin-like molecules. *J Biol Chem*. 1992;267(9):6093-6098.

117. Sarrazin S, Lamanna WC, Esko JD. Heparan sulfate proteoglycans. *Cold Spring Harb Perspect Biol*. 2011;3(7).

118. Delehedde M, Deudon E, Boilly B, Hondermarck H. Production of sulfated proteoglycans by human breast cancer cell lines: binding to fibroblast growth factor-2. *J Cell Biochem*. 1997;64(4):605-617.

119. Delehedde M, Deudon E, Boilly B, Hondermarck H. Heparan sulfate proteoglycans play a dual role in regulating fibroblast growth factor-2 mitogenic activity in human breast cancer cells. *Exp Cell Res*. 1996;229(2):398-406.

120. Harmer NJ, Ilag LL, Mulloy B, Pellegrini L, Robinson C V, Blundell TL. Towards a Resolution of the Stoichiometry of the Fibroblast Growth Factor (FGF)–FGF Receptor–Heparin Complex. *J Mol Biol*. 2004;339(4):821-834.

121. Huang SM, Bock JM, Harari PM. Epidermal growth factor receptor blockade with C225 modulates proliferation, apoptosis, and radiosensitivity in squamous cell carcinomas of the head and neck. *Cancer Res*. 1999;59(8):1935-1940.

122. Nyati MK, Morgan MA, Feng FY, Lawrence TS. Integration of EGFR inhibitors with radiochemotherapy. *Nat Rev Cancer*. 2006;6(11):876-885.

123. Kruser TJ, Wheeler DL. Mechanisms of resistance to HER family targeting antibodies. *Exp Cell Res*. 2010;316(7):1083-1100.
124. Wheeler DL, Huang S, Kruser TJ, et al. Mechanisms of acquired resistance to cetuximab: role of HER (ErbB) family members. *Oncogene*. 2008;27(28):3944-3956.
125. Sergina N V, Rausch M, Wang D, et al. Escape from HER-family tyrosine kinase inhibitor therapy by the kinase-inactive HER3. *Nature*. 2007;445(7126):437-441.
126. Tebbutt N, Pedersen MW, Johns TG. Targeting the ERBB family in cancer: couples therapy. *Nat Rev Cancer*. 2013;13(9):663-673.
127. Francis DM, Huang S, Armstrong EA, et al. Pan-HER receptor inhibition augments radiation response in human lung and head and neck cancer models. *Clin Cancer Res*. September 2015.
128. Fujimori K, Covell DG, Fletcher JE, Weinstein JN. A modeling analysis of monoclonal antibody percolation through tumors: a binding-site barrier. *J Nucl Med*. 1990;31(7):1191-1198.
129. Saga T, Neumann RD, Heya T, et al. Targeting cancer micrometastases with monoclonal antibodies: a binding-site barrier. *Proc Natl Acad Sci U S A*. 1995;92(19):8999-9003.
130. Tavecchio M, Simone M, Bernasconi S, Tognon G, Mazzini G, Erba E. Multi-parametric flow cytometric cell cycle analysis using TO-PRO-3 iodide (TP3): Detailed protocols. *Acta Histochem*. 2008;110(3):232-244.
131. Tomlinson IM, Walter G, Jones PT, Dear PH, Sonnhammer EL, Winter G. The imprint of somatic hypermutation on the repertoire of human germline V genes. *J Mol Biol*. 1996;256(5):813-817.
132. Park PW, Reizes O, Bernfield M. Cell surface heparan sulfate proteoglycans: selective regulators of ligand-receptor encounters. *J Biol Chem*. 2000;275(39):29923-29926.
133. Yang WP, Green K, Pinz-Sweeney S, Briones AT, Burton DR, Barbas CF. CDR walking mutagenesis for the affinity maturation of a potent human anti-HIV-1 antibody into the picomolar range. *J Mol Biol*. 1995;254(3):392-403.

134. Schier R, McCall A, Adams GP, et al. Isolation of picomolar affinity anti-c-erbB-2 single-chain Fv by molecular evolution of the complementarity determining regions in the center of the antibody binding site. *J Mol Biol*. 1996;263(4):551-567.

135. Sliwkowski MX, Mellman I. Antibody therapeutics in cancer. *Science*. 2013;341(6151):1192-1198.

136. Huang SM, Bock JM, Harari PM. Epidermal growth factor receptor blockade with C225 modulates proliferation, apoptosis, and radiosensitivity in squamous cell carcinomas of the head and neck. *Cancer Res*. 1999;59(8):1935-1940.

137. Wild R, Fager K, Flefleh C, et al. Cetuximab preclinical antitumor activity (monotherapy and combination based) is not predicted by relative total or activated epidermal growth factor receptor tumor expression levels. *Mol Cancer Ther*. 2006;5(1):104-113.

138. Overholser JP, Prewett MC, Hooper AT, Waksal HW, Hicklin DJ. Epidermal growth factor receptor blockade by antibody IMC-C225 inhibits growth of a human pancreatic carcinoma xenograft in nude mice. *Cancer*. 2000;89(1):74-82.

139. du Manoir JM, Francia G, Man S, et al. Strategies for delaying or treating in vivo acquired resistance to trastuzumab in human breast cancer xenografts. *Clin Cancer Res*. 2006;12(3 Pt 1):904-916.

140. Ni H, Bockus A, Wozniak AL, et al. Dissecting the dynamic turnover of GFP-LC3 in the autolysosome. Autophagy. 2011 Feb;7(2):188-204